MICROCOPY RESOLUTION TEST CHART
NATIONAL BUREAU OF STANDARDS-1963-A

AD A 124326

NOISE AND THERMAL CONTRIBUTIONS IN TRANSFERRED
ELECTRON TWO AND THREE TERMINAL DEVICES

FINAL REPORT: R930007-F

H. L. Grubin

J. P. Kreskovsky

January 1983

U. S. Army Research Office

Contract DAAG29-81-C-0033

DTIC

FEB 1 4 1983

H

Prepared by

Scientific Research Associates, Inc.

P. O. Box 498

Glastonbury, CT 06033

83 02 014 002

THE VIEW, OPINIONS, AND/OR FINDINGS CONTAINED IN THIS REPORT ARE THOSE
OF THE AUTHOR(S) AND SHOULD NOT BE CONSTRUED AS AN OFFICIAL DEPARTMENT
OF THE ARMY POSITION, POLICY, OR DECISION, UNLESS SO DESIGNATED BY
OTHER DOCUMENTATION.

REPORT DOCUMENTATION PAGE	READ INSTRUCTIONS BEFORE COMPLETING FORM

1. REPORT NUMBER	2. GOVT ACCESSION NO.	3. RECIPIENT'S CATALOG NUMBER
R930007-F	AD-A124 336	

4. TITLE (and Subtitle)	5. TYPE OF REPORT & PERIOD COVERED
Noise and Thermal Contributions in Transferred Electron Two and Three Terminal Devices	Final Report 15 Aug 1981 – 30 Sept 1982
	6. PERFORMING ORG. REPORT NUMBER

7. AUTHOR(s)	8. CONTRACT OR GRANT NUMBER(s)
H. L. Grubin, J. P. Kreskovsky	DAAG29-81-C-0033

9. PERFORMING ORGANIZATION NAME AND ADDRESS	10. PROGRAM ELEMENT, PROJECT, TASK AREA & WORK UNIT NUMBERS
Scientific Research Associates, Inc. P.O. Box 498 Glastonbury, CT 06033	

11. CONTROLLING OFFICE NAME AND ADDRESS	12. REPORT DATE
U.S. Army Research Office P. O. Box 12211 Research Triangle Park, NC 27709	21 Jan 1983
	13. NUMBER OF PAGES
	109

14. MONITORING AGENCY NAME & ADDRESS(if different from Controlling Office)	15. SECURITY CLASS. (of this report)
	Unclassified
	15a. DECLASSIFICATION/DOWNGRADING SCHEDULE

16. DISTRIBUTION STATEMENT (of this Report)

Approved for public release; distribution unlimited

17. DISTRIBUTION STATEMENT (of the abstract entered in Block 20, if different from Report)

N/A

18. SUPPLEMENTARY NOTES

The view, opinions, and/or findings in this report are those of the author(s) and should not be contrued as an official Department of the Army position, policy, or decision, unless so designated by other documentation.

19. KEY WORDS (Continue on reverse side if necessary and identify by block number)

Nonlinear transport, semiconductors, microelectronics, quantum transport, Boltzmann transport, drift and diffusion, gallium arsenide, indium phosphide, Gunn diodes, FET's, space charge injection, noise, thermal conductivity, nonlocal effects, small signal "Y" parameters, numerical simulation, transferred electron effect

20. ABSTRACT (Continue on reverse side if necessary and identify by block number)

A description of recent studies on noise in two and three terminal compound semiconductor devices, as well as numerical studies of GaAs FET "Y" parameters is given. Studies of thermal effects and space charge limited FET behavior in compound semiconductors is briefly described.

TABLE OF CONTENTS

1. INTRODUCTION

This Final Report R930007-F summarizes activities sponsored by the U.S. Army Research Office under Contract No. DAAG29-81-C-0033. The technical period extended from 15 August 1981 to 30 September 1982.

Three distinct levels of study were involved and used in ARO-sponsored programs. The most fundamental level addressed quantum transport effects in nanometer scale devices, through solutions to the Wigner-Boltzmann transport equation. The second level addressed non-equilibrium transport on a submicron scale through solutions to the Boltzmann-Block transport equation. Here such phenomena as velocity overshoot enter. The third level examined transport on a near micron scale through solutions to the semiconductor drift and diffusion equations. This last level of study has been the mainstay of semiconductor devices for the last thirty to forty years.

During the course of the ARO program, several papers appeared in print in which quantum transport effects were studied. The motivation for the study was high USER (ultra submicron electronics research) interest in determining the range of validity of the Boltzmann transport equation for submicron devices. Difficulties are suggested by the fact that within the effective mass approximation the thermal deBroglie wavelength is of the order of ultrasubmicron dimensions (e.g., 250°A for GaAs). With this as motivation, a quantum transport equation suitable for numerical device computation was developed. Here the equation of motion for the Wigner distribution function was generalized to include scattering contributions. Balance equations for density, momentum and energy and their quantum contributions have been derived. The study has demonstrated that quantum corrections are non-negligible when the carrier transit lengths are of the order of the thermal deBroglie wavelength. Copies of two publications on this subject have already been submitted to ARO.

During the study a numerical technique was developed to analyze the small signal transient characteristics of semiconductor micron length and submicron length devices. In this study the device (either two or three-terminal) was brought to steady state and then subjected to a small voltage pulse. The resulting time-dependent response was subsequently determined self-consistantly, and then analyzed in terms of frequency dependent Fourier components. For submicron length devices, the transient analysis was coupled to solutions to the Boltzmann transport equation and the small

1

signal upper frequency limit of gallium arsenide two-terminal devices, operating under transient overshoot conditions was determined. The results were incorporated into a major review article and were published.

The small signal analysis was also applied to the semiconductor drift and diffusion equation to obtain the small signal microwave parameters of gallium arsenide field effect transistors. The frequency and bias dependence of these parameters are thought to directly reflect the distribution of electrons within the device. In this study the device was brought to a steady state voltage level and then subjected to a small voltage pulse on the drain contact. The resulting time-dependent device response was obtained through two-dimensional solutions of the relevant semiconductor equations. The time-dependent response was analyzed into frequency dependent (Fourier) components and expressed in suitable microwave ("Y") parameter form. The calculations were repeated for a pulse on the gate contact. The microwave parameter calculation which showed general agreement with experiments was extremely sensitive to the electron distribution within the device. One calculation demonstrated that microwave parametric measurements could reveal the presence of local dipole layers of charge within the device. The results of this study are new and are summarized in this report. The study is being prepared for publication.

Another area of study involving the drift and diffusion equation concerns calculating the noise in semiconductor devices. Particularly in the case of gallium arsenide devices, there is a large body of experimental evidence showing an increase in noise prior to the onset of Gunn oscillations. Indeed, this result led some early investigators to speculate that high field cathode-to-anode transit time oscillations were triggered by shot noise. In contrast to this, theoretical studies show a decrease in FET channel noise when the field is in the region of negative differential mobility. These ostensibly conflicting results need reconciliation. One phase of the ARO study involves an analytic study of the effects of contact originated or operational originated (e.g., an FET at high voltage levles) nonuniform field profiles on the noise properties of negative differential mobility devices. In particular with the "fixed cathode boundary" field model developed to explain cathode originated Gunn instabilities, the mean square noise voltage per unit band width has been obtained analytically using the "impedence field technique". The computed results demonstrate that as the threshold for current instabilities is approached, the noise component increases. This is the first theoretical

demonstration of enhanced noise as the instability threshold - rather than the electron transfer threshold is approached. The results were summarized in a keynote paper presented at the Surface and Interface Conference in Trieste, August 1982, and are discussed in this report.

One of the significant conclusions of the two-terminal noise study is that in an active media noise disturbances propagate and simultaneously are amplified. Generally, amplification within the active region of an FET has been accounted for by introducing an effective electron temperature. To some extent this approach is incomplete insofar as it ignores the physics of growth through transit of the carriers. To overcome this difficulty, we have generalized the standard noise theory of FETs within the framework of the analytical gradual channel approximation. For analytical purposes, the essential features of growth are retained within this approximation. In addition to the analytical noise theory, the small signal study demonstrates that the dc space charge profiles will significantly affect the noise characteristics of the device. We have qualitatively coupled the two-dimensional "Y" parameter calculation with the analytical noise study. This is also summarized below. It too is being prepared for publication.

Most device simulations involving the compound semiconductors assume a uniform ambient temperature. Typically, however, the actual device is subject to significant temperature variations which can sometimes permanently alter device properties and often degrade device operation. In order to introduce design changes to minimize these deleterious temperature effects, the detailed temperature profiles must be determined. Under the present ARO contract the semiconductor device numerical code has been generalized to include the heat flow in gallium arsenide devices. Additionally, current flow now includes transport by holes as well as electrons. The results of this study are summarized below.

A new study was initiated to determine the electrical characteristics of a space charge limited injection field effect transistor. The motivation for this study was the superior performance of submicron scale injection FETs. The study discussed below utilized the drift and diffusion equations and is regarded as a benchmark calculation to which submicron calculations may be compared. The results are briefly summarized below.

The technical discussion is contained in the next four sections. Section 2 consists of a one-dimensional analytical study of the effects of cathode originated nonuniformities on the noise properties of transferred electron devices. Section 3 contains the discussion of the numerical "Y" parameter determination and the analytical formulation of the FET noise problem. Section 4 includes the temperature dependent study, while Section 5 contains the discussion of the injection FET.

A list of recent ARO sponsored papers is also included.

2. Noise Properties of Transferred Electron Devices

2.1 Introduction

When a signal is applied to a transferred electron semiconductor such as gallium arsenide or indium phosphide, space charge waves grow as they propagate downstream from the disturbance. This growth mechanism is indiscriminate, and both desired as well as undesired disturbances (noise) are amplified. In the study summarized in this report, two types of noise calculations were considered. The first type was one dimensional, for which analytical calculations were performed. In this calculation the goal was to determine whether noise calculations could provide insight into the nature of the cathode contract conditions, and how they would be modified by nonuniform field profiles. The calculations represent the first detailed analytical study of noise under nonuniform space charge conditions appropriate to the onset of transferred electron oscillations. The second type of noise calculation is associated with noise in FET's. This calculation is a combination of both analytical and numerical studies. Both calculations are designed to demonstrate the effects of nonuniform profiles on the noise properties of devices.

2.2 One-Dimensional Calculations

The calculational approach to one-dimensional noise problems is discussed with reference to Figure 2-1. Figure 2-1 displays a one-dimensional device of length L and carrier density N_o. A small imposed signal at the source of the device manifests itself as a change in voltage across the device, $\delta\psi(t)$. Similarly, a small fluctuation in current, of magnitude $A(X_1)$ at the point $X = X_1$, will propagate toward the anode and manifest itself as a change in voltage $\delta\psi_{X1}(t)$. Shockley, et al (1966) considered two such disturbances: one where the fluctuation resulted in an _increase_ in local charge density, the second in which the fluctuation resulted in an equal _decrease_ in local charge density. Each disturbance results in an impedance change $Z(X_1)$ and $Z(X_2)$. Of relevance for $X_2 = X_1 + \Delta X$, is the differential impedance and "the impedance field defined as

$$\nabla Z = \frac{Z(X_2) - Z(X_1)}{\Delta X} \qquad \text{2.2-1}$$

in which terms the mean square noise voltage per unit band width is defined [Shockley, et al (1966)]

$$\frac{\langle \delta V_n^2 \rangle}{\Delta \Omega / 2\pi} = \int_{\text{Vol.}} |\nabla Z|^2 4e^2 NDd^3X \qquad \text{2.2-2}$$

In the above N is the carrier density, D the diffusivity, and e the magnitude of the electron charge. In the analytical calculations D is taken as constant.

Since the noise calculation describe departures from steady state, the relevant equations are: (1) The equation for total current

$$J = e(NV - \underline{\underline{D\nabla N}}) + \frac{\epsilon \partial F}{\partial T} \qquad \text{2.2-3}$$

and (2) Poisson's equation,

$$\nabla^2 \Psi = \frac{-e}{\epsilon} (N - N_o). \qquad \text{2.2-4}$$

The electric field in these equations is

$$F = -\nabla \Psi \qquad \text{2.2-5}$$

and the potential drop Ψ_o is

$$\Psi_o = \int_0^L FdX \qquad \text{2.2-6}$$

In the analytical noise calculations the underlined terms are ignored.

In the calculations that follow, two types of structures are considered: (1) space charge limited diodes, and (2) diodes with thermally generated carriers. In both cases the effects of boundaries on the noise properties are emphasized. In these calculations it is convenient to work with a set of dimensionless variables identified in Table 1.

6

In dimensionless terms, the relevant equations are (in one dimension)

$$j = nv + \frac{\partial f}{\partial t}.$$
$$\qquad 2.2\text{-}7$$

$$\frac{\partial f}{\partial x} = n-1 \quad \text{or} \quad \frac{\partial f}{\partial x} = n$$
$$\qquad 2.2\text{-}8$$

$$\psi_o = \int_0^{\ell} f dx$$
$$\qquad 2.2\text{-}9$$

and

$$\frac{\langle \delta \psi_n^2 \rangle}{\Delta \Omega / 2\pi} = \frac{4kTR_o}{\ell} \int_0^{\ell} nD \left| \frac{\partial z}{\partial x} \right|^2 dx$$
$$\qquad 2.2\text{-}10$$

In equation 2.2-8, the second differential equation is relevant to space charge limited (SCL) diodes. (Note: the left hand part of equation 2.2-10 is in ordinary units).

In examining noise, small signal perturbations from the steady state are considered, thus

$$j \Rightarrow j_o + \delta j$$
$$\qquad 2.2\text{-}11$$

$$f \Rightarrow f_o(x) + \delta f$$
$$\qquad 2.2\text{-}12$$

$$v \Rightarrow v_o + \delta v = v_o + \mu \delta f$$
$$\qquad 2.2\text{-}13$$

where

$$\mu = \frac{dv}{df}$$
$$\qquad 2.2\text{-}14$$

for simplicity v is taken to be represented by three linear pieces, as in Figure 2.2.

The relevant small signal current equation is

$$\delta j = \left(\frac{\mu_o j_o}{v_o} + i\omega \right) \delta f + v_o \frac{\partial \delta f}{\partial x}$$
$$\qquad 2.2\text{-}15$$

7

for either doped or SCL diodes. In the above, the time dependence is taken as $e^{i\omega t}$. The solution to equation 2.2-15 for both uniform and nonuniform fields is part of an extensive literature [see, e.g., Shaw, et al 1979)]. By way of introduction we carry this solution for uniform fields to the point where the impedance field is obtained [see also Thim (1971)]. It is then generalized for nonuniform fields.

For uniform fields, a disturbance originating at the point x_1, with amplitude $A(x_1)$ results in a perturbed field

$$\delta f(x > x_1, x) = \frac{A(x_1)}{\lambda}\left(1 - e^{-\lambda(x-x_1)/v_0}\right) \qquad 2.2\text{-}16$$

where

$$\lambda = \mu + i\omega \qquad 2.2\text{-}17$$

The potential drop arising from this disturbance is

$$\delta\psi(x_1, \omega) = \int_{x_1}^{\ell} \delta f(x > x_1, x)\, dx$$

$$= \frac{A(x_1)}{\lambda}\left[\ell - x_1 + \frac{v_0}{\lambda}\left(e^{-\lambda(\ell-x_1)/v_0} - 1\right)\right] \qquad 2.2\text{-}18$$

And the impedance field

$$\frac{\partial z(x_1)}{\partial x} = \frac{\left[1 - e^{-\lambda(\ell-x_1)/v_0}\right]}{\lambda} \qquad 2.2\text{-}19$$

which is equation (6) of Thim (1971).

For nonuniform fields the solutions are more complex. For both doped and SCL diodes the solution to equation 2.2-15 is

$$\delta f(x, \omega) = e^{-\int^x g(\zeta)d\zeta}\left\{a(\omega) + \delta j(\omega)\int^x \frac{d\zeta}{v(\zeta)}\, e^{+\int^\zeta g(\zeta')d\zeta'}\right\} \qquad 2.2\text{-}20$$

where

$$g(x) = \left\{\frac{\mu j_0}{v_0(x)} + i\omega\right\}\frac{1}{v_0(x)} \qquad 2.2\text{-}21$$

8

Differences in the results of SCL and doped diodes arise after integration. For doped diodes

$$\int_{x_1}^{x_2} g(\zeta)d\zeta = i\omega t(x_1,x_2) + \log\left\{\frac{j_o/v(x_1)-1}{j_o/v(x_2)-1}\right\} \qquad 2.2\text{-}22$$

$$t(x_1,x_2) = \int_{x_1}^{x_2}\frac{d\zeta}{v_o(\zeta)} = -\frac{1}{\mu}\log\left\{\frac{j_o-v(x_2)}{j_o-v(x_1)}\right\} \qquad 2.2\text{-}23$$

and

$$\delta f(x,\omega) = a(\omega)e^{-\int_{x_1}^{x}g(\zeta)d\zeta} + \delta j(\omega)\int_{x_1}^{x}\frac{d\zeta}{v(\zeta)}\left(\frac{j/v(x)-1}{j/v(\zeta)-1}\right)e^{i\omega t(x_1\zeta)} \qquad 2.2\text{-}24$$

For SCL diodes

$$\int_{x_1}^{x_2} g(\zeta)d\zeta = i\omega t(x_1,x_2) + \log\frac{v(x_2)}{v(x_1)} \qquad 2.2\text{-}25$$

$$t(x_1,x_2) = \frac{v(x_2)-v(x_1)}{\mu j_o} \qquad 2.2\text{-}26$$

and

$$\delta f(x,\omega) = a(\omega)e^{-\int_{x_1}^{x}g(\zeta)d\zeta} + \delta j(\omega)\int_{x_1}^{x}\frac{d\zeta}{v(\zeta)}\frac{v(\zeta)}{v(x)}e^{i\omega t(x_1\zeta)} \qquad 2.2\text{-}27$$

9

Integrating, we obtain, for doped diodes

$$\delta f(x,\omega) = a(\omega) \, e^{-\int_{x_1}^{x} g(\zeta)d\zeta} +$$

$$\delta j(\omega)\left[\left(\frac{1-j}{v(x)}\right)\left(\frac{1-e^{-i\omega t(x_1,x)}}{i\omega}\right)\frac{+j}{v(x)}\left(\frac{1-e^{-\lambda t(x_1,x)}}{\lambda}\right)\right] \qquad 2.2\text{-}28$$

and for SCL diodes

$$\delta f(x,\omega) = a(\omega) \, e^{-\int_{x_1}^{x} g(\zeta)d\zeta} +$$

$$\delta j(\omega)\left[\frac{1}{i\omega}\left(1 - \frac{v(x_1)}{v(x)} \, e^{-i\omega t(x_1,x)}\right) + \right. \qquad 2.2\text{-}29$$

$$\left. \frac{1}{v(x)} \frac{\mu j}{\omega^2}\left(1 - e^{-i\omega t(x_1,x)}\right)\right]$$

10

For fixed cathode fields, as in the case of gallium arsenide devices, $a(\omega) = 0$. For fixed cathode conduction currents as in the case of some indium phosphide devices $a(\omega) = \delta j(x = 0)/i\omega$. These latter results will be included at a later time.

We now examine the field response when a disturbance originates somewhere within the device. In particular: for a disturbance originating at a point x_1, and within either the ohmic, NDM or saturated drift velocity region, the potential drop due to this disturbance is required. For the doped diode

$$\delta\phi(x_1,\Delta,\omega) = \int_{x_1}^{\Delta} \delta f(x \geq x_1, x\omega)dx \qquad 2.2\text{-}30$$

with $\delta f(x > x_1, x, \omega)$ given by equation 2.2-28 with $a(\omega)=0$ and $\delta j(\omega)$ replaced by $A(x_1)$. Integrating the above, and including a disturbance originating at the point $x_2 > x_1$ leads to an impedance field

$$\frac{\partial z(x_1)}{\partial x} = \frac{1-e^{-\lambda t(x_1,\Delta)}}{\lambda} \qquad 2.2\text{-}31$$

which has the same form as that of equation (2.2-19). For SCL diodes

$$\frac{\partial z(x_1)}{\partial x} = \frac{1-e^{-i\omega t(x_1\Delta)}}{i\omega} \qquad 2.2\text{-}32$$

[see also Thornber (1973)].

With the above result, we are in a position to evaluate the noise within either a doped or space charge limited diode. We first illustrate the result for uniform fields and doped diodes.

For uniform fields, with $D = 1$, and $n = 1$

$$\frac{\langle \delta Y_n^2 \rangle}{\Delta\Omega/2\pi} = \frac{4kTR_0}{\ell} \int_0^\ell dx' \left| \frac{1-e^{-\lambda(\ell-x_1)/v_0}}{\lambda} \right|^2 \qquad 2.2\text{-}33$$

$$= \frac{4kTR_0}{\mu^2+\mu^2} \left[1\frac{-j_0}{2\mu\ell} \left(e^{-2\mu\ell/j_0}-1 \right) + \frac{2j_0}{(\mu^2+\omega^2)\ell} \left[\mu\left(e^{-\mu\ell/j_0}\cos\theta-1 \right) - \omega e^{-\mu\ell/j_0}\sin\theta \right] \right] \qquad 2.2\text{-}34$$

11

(See also Thim (1971). In the above, θ is the transit angle

$$\theta = \frac{\ell-x_1}{v_o} \omega \qquad 2.2\text{-}35$$

We note that for ohmic conduction $\mu = 1$, and for ℓ sufficiently large

$$\frac{\left\langle \delta y_n^2 \right\rangle}{\Delta\Omega/2\pi} = \frac{4kTR_o}{1+\omega^2} \qquad 2.2\text{-}36$$

For conduction within the NDM region $\mu < 0$ and the mean square noise voltage per unit bandwidth increases as $e^{+2\mu\ell/j_o}$. For nonuniform fields originating within and remaining within the NDM region

$$\frac{\left\langle \delta y_n^2 \right\rangle}{\Delta\Omega/2\pi}\Delta = \frac{4kTR_o}{\mu_o^2+\omega^2} \cdot \frac{\Delta}{\ell} \cdot \frac{j_o}{\Delta} \left[t(0\Delta) - \frac{1}{2\mu}\left(e^{-2\mu t(0,\Delta)}-1\right)_+ \right.$$

$$\left. \frac{2}{\mu^2+\omega^2}\left[\mu\left(e^{-\mu t(0,\Delta)}\cos\omega t(0,\Delta)-1\right) - \omega e^{-\mu t(0\Delta)}\sin\omega t(0\Delta)\right]\right] \qquad 2.2\text{-}37$$

which bears a clear similarity to equation 2.2-34. There are important differences between the two. In the uniform field case the noise depends critically on length, in which the longer the device the greater the noise. For the case represented by equation 2.2-37, the noise is dependent on the relative values of the mean carrier velocity j_o and the velocity of the entering carriers. This occurs through the relation

$$e^{-\mu t(o,\Delta)} = \frac{j_o-v(\Delta)}{j_o-v(0)} \qquad 2.2\text{-}38$$

Thus, as $j_o \to v(0)$ the noise increases. The context in which this occurs is contained in Figure 2-3 which shows a nonuniform field profile for a ten micron long gallium arsenide element. Here, as the bias is increased that portion of the element within the NDM region increases, and this feature leads to enhanced noise. Thus, from this point of view, the content of equation 2.2-37 is similar to the length dependence of equation 2.2-34.

For the diode whose structure is represented by figure 2.3, which is common to that of a diode just prior to that of a Gunn type oscillation the mean squared noise voltage per unit frequency range is

$$\frac{\langle \delta\gamma_n^2 \rangle}{\Delta\Omega/2\pi} \cong \frac{(1+|\mu|)}{1+\omega^2} \cdot \frac{\langle \delta\gamma_n^2 \rangle_\Delta}{\Delta\Omega/2\pi} + \frac{4kTR_o}{1+\omega^2}\left(1-\frac{\Delta}{\ell}\right) \qquad \text{2.2-39}$$

Rather than deal with this equation, we follow Thim (1971) and examine the noise figure F of a high gain amplifier

$$F \approx 1 + M \qquad \text{2.2-40}$$

where

$$M = \frac{\langle \delta\gamma_n^2 \rangle}{\Delta\Omega/2\pi} \cdot \frac{1}{4kTR_o |Re\, z(\omega)|} \qquad \text{2.2-41}$$

and Re z(w) is the real part of the device impedance. Z(w) is displayed in figure 2-4 (see Grubin et al 1975) for a range of bias values. We note that z(ω) exhibits zeroes, and that the separation of zeroes is an estimate of the extent to which the nonlinear element sustains electric field values within the NDM region. This in turn introduces structure into F [see also Sitch et al (1976)] which is shown in figure 2-5.

The noise figure thus provides two pieces of information.
First the noise figure increases with increasing bias, reflecting enhanced contributions from the NDM region. This increased noise prior to the onset of Gunn oscillations is an important feature of Gunn devices (Gunn 1964). Secondly, the noise figure provides a means of tracing the extent of the NDM region, as shown in figure 2-5. As the bias increases the edges of maximum F, which are associated with ReZ → 0, move closer, reflecting an increase in Δ. This narrowing frequency range is a measure of transit across the NDM region where gain is occurring. The significance of the above unit is that noise measurements may be utilized to provide information about the structure of the space charge layer within the device. Further application for both accumulation layers and constant cathode conduction current boundary conditions and SCL diodes is planned for the future.

Table 1
Normalization

Current Density
$J = (N_o e V_p)j$

Carrier Density
$N = N_o n$

Velocity
$V = V_p v$

Poetntial
$\Psi = (V_p^2 T_o / \mu_o)\psi$

Time
$T = T_o t$

Field
$F = V_p / \mu_o f$

Distance
$X = (V_p T_o)x$

Impedance
$Z = R_o (V_p T_o / L)z$

Diffusion
$D = (\mu kT/e)$

Angular Frequency
$\Omega = T_o^{-1}\omega$

Typical Valves

$N_o \approx 10^{15}/cm^3$

$V_p \approx 2 \times 10^7 cm/sec$

$T_o \approx \varepsilon / N_o e \mu_o \approx 1ps$

$\mu_o \approx 8600\ cm^2/V\text{-}sec$

14
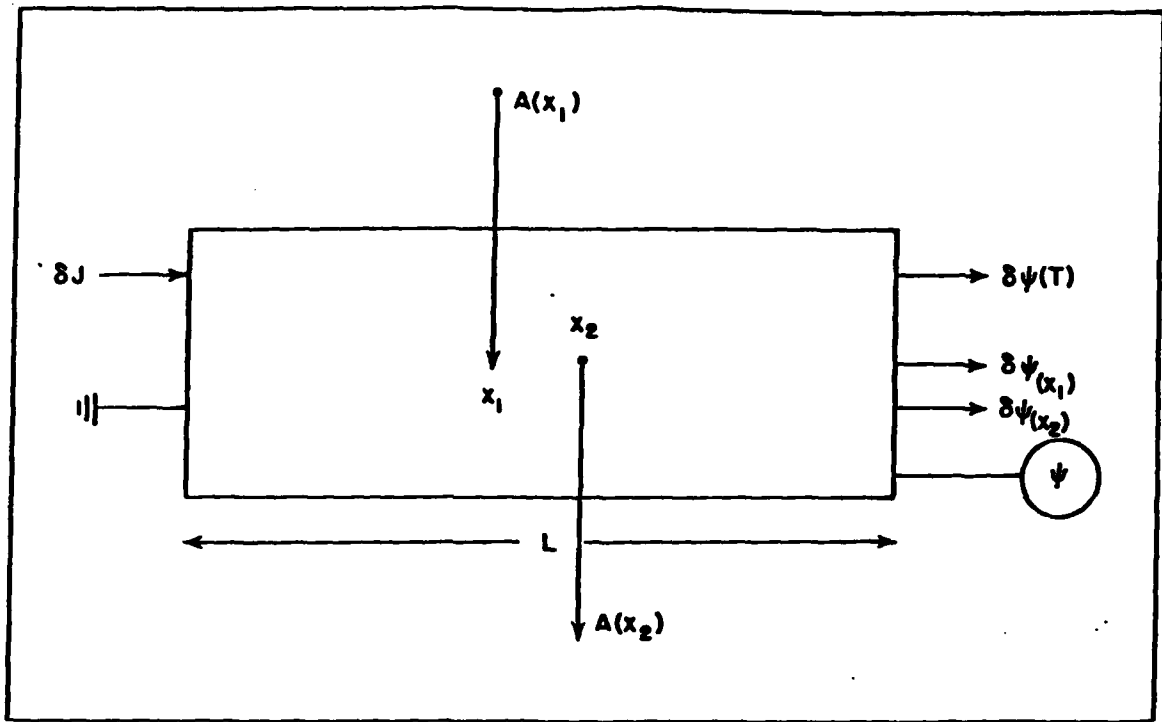
Figure 2.1. Schematic of small signal calculations. A small current disturbance at source results in potential change $\delta\psi(T)$ at anode. For noise calculations a disturbance at x_1 results in a change in anode potential $\delta\psi x_1$.
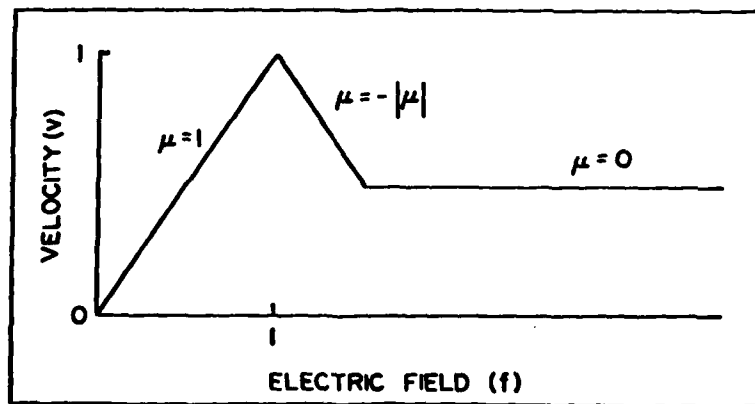
Figure 2.2. Three linear-piece representation of a nonlinear velocity-field curve. In normalized variables (see Table 1), the velocity as well as the threshold field for negative differential mobility are unity. The quantities μ, are differential mobilities, expressed in normalized units.

15
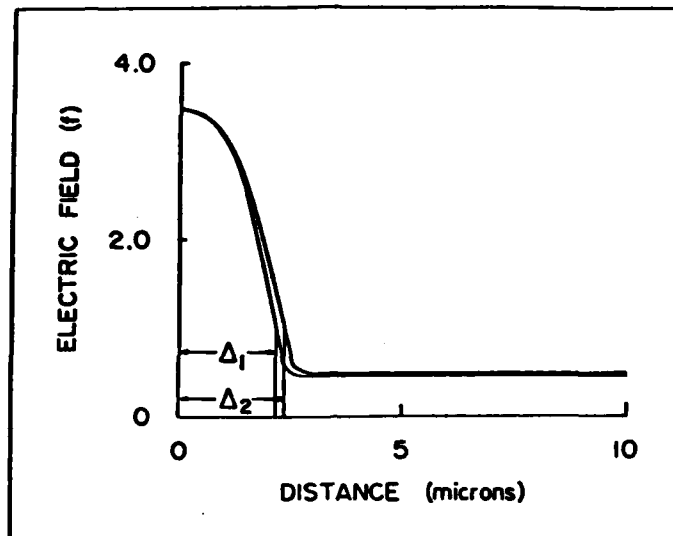
Figure 2.3. Electric field versus distance profiles
for a dimension long NDM with a fixed cathode field
F_c= 3.5F_T, and a normalized negative differential
mobility of -0.2. Normalized cathode velocity is 0.5.
The normalized current density for the two calculations
are 0.485 and 0.488 respectively. Note that the NDM
region, represented by Δ is wider at the higher current
density. [From Grubin et al (1975)].
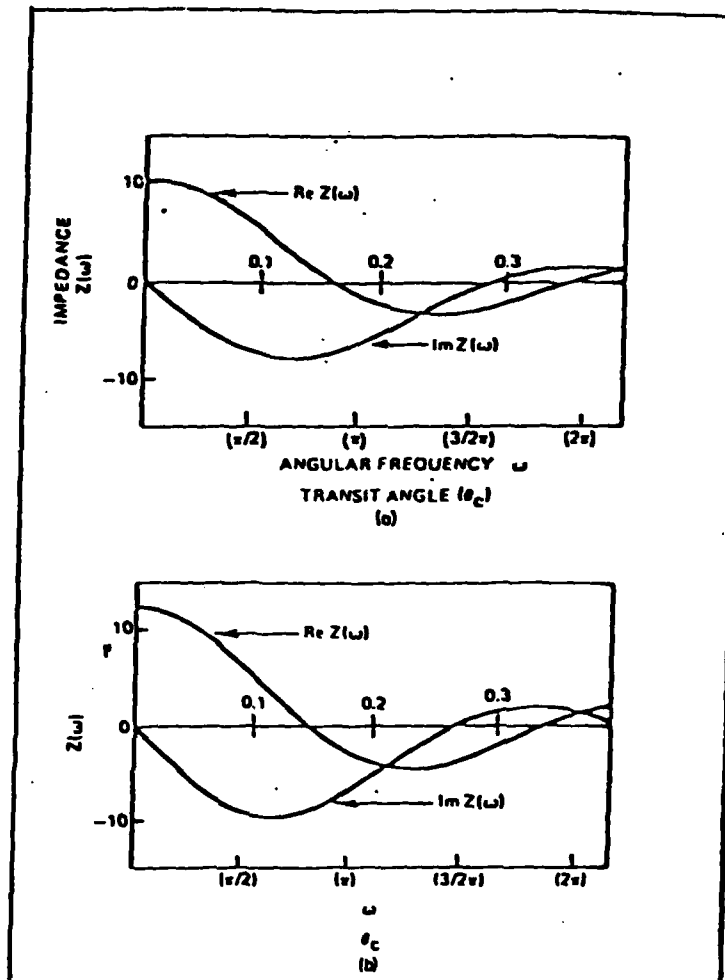
Figure 2.4. Small signal impedance (in multiples of R_o) for a negative differential mobility element with the parameters of figure 2.3. The abscissa displays both angular frequency and transit angle. For part (a) $j_o=0.485$, for (b) $j_o=0.488$. [From Grubin et al (1975)].
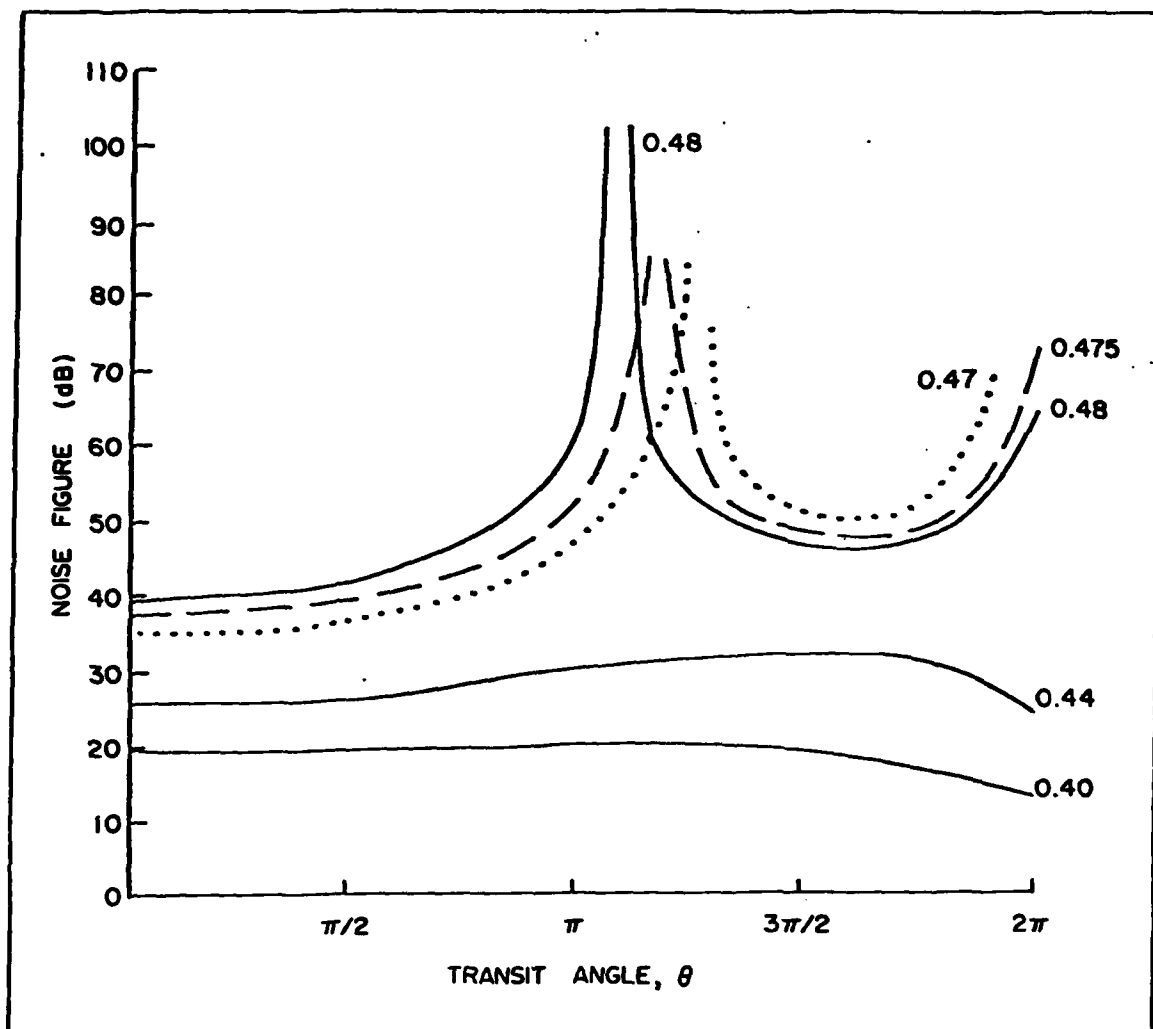
Figure 2.5. Noise figure versus transit angle keyed to normalized bias current $j = J_o/N_o eV_p$, for a ten micron long element with a depletion layer profile.

3. Noise in Field Effect Transistors

3.1 Introduction

One of the significant conclusions of the two-terminal noise study is that in an active media noise disturbances propagate and simultaneously are amplified. Generally, amplification within the active region has been accounted for by introducing an effective electron temperature [Pucel, et al (1975), Baechtold (1972)]. To some extent this approach is incomplete insofar as it ignores the physics of growth through transit of the carriers. To overcome this difficulty, we have generalized the standard noise theory within the framework of the gradual channel approximation. For analytical purposes, the essential features of growth are retained within this approximation. This is discussed below.

In addition to the analytical noise theory, it is clear from the previous section that the dc space charge profiles will significantly affect the noise characteristics of the device. Thus, we need a full set of bias dependent small signal parameters. These parameters have been calculated numerically and are discussed in Section 3.2. Section 3.3 formulates the noise problem, and 3.4 contains the analytical contributions to the FET noise study.

3.2 Calculation of the Small Signal "Y" Parameters

This calculation is a numerical one. The equations solved are the two-dimensional continuity equation

$$-e \frac{\partial N(\vec{X},T)}{\partial T} + \text{div} \cdot \vec{J} = 0 \qquad 3.2\text{-}1$$

the drift and diffusion equation

$$\vec{J} = -e \left\{ N(\vec{X},T) \ \vec{V}(\vec{F}) - D(\vec{F}) \ \nabla N(\vec{X},T) \right\} \qquad 3.2\text{-}2$$

Poisson's equation

$$\nabla^2 \psi \ (\vec{X},T) = + \frac{e}{\varepsilon} \left(N \ (\vec{X},T) - N_o(\vec{X}) \right) \qquad 3.2\text{-}3$$

and the relevant circuit equations. In the above $\vec{X}$ denotes the two-dimensional position vector. The FET configuration is shown in figure 3-1.

The small signal calculations are obtained as small time dependent perturbations of time independent steady state solutions. Since we are treating gallium arsenide, the possibility of large signal domain transit time oscillations must be considered. Since this would only serve to complicate matters and render the concept of small signal parameters specious, attention was concentrated on thin "ND" product FETs that do not sustain instabilities [Grubin, et al (1980)].

The steady state, or dc characteristics of the device, were self-consistently computed and are displayed in figure 3-2. Typical carrier density profiles are represented in figures 3-3 and 3-4. Figure 3-3 displays results for a bias sufficiently high to generate a high field domain under the gate contact. Figure 3-4 shows a result for broad depletion layer under the gate contact.

Figures 3-3 and 3-4 and their respective current and voltage values represent the starting point of the calculation. Subsequently, a small signal square wave voltage (see, e.g., figure 3-5) was superimposed on the drain contact potential, with the gate contact potential fixed at its steady state value. The resulting change in source, gate and drain currents are then computed subject to the constraint

$$\delta I_s(T) = \delta I_d(T) + \delta I_g(T) \qquad 3.2-4$$

The gate and drain current, and the drain potential are then Fourier analyzed. The ratios for a fixed gate potential are identified as the admittance parameters:

$$Y_{12}(\Omega) = \delta I_G(\Omega)/\delta \psi_D(\Omega) \qquad 3.2-5$$

$$Y_{22}(\Omega) = \delta I_D(\Omega)/\delta \psi_D(\Omega) \qquad 3.2-6$$

A similar exercise is performed for a perturbation on the gate contact, with the identification of two additional admittance parameters

$$Y_{11}(\Omega) = \delta I_G(\Omega)/\delta\psi_G(\Omega) \qquad \text{3.2-7}$$

$$Y_{21}(\Omega) = \delta I_D(\Omega)/\delta\psi_G(\Omega) \qquad \text{3.2-8}$$

The "Y" or admittance parameters are dependent on the space charge and potential profiles and are thus bias dependent. In addition it is generally assumed that, about a given bias point, the small signal currents add in a linear way; i.e.,

$$\delta I_G(\Omega) = Y_{11}(\Omega)\ \delta\psi_G(\Omega) + Y_{12}(\Omega)\ \delta\psi_D(\Omega) \qquad \text{3.2-9}$$

$$\delta I_D(\Omega) = Y_{21}(\Omega)\ \delta\psi_G(\Omega) + Y_{22}(\Omega)\ \delta\psi_D(\Omega) \qquad \text{3.2-10}$$

Calculations of the "Y" parameters represent the core of the small signal calculation. The calculation takes on added significance when placed in the context of an equivalent circuit model. A purely formal manipulation of equations 3.2-9 and 3.2-10 provides the necessary direction

$$\delta I_G = (Y_{11} + Y_{12})\ \delta\psi_G - Y_{12}\ (\delta\psi_G - \delta\psi_D) \qquad \text{3.2-11}$$

$$\delta I_D = (Y_{21} - Y_{12})\ \delta\psi_G + Y_{12}\ (\delta\psi_G - \delta\psi_D) + (Y_{22} + Y_{12})\ \delta\psi_D \qquad \text{3.2-12}$$

with the equivalent circuit as shown in figure 3-6.

The terms $Y_{11} + Y_{12}$ are generally identified as source-gate admittance parameters, while $-Y_{12}$ is referred to as the gate-drain admittance.

In the discussion that follows we have attempted to construct the simplest type of equivalent circuit consistent with the numerical calculations. The essential features of the calculations are represented by the equivalent circuit of figure 3-7 where R_d represents channel resistance in the drain loop away from the gate contact. The equivalent circuit of figure 3-7 will require modifications which will be discussed in the conclusions, but it represents the essential features of the calculation. Identifying zeroth order "Y" parameters by the subscript "o", the "Y" parameters are obtained from the equations

21

$$\delta I_g = Y_{110} (\delta\psi_G - R_g \, \delta I_g) + Y_{120} (\delta\psi_D - R_d \, \delta I_d) \qquad \text{3.2-13}$$

$$\delta I_d = Y_{210} (\delta\psi_G - R_g \, \delta I_g) + Y_{220} (\delta\psi_D - R_d \, \delta I_d) \qquad \text{3.2-14}$$

Defining

$$\det Y^2 \equiv Y_{110} Y_{220} - Y_{120} Y_{210} \qquad \text{3.2-15}$$

and

$$D = 1 + R_g Y_{110} + R_d Y_{220} + R_g R_d \det Y^2 \qquad \text{3.3-16}$$

the "Y" parameters are

$$Y_{11} = \frac{Y_{110} + R_d \det Y^2}{D} \qquad \text{3.2-17}$$

$$Y_{12} = \frac{Y_{120}}{D} \qquad \text{3.2-18}$$

$$Y_{21} = \frac{Y_{210}}{D} \qquad \text{3.2-19}$$

$$Y_{22} = \frac{Y_{220} + R_g \det Y^2}{D} \qquad \text{3.2-20}$$

For our immediate discussion it is sufficient to consider the case when $R_g = 0$; thus

$$Y_{11} = Y_{110} - \frac{Y_{120} Y_{210} R_d}{1 + Y_{220} R_d} \qquad \text{3.2-21}$$

$$Y_{12} = \frac{Y_{120}}{1 + Y_{220} R_d} \qquad \text{3.2-22}$$

$$Y_{21} = \frac{Y_{210}}{1 + Y_{220} R_d} \qquad \text{3.2-23}$$

$$Y_{22} = \frac{Y_{220}}{1 + Y_{220} R_d} \qquad \text{3.2-24}$$

With reference to figure 3-7, the zeroth order "Y" parameters are

$$Y_{120} + Y_{220} = G_{DS} \qquad\qquad 3.2\text{-}25$$

where G_{DS} is the drain conductance;

$$Y_{210} - Y_{120} = G_m \qquad\qquad 3.2\text{-}26$$

where G_m is the transconductance, and

$$Y_{110} + Y_{120} = -j\Omega C_{gs}/(1 + j\Omega C_{gs} R_{gs}) \qquad\qquad 3.2\text{-}27$$

Thus, the central circuit parameter to identify is the gate-drain admittance Y_{120}. This parameter contains the essential physics of domain formation. At low drain bias levels, or rather a bias level in which high field domains are not present, Y_{120} is adequately represented by the capacitance C_{dg} as shown in figure 3-7. At high bias levels C_{gd} is replaced by the element shown in figure 3-8, where the conductance at high bias levels will exhibit a small region of negative differential conductivity. In the qualitative discussion that follows, we will ignore the real part of Y_{120} insofar as it modifies the equivalent circuit representation, although its contribution is incorporated in the numerical contributions. The bias dependence of C_{gd} will, however, enter prominently in the following discussion. In terms of figure 3-7

$$Y_{110} = -j\Omega C_{gs} - j\Omega C_{gd} \qquad\qquad 3.2\text{-}28$$

$$Y_{120} = j\Omega C_{gd} \qquad\qquad 3.2\text{-}29$$

$$Y_{210} = G_m + j\Omega C_{gd} \qquad\qquad 3.2\text{-}30$$

$$Y_{220} = G_{ds} - j\Omega C_{gd} \qquad\qquad 3.2\text{-}31$$

Thus

$$Y_{11} = \frac{\Omega^2 C_{gd} R_d (1 + R_d G_1)}{D} - j\Omega \left\{ C_{gs} + \frac{C_{gd} (1 + R_d G_1) (1 + R_d G_{ds})}{D} \right\} \quad 3.2\text{-}32$$

where

$$G_1 = G_{ds} + G_m \quad 3.2\text{-}33$$

and

$$D = (1 + G_{ds} R_d)^2 + \Omega^2 R_d^2 C_{gd}^2) \quad 3.2\text{-}34$$

Also,

$$Y_{12} = \frac{-\Omega^2 C_{gd}^2 R_d}{D} + \frac{j\Omega C_{gd} (1 + R_d G_{ds})}{D} \quad 3.2\text{-}35$$

$$Y_{21} = \frac{G_m (1 + R_d G_{ds}) - \Omega^2 C_{gd}^2 R_d}{D} + \frac{j\Omega C_{gd} (1 + R_d G_1)}{D} \quad 3.2\text{-}36$$

and

$$Y_{22} = \frac{G_{ds} (1 + R_d G_{ds}) + \Omega^2 C_{gd} R_d}{D} - \frac{j\Omega C_{gd}}{D} \quad 3.2\text{-}37$$

Selective "Y" parameter versus frequency are displayed in figures 3-9 through 3-12 for a range of drain bias values and a moderate value of gate bias. Figures 3-13 and 3-14 show the effects of increasing the gate bias. In these figures, the admittance parameters are expressed units of G_0, where

$$G_0 = \frac{N_0 \ e\mu o \ HW}{L} \quad 3.2\text{-}38$$

the frequency is in multiples of f_0

$$f_0 = 0.542 \ GHZ \quad 3.2\text{-}39$$

24

and the bias levels are in multiples of $F_T L$, where F_T is the threshold field for negative differential mobility in gallium arsenide. Some broad general features are clear from equations 3.2-32 through 3.2-37.

Consider first, Re Y_{11}. It is approximately zero at low frequency values and shows an increase in value with increasing frequency. The imaginary part is always negative. Y_{11} displays interesting structure as domains form. (We note that the space charge distribution accompanies each figure.) Next consider Y_{12}. In the absence of domain formation Re Y_{12} is small under dc conditions and then everywhere negative. Under domain formation there is a significant change in Re Y_{12}, requiring the addition of a small negative conductance, as in figure 3-8. For this case Re Y_{12} reads

$$\text{Re } Y_{12} = \frac{gm \ (1 + R_d \ G_{ds}) - \Omega^2 \ C_{gd}^2 \ R_d}{D} \qquad \text{3.2-40}$$

where gm is the parallel conductance. Thus, under weak domain formation Re Y_{12} < 0. Of course, there is a frequency dependance to gm and if gm becomes positive at high frequencies, Re Y_{12} may become positive. The possibility also exists that G_{ds} will become negative when domains are present and again change the sign of Re Y_{12}. The quantities Y_{21} and Y_{22} shows the general trends of equations 3.2-36 and 3.2-34, but also appear to show some unusual structure when high field domains are present. The details of this structure are discussed below. As the discussion progresses, necessary changes to the equivalent circuit will become apparent.

We begin with the detailed discussion of the "Y" parameter with an examination of the drain components Y_{12} and Y_{22}. An examination of these Y-parameters for a fixed gate bias of -0.1 normalized units (figures 3-9 through 3-13) indicates that at low values of drain bias, $|\text{Im } Y_{22}| < |\text{Im } Y_{12}|$. This situation remains until a high field domain forms within the channel and $|\text{Im } Y_{22}| > |\text{Im } Y_{12}|$. The situation in which the drain bias is fixed and the gate bias is increased, result in movement of the depletion layer toward the bottom of the channel. It is seen that $|\text{Im } Y_{22}| > |\text{Im } Y_{12}|$. Thus, the drain element Y_o appears to require the

inclusion of a capacitor. In any case, at high bias levels, $|\text{Im } Y_{22}| \approx |\text{Im } Y_{12}|$ as suggested by equations 3.2-35 and 3.2-36. Further, the frequency dependence and bias dependent nature of both Y_{12} and Y_{22} suggest a rich space charge dependency. Consider the broad frequency dependence of Y_{12}. The first point we note is that Re Y_{12} at low bias levels is negative. This is accounted for by the presence of the parasitic resistance R_d associated with those portions of the semiconductor element not directly under the gate.

Apart from the frequency dependence of the real part of Y_{12}, the most dramatic changes are those associated with the imaginary path. As seen in figure 3-15, the capacitance of the system undergoes a percipitous drop, a feature also seen experimentally [Englemann, et al (1977)] figure 3-16. The broad features of this result were discussed by Englemann, et al (1977), and is represented in figure 3-8. Essentially, the presence of the high field domain is cutting off the gate-drain coupling.

We recall that C_{gd} represents the gate-to-channel capacitance on the drain side of the channel as indicated in figure 3-17, and is a measure of the change in channel depletion charge as a result of changes in drain bias. Now, while a capacitance change is expected as the edge of the depletion layer moves toward the bottom of the channel, the enhanced drop in capacitance suggests that most of the modulation is across the dipole layer. This is illustrated in figure 3-15.

There are basically two sets of data in figure 3-15. The bold line is primarily for a moderate value of gate bias. The most significant drop in capacitance occurs when a domain forms. The situation when the increase in gate to drain voltage is a result of an increased gate bias, does not result in the dramatic decrease in capacitance. For the latter case, dipole domain do not form. We note that the qualitative features of this calculation are in agreement with the experimental results of Englemann, et al (1977).

For the parameter Y_{22}, we simply note that at low bias levels $G_{ds} > 0$, whereas at high values of bias the results strongly suggest a frequency dependent region of small signal negative conductance.

We next consider Y_{11} and note again that to account for the high frequency high bias behavior of Y_{11} it is necessary that G_{ds} exhibit a frequency dependence which allows for a range of small signal negative conductance. With regard to Im Y_{11}, which we write as

$$\text{Im } Y_{11} = -\Omega \, C_{11} \, (\Omega) \qquad\qquad 3.2-41$$

we note from figures 3-18 and 3-15 that at low bias levels C_{11} is somewhat greater than twice C_{gd}. At high bias levels when domains form $C_{11}(\Omega)$ is at least an order of magnitude greater than C_{gd}. Under low or moderate gate bias levels $C_{11}(\Omega)$ does not exhibit a precipitous drop in value. Rather, at first the capacitance decreases corresponding to a movement of the depletion layer toward the bottom of the channel. This was also the initial behavior of the gate to drain capacitance. Further increases in drain bias result in domain formation and space charge injection into the depleted zone. The effective capacitance shows a corresponding increase. This is displayed in figure 3-18. For the situation where the net voltage increase is due to an increase in gate bias, where no domains form there is the expected drop in capacitance, as reflected in the gate to drain capacitance without domains. This is also shown in figure 3-18. The experimental situation shows broad agreement with the numerical results and is displayed in figure 3-19.

The two remaining items of interest here are theoretical/experimental comparison of the transconductance, and current-gain cutoff frequency. Figure 3-20 displays the transconductance, Re Y_{21}, versus $V_{DS} - V_{GS}$, for two values of gate bias. We see the presence of near saturation in both sets of data. This is also seen experimentally. Our data does not extend to high enough drain bias levels to determine whether a corresponding decrease in transconductance occurs. The experimental results are shown in figure 3-21.

The current-gain cutoff frequency is obtained from the expression

$$f_T = \frac{\Omega \text{ Re } Y_{21}}{2\pi \left| \text{Im } (Y_{11} + Y_{12}) \right|} \qquad\qquad 3.2-42$$

and is shown in figure 3-22. It is seen that saturation in f_T occurs under the presence of domain formation. The decrease in f_T at the higher drain bias levels appears to be associated with an increase in the source-gate capacitance. Experimental observations are displayed in figure 3-23, and again show qualitative agreement with theory.

The results of the above study show a clear indication of the role of the high field domain on the small signal characteristics of the FET. These will be used in the qualitative discussion of noise contributions to the FET in the next section. One of the more interesting results is the presense of negative values of Re Y_{22}. This requires further examination.

3.3 Circuit Representation of Noise Sources

As discussed in section 3.2, the small signal properties of the FET can be expressed in terms of a set of "Y" parameters, where when noise is included the circuit is as shown in figure 3-24. For a network of this type it has been established that the noise character-istics of the network can be completely specified in terms of two noise generators [see e.g., Talpey (1959)] as in figure 3-25 or equivalently figure 3-26. In figure 3-26

$$\delta I = \delta I_g - Y_{11} \, \delta I_d / Y_{21} \qquad 3.3-1$$

$$\delta \psi = \delta I_d / Y_{21} \qquad 3.3-2$$

As discussed earlier, a quantitative measure by which the FET noise characteristics are generally judged is the noise figure. The noise figure is defined as the ratio of the output noise power of the actual device to the output noise power that would be obtained from a hypothetical device, identical in all respects except that it contains no noise sources. The output noise in the ideal case is then amplified thermal noise from the signal source connected to the input terminals. Thus

$$F = \frac{\hat{N}_o}{\hat{N}_s} = \frac{\hat{N}_s + \hat{N}_a}{\hat{N}_s} \qquad 3.3-3$$

28

where $\hat{N}_o$ is the output noise of the device, $\hat{N}_s$ is the output noise owing its origin to thermal noise in the signal source, and $\hat{N}_a$ is the noise contribution produced by noise sources within the device. With reference to figure 3-27, where Y_s represents the admittance of the signal source,

$$F = \frac{|i_s + Y_s \delta\psi + \delta i|^2}{|i_s|^2} \qquad 3.3\text{-}4$$

and while i_s is not correlated with either δI or $\delta\psi$, the latter have components that are correlated. Thus

$$F = 1 + \frac{|Y_s \delta\psi + \delta I|^2}{|i_s|^2} \qquad 3.3\text{-}5$$

Using the definitions of δI and $\delta\psi$

$$F = 1 + \frac{\left| \delta I_g - \dfrac{\{Y_s + Y_{11}\}\delta I_d}{Y_{21}} \right|^2}{|i_s^2|} \qquad 3.3\text{-}6$$

$$= 1 + \frac{|\delta I_g|^2 + \dfrac{|Y_s + Y_{11}|^2|\delta I_d^2|}{Y_{21}} - 2|\delta I_d \delta I_g^*| \dfrac{|Y_s + Y_{11}|}{Y_{21}}}{|i_s^2|} \qquad 3.3\text{-}7$$

with $|i_s^2| = 4kTY_s\Delta f = 4kTR_s\Delta f Y_s^2$, assuming Y_s is real

$$F = 1 + \frac{1}{4kTR_s\Delta f}\left\{ |\delta i_d^2| \left| \frac{Y_{11}R_s+1}{Y_{21}} \right|^2 + |\delta i_g^2| R_s^2 - 2|\delta I_d \delta I_g^*| \left| \frac{1 + Y_{11}R_s}{Y_{21}} \right| R_s \right\} \qquad 3.3\text{-}8$$

(see also Cobbold eq. 9.85). Thus, the noise figure depends in a critical way on the noise sources and the circuit parameters introduced earlier.

3.4 Calculation of Noise Sources

3.4.1 Introduction

The quantities of interest in evaluating the noise figure are
the noise current sources and the circuit "Y" parameters. The "Y"
parameters are computed self-consistently. The noise parameters are
not. Instead, we have sought to develop conceptual ideas associated
with the propagation of noise sources, which we have seen tend to
dominate two-terminal device behavior. Thus, while the frequency and
bias dependence of the noise current generators are dependent on the
circuit elements and should be obtained self-consistently, we will rely
heavily on a small signal formulation that is consistent with the gradual
channel approximation. It may be argued that the gradual channel
approximation will not properly describe the electrical behavior of gal-
lium arsenide field effect transistors, and this author would agree.
Nevertheless, from the view point of highlighting important physical
concepts it remains extremely valuable. It is from this latter point
of view that it is used below.

3.4.2 Critique of Noise Calculations, Nonlocal Equations

With reference to figure 3-28, the total channel current between
source and drain, ignoring diffusion contribution is

$$I_d = \left(eNV + \epsilon \, \frac{\partial F}{\partial T}\right) W(H-h(x)) \qquad 3.4-1$$

In the absence of any gate current I_d is independent of x, although in
general I_d is position dependent.

The approach of this author to performing noise calculations
was expressed in the one-dimensional section. It was assumed that a
local fluctuation somewhere within the device caused a change in current,
and that the resulting time-dependent behavior was described by a small
signal perturbation equation. For the FET study we assume, therefore,
that prior to the fluctuation there is no gate current, while after the
fluctuation, gate current can flow. Within the spirit of the small
signal analysis we take

$$I_d \Rightarrow I_{do} + \delta I_d$$

$$h(x,T) \Rightarrow h_o(x) + \delta h$$

$$N(x,T) \Rightarrow N_o(x) + \delta N \qquad \text{3.4-2}$$

$$V \Rightarrow V_o + \mu \delta F$$

$$F(x,T) \Rightarrow F_o(x) + \delta F$$

where

$$\mu = \frac{dV_o}{dF_o} \qquad \text{3.4-3}$$

Incorporating Poisson's equation and rearranging equation 3.4-1 we obtain the small signal equation:

$$\frac{I_{do} + \delta I_d}{W(H - h_o(x) - \delta h(x))} \quad \frac{-Id_o}{W(H - h_o(x))} = \epsilon \left(\frac{\partial}{\partial T} + V_o \frac{\partial}{\partial X} + \frac{N_o(x)e\mu}{\epsilon} \right) \delta F \qquad \text{3.4-4}$$

where

$$\frac{I_{do}}{W(H - h_o(x))} = N_o e V_o(x) \qquad \text{3.4-5}$$

To place equation 3.4-4 in a form useful for analytical work, we introduce the depletion layer approximation for h(x). If ψ represents the potential along the channel, and ψ_g is the potential on the gate contact

$$h(x,T) = \sqrt{(\psi(x,T) - \psi_g) \frac{2\epsilon}{eN_o}} \qquad \text{3.4-6}$$

We note that while ψ_g can be time dependent, it is not spatially dependent. Defining ψ_H through the equation

$$H \equiv \sqrt{\psi_H \frac{2\epsilon}{eN_o}} \qquad \qquad 3.4\text{-}7$$

and

$$\psi(x) = \psi_H \phi(x) \quad , \qquad \qquad 3.4\text{-}8$$

then in terms of dimensionless potentials

$$h(x) = H\sqrt{\phi - \phi_g} \qquad \qquad 3.4\text{-}9$$

I_{do} which is spatially independent is found by direct integration:

$$I_{do} = \frac{1}{L} \int_0^L I_{do} \, dx = \frac{1}{L} \int_0^L N_o(x) e V_o(x) W(H - h_o(x) \, dx \qquad 3.4\text{-}10$$

$$= \frac{WN_o e}{L} \int_0^L V_o(x)(H - H_o(x)) \, dx + \frac{We}{L} \int_0^L (N_o(x) - N_o) \, V_o(x)(H - h_o(x)) \, dx$$

$$\qquad \qquad 3.4\text{-}11$$

$$= -G_o \psi_H \int_0^L (1 - \sqrt{\phi - \phi_g}) \, d\phi + G_o \psi_H \cdot \frac{H^2}{4} \int_0^L \left[\frac{d}{dx}\left(\frac{d\phi}{dx}\right)^2\right](1 - \sqrt{\phi - \phi_o}) \, dx$$

$$\qquad \qquad 3.4\text{-}12$$

where

$$G_o = N_o e \mu W H / L \qquad \qquad 3.4\text{-}13$$

Writing

$$I_{Do} = I_{Do}(1) + I_{Do}(2) \qquad \qquad 3.4\text{-}14$$

32

$I_{Do}(1)$ is directly integrable:

$$I_{Do}(1) = -G_o\psi_H \left[\phi_D - \frac{2}{3}(\phi_D - \phi_g)^{3/2} + \frac{2}{3}(-\phi_g)^{3/2}\right] \qquad 3.4\text{-}15$$

$I_{Do}(2)$ requires numerical integration. The significance of this separation is that $I_{Do}(2)$ is zero when N_o is spatially independent; <u>an assumption made in virtually all analytical FET calculations</u> [see e.g. Pucel, et al (1975)]. Finally, $\delta h(x)$ is given by

$$\delta h(x) = \frac{H(\delta\phi - \phi_g)}{2\sqrt{\phi - \phi_g}} \qquad 3.4\text{-}16$$

Writing the small signal equations in terms of the reduced potential ϕ, we obtain

$$\frac{1}{1 - \sqrt{\phi - \phi_g}} \left\{\delta id + \frac{1}{2}\, id_o \frac{\delta(\phi - \phi_g)}{\sqrt{\phi - \phi_g}}\right\} \qquad 3.4\text{-}17$$

$$= L\left\{\frac{\partial}{\partial t} + V_o\tau\frac{\partial}{\partial x} + n'(x)\right\}\frac{\partial}{\partial x}\delta\phi$$

In the above

$$I_{do} = G_o\psi_H i_{do} \qquad 3.4\text{-}18$$

Similarily for δid. We have also used the Table 1 normalization for t and $n(x)$.

<u>Equation 3.4-17 is the nonlocal equation governing small signal transport within an FET</u>. It is more general than hitherto proposed, [see e.q. Pucel, et al (1975), Van der Zeil (1963)] insofar as it contains the seeds of a propagating disturbance. For example, if the underlined term on the left hand side of equation 3.4-17 is ignored, the equation is essentially that of Section 2 in which the one-dimensional transport equation was studied. Here it is seen that a disturbance within the FET will grow if the field were within the NDM region, while decay would occur for transport within the ohmic or lossy region. <u>The standard calculation,</u>

however, ignores the underlined terms on the right hand side, assumes transport is local within the ohmic region and that $n(x) = 1$. Under these more common assumptions the governing equation, with

$$i_{do} = -L \left(1 - \sqrt{\phi - \phi_g}\right) \frac{d\phi}{dx} \quad , \qquad 3.4\text{-}19$$

is

$$\delta i_d = -L \frac{d}{dx} \left\{\delta\phi(1 - \sqrt{\phi - \phi_g})\right\} \qquad 3.4\text{-}20$$

See e.q. Van der Ziel and Ero (1964), equation 14.

In the absence of numerical calculations, the question that must be asked in assessing the standard approximations to equation 3.4-17 is how significant are the propagating solutions and how well does equation 3.4-20 represent the essential physics. These questions are independent of whether the dc gradual channel approximation is extended into the region of negative differential mobility.

In the one-dimensional noise study it was seen that disturbances within the ohmic region decay very rapidly away from their origin. For this case, equation 3.4-20 is likely to be an excellent approximation for a zeroth order charge density that is approximately uniform. For disturbances within the NDM regime the full perturbation, equation 3.4-17, is needed.

3.4.3 Drain Noise Current; Qualitative Effects of Nonlocality

We now consider an application of these equations to the problem of determining the equivalent noise source in the FET. Consider equation 3.4-20, within the framework of the impedance field. With reference to figure 2-1, we assume a small fluctuation in current is inserted at x_1 and removed at x_2. The effect of the current pulse at x_1 is to cause a voltage change at the drain of magnitude $\delta\phi_{d1}$, such that

$$\delta i_{d1}(L - x_1) = \delta\phi_{d1}(1 - \sqrt{\phi_d - \phi_g}) \qquad 3.4\text{-}21$$

where $\delta\phi(x_1) = 0$. A similar change at x_2 where $\delta i_{d2} = -\delta i_{d1}$ results in

$$-\delta i_{d1}(L - x_2) = \delta\phi_{d2}\left(1 - \sqrt{\phi_d - \phi_g}\right) \qquad \text{3.4-22}$$

with a net voltage change

$$\delta\phi = \frac{\delta i_{d1}(x_2 - x_1)}{1 - \sqrt{\phi_d - \phi_g}} \qquad \text{3.4-23}$$

When expressed in dimensioned units

$$\delta\psi = \frac{1}{G_o} \frac{\delta I_d}{1 - h(L)/H} (x_2 - x_1) \qquad \text{3.4-24}$$

and the impedance field is

$$\nabla Z = \frac{1}{G_o L(1 - h(L)/H} \qquad \text{3.4-25}$$

From equation 2.2-2 for the mean square noise voltage per unit band width, the mean square noise <u>current</u> per unit band width is

$$\frac{\left\langle \delta I_d^2 \right\rangle}{\Delta\Omega/2\pi} = \frac{\left\langle \delta\psi_d^2 \right\rangle}{\Delta\Omega/2\pi} \cdot \frac{1}{R_d^2} \qquad \text{3.4-26}$$

where

$$\frac{1}{R_d} = \frac{\partial I_d}{\partial\psi_d} = G_o(1 - h(L)/H) \qquad \text{3.4-27}$$

Thus

$$\frac{\left\langle \delta I_d^2 \right\rangle}{\Delta\Omega/2\pi} = \frac{4e^2}{L^2} \int_{volume} ND d^3X \qquad \text{3.4-28}$$

Within the spirit of the approximation in which the mobile charge density is assumed to be uniform, equation 3.4-28 integrates to

$$\frac{\left\langle \delta I_d^2 \right\rangle}{\Delta\Omega/2\pi} = 4e^2 N_o \frac{\mu kT \cdot W}{e} \frac{1}{L^2} \int_o^L (H - h(x)dx. \qquad \text{3.4-29}$$

35

To integrate equation 3.4-29, note is taken of the fact that

$$\frac{dx}{d\psi} = \frac{- N_o e \mu_o W(H_. - h(x))}{Id_o} \qquad\qquad 3.4\text{-}30$$

leading to

$$\frac{\langle \delta I_d^{\,2} \rangle}{\Delta\Omega/4\pi} = 4kTG_o \cdot P(\phi_D \ \phi_G) \qquad\qquad 3.4\text{-}31$$

where

$$P(x,y) = \frac{x - \frac{4}{3}\left[(x-y)^{3/2} - (-y)^{3/2}\right] + \frac{1}{2}\left[(x-y)^2 - (-y)^2\right]}{x - \frac{2}{3}\left[(x-y)^{3/2} - (-y)^{3/2}\right]} \equiv \frac{g_1(x,y)}{f_1(x,y)}$$

$$3.4\text{-}32$$

Here $g_1(x,y)$ and $f_1(x,y)$ represent the numerator and denominator, respectively of equation 3.4-32. [See e.g. Van der Ziel (1963), equation 17)] where P is of the order of magnitude of unity. The above results are the low frequency results, and ignore nonlocality. The interest here is, however, in the propagating terms. The discussion below is concerned with this point and the approach is qualitative. We begin in a manner that is analogous to the one-dimensional noise problem.

For the one-dimensional noise problem, and with uniform fields, the impedance field, in dimensioned units is

$$\frac{\partial Z}{\partial X} = \frac{R_o}{L\tau}\left[\frac{1 - \exp - \left[i\Omega + \frac{\mu/\mu_o}{\tau}\right]\frac{L - X}{V}}{i\Omega + \frac{\mu/\mu_o}{\tau}}\right] \qquad\qquad 3.4\text{-}33$$

where

$$\tau = \frac{\epsilon}{N_o e \mu_o} \equiv R_o C_o \qquad\qquad 3.4\text{-}34$$

For low, or zero frequency

$$\frac{\partial Z}{\partial X} = \frac{R_o}{L\mu/\mu_o}\left[1 - \exp - \left(\frac{\mu/\mu_o}{\tau} \cdot \frac{L - x}{v}\right)\right] \qquad\qquad 3.4\text{-}35$$

36

For disturbances within the ohmic region, the exponential contribution is negligible and with $\mu = \mu_o$

$$\frac{\partial z}{\partial x} \approx \frac{R_o}{L} \qquad \qquad 3.4-36$$

With the exception of a variable cross-sectional area this, of course, is similar to the results of equation 3.4-25. The situation with the drain current noise, as dictated by equation 3.4-17 is that the impedance field should have a form qualitatively similar to that of equation 3.4-33 and that for the FET, equation 3.4-25 should be generalized to read

$$\nabla Z^{qual} = \frac{R_o}{L \tau_{eff}} \left[\frac{1 - \exp\left(\left[i\Omega + \frac{\mu/\mu_o}{\tau_{eff}} \right] \frac{L - x}{v} \right)}{i\Omega + \frac{\mu/\mu_o}{\tau_{eff}}} \right] \qquad 3.4-37$$

where τ_{eff} is a generalized "RC" time constant to account for the fact that the cross-sectional area is variable

If equation 3.4-37 is intuitively accepted as a reasonable representation of the nonlocal contributions then modifications to equation 3.4-31 are in order. To introduce these modifications, we turn for guidance again to the one-dimensional case concentrating on equation 2.2-33. This equation, under dc conditions, yields for the mean square current per unit bandwidth.

$$\frac{\langle \delta I^2 \rangle}{\Delta \Omega / 2\pi} = \frac{4kTG_o}{\mu^2} \left[1 + \frac{V_o \tau}{2L|\mu|} \left[A^2 - 4(A - 1) \right] \right] \qquad 3.4-38$$

where

$$\mu = \frac{dV/dF}{\mu_o} \qquad \qquad 3.4-39$$

and

$$A = \exp |\mu/L| V_o \tau \qquad \qquad 3.4-40$$

The above expression is for a disturbance within the negative differential mobility region. The above equation indicates that a fluctuation within the NDM region will be amplified, as expected. Now within an FET only a fraction of the device may be expected to be within the NDM region. Thus, qualitatively, if $< \Delta >$ represent an average length of the NDM region, we expect that equation 3.4-31 will be modified to read

$$\frac{\left\langle \delta I_d^2 \right\rangle}{\Delta\Omega/4\pi} \cong 4kTG_0 \left\{ P(\phi_D, \phi_G) + \frac{1}{\mu^2} \left[1 + \frac{V_0 \tau}{2<\Delta>|\mu|} \left[A^2 - 4(A-1) \right] \right] - \hat{P}_{<\Delta>} \right\}$$

3.4-41

In the above, the length dependance of A is determined by replacing L in equation 3.4-40 by $< \Delta >$. The meaning of equation 3.4-41 is that in the absence of amplification within the NDM region noise is given by the well established classical expression. In the presence of NDM gain over a distance $< \Delta >$, the excess noise over and above that associated with classical noise over a distance $< \Delta >$, $\hat{P}_{< \Delta >}$, is given by

$$4kTG_0 \left\{ \frac{1}{\mu^2} \left[1 + \frac{V_0 \tau}{2<\Delta>|\mu|} \left[A^2 - 4(A-1) \right] \right] - \hat{P}_{<\Delta>} \right\} \qquad 3.4-42$$

In an FET and within a region of negative differential mobility the electron velocity can change by, in many cases a factor of two in going from one region to another. Thus, it is not clear from this expression how a current increase will enhance the noise, as seen experimentally, if all interpretation is through velocity increases. On the other hand, numerical calculations reveal that the length $< \Delta >$ of the NDM region increases with increasing drain bias. This will increase A and the noise.

3.4.4 Current Noise; Quantitative Formulation Including Nonlocality

In many ways the formulation of 3.4.3 is more general than the approach which assumes a variable electron temperature within the channel [Pucel, et al (1975)]. Certainly carriers in the central valley of gallium arsenide experience an increase in electron temperature prior to and during transfer. But once in the satellite valley, the mean carrier temperature decreases. This feature is reflected in the dif-fusion coefficient, whose field dependence is representative of only

moderate mean temperature variations. The crucial component of the
electron transfer mechanism is _gain_ through negative differential mobility.
This result is expressed qualitatively in equation 3.4-41. It is worth-
while noting that if the mechanism of negative differential mobility is
ignored and all enhanced noise is due to variations in electron temperature,
then, fundamentally, silicon should be qualitatively similar to gallium
arsenide. In silicon, high fields also result in increased values of
electron temperature, but there is no gain due to negative differential
mobility.

Equation 3.4-37 indicates the presence of transit time effects
associated with the region of negative differential mobility. In view
of the fact that this region is often shorter than such critical dimensions
as the gate to drain spacing [Grubin, et al (1980)] such transit time
effects are likely to be important only at very high frequencies. Further,
the fairly complex spatial distribution associated with an actual dipole
layer, as determined from simulations, suggests that a distinct transit-
time frequency is likely to be absent. Instead a spread in values occurs.

To summarize; the contribution of the drain noise component to the
noise figure (see equation 3.3-8):

$$\left\langle \delta I_d^2 \right\rangle \left| \frac{Y_{11}Y_s + 1}{Y_{21}} \right|^2 \qquad \qquad 3.4\text{-}43$$

will show amplification within the NDM region through $\left\langle \delta I_d^2 \right\rangle$,
while the significant frequency dependence is through the term

$$\left| \frac{Y_{11}Y_s + 1}{Y_{21}} \right|^2 \qquad \qquad 3.4\text{-}44$$

The frequency dependence is discussed at the end of the section.

A quantitative evaluation of nonlocal noise contributions is now con-
sidered. For this case intuitive generalizations associated with the impedance
field method are not as direct and an alternative derivation is sought. This
method is first illustrated with an alternative calculation of the
nonlocal contribution to $\delta\phi$ following a fluctuation. We begin with
equation 3.4-17 ignoring the time derivative, a nonessential approximation
that will be relaxed at a later time [see, e.g., Richer (1973)]. Thus

$$\frac{\delta i_d}{L} = \frac{d}{dx}\left\{\delta\phi\left(1 - \sqrt{\phi(x) - \phi_g}\right)\right\} + \left(1 - \sqrt{\phi(x) - \phi_g}\right) V_o\tau \frac{d^2\delta\phi}{dx^2} \qquad .3.4\text{-}45$$

where we have again assumed that the dc mobile carrier density is uniform. Under open circuit conditions $\delta id = 0$ and a solution to the resulting homogeneous equation is sought. An expansion of equation 3.4-45 yields

$$\lambda \frac{d^2\delta\phi}{dx^2} + \frac{d\delta\phi}{dx} \cdot b(x) + \delta\phi \cdot a(x) = 0 \qquad 3.4\text{-}46$$

where

$$a(x) = \frac{d}{dx} \ln\left[1 - \sqrt{\phi(x) - \phi_g}\right] , \quad b(x) = 1 \qquad 3.4\text{-}47$$

and

$$\lambda = V_o\tau \qquad 3.4\text{-}48$$

Typically λ is fo the order of 10^{-5} cm and the contribution of the second derivative term may be safely ignored when disturbances are in the ohmic region. Nevertheless, the approach we are taking is a new one and the discussion will, therefore, concentrate on disturbances within this regime. The *effects of* propagation and nonlocality within the NDM region will be treated qualitatively, at this time. We consider solutions of the type (see e.g., Cole (1968), section 2.2 on the singular problem).

$$\delta\phi = \exp S(x) \qquad 3.4\text{-}49$$

with

$$S(x) = S_o(x) + \lambda S_1(x) + \lambda^2 S_2(x) \qquad 3.4\text{-}50$$

Rigorously the expansion in terms of λ may be justified only if convergence is rapid. We are also confining ourselves to perturbations near one boundary. The quantities $S_o(x)$, $S_1(x)_1$, . . . are obtained by equating terms with equal values of λ, as below:

$$(\delta\phi)_x = S_x\delta\phi \qquad 3.4\text{-}51$$

$$(\delta\phi)_{xx} = S_{xx}\delta\phi + (S_x)^2\delta\phi \qquad 3.4\text{-}52$$

40

Thus

$$\lambda \left[S_{xx}\delta\phi + (S_x)^2\,\delta\phi \right] + S_x\delta\phi + a(x)\delta\phi = 0 \qquad 3.4\text{-}53$$

and

$$\frac{d\,S_o(x)}{dx} + a(x) = 0 \qquad 3.4\text{-}54$$

$$\left[So_{xx} + (S_{ox})^2 \right] + \frac{d\,S_1(x)}{dx} = 0 \qquad 3.4\text{-}55$$
$$\vdots \qquad \vdots \qquad \vdots \qquad \cdot\ \vdots$$

The problem is solved subject to the condition

$$\delta\phi\ (X_o) = \Delta\phi\ (X_o) = \exp S(X_o) \qquad 3.4\text{-}56$$

where $\Delta\phi\ (X_o)$ is presumed to be known. It is then asserted that this
must hold for any value of λ. Thus

$$S_1\ (X_o) = S_2(X_o) = \ldots \qquad\qquad = 0 \qquad 3.4\text{-}57$$

Solution to equation 3.4-54, then yields

$$S_o(x) = \ell n \left\{ \Delta\phi(X_o)\ \left[\frac{1 - \sqrt{\phi(X_o) - \phi g}}{1 - \sqrt{\phi(X) - \phi g}} \right] \right\} \qquad 3.4\text{-}58$$

and

$$\delta\phi_o(x) \equiv \exp S_o(x) \qquad 3.4\text{-}59$$

or

$$\delta\phi_o\ (X) = \Delta\phi\ (X_o) \left[\frac{1 - \sqrt{\phi(X_o) - \phi g}}{1 - \sqrt{\phi(X) - \phi g}} \right] \qquad 3.4\text{-}60$$

41

Equation 3.4-60 is the same as equation (10) of Van der Ziel (1962) and when used to calculate the mean squared drain noise, yields equation 3.4-32. The first correction $S_1(X)$ is obtained by direct integration and is equal to

$$S_1(X) = \left[\phi_D - \frac{2}{3}(\phi_D - \phi_G)^{3/2} + \frac{2}{3}[-\phi_G]^{3/2}\right]\left(\theta(X) - \theta(X_o)\right) \times$$

$$x \quad \left\{\frac{1}{\theta(X)\,\theta(X_o)} + \frac{1}{1-\theta(X)} \cdot \frac{1}{1-\theta X_o)}\right.$$

$$\left. + \frac{2}{\theta(X) - \theta(X_o)} \; \ell_n\left[\frac{\theta(X)}{1-\theta(X)} \cdot \frac{1-\theta(X_o)}{\theta(X_o)}\right]\right\} \qquad \text{3.4-61}$$

where

$$\theta(X) = h(X)/H \qquad \text{3.4-62}$$

(see equation 3.4-9). Although $\theta(X) > \theta(X_o)$ for $X > X_o$, and the logarithm term is slightly negative, $S_1(X)$ is negative and

$$\lambda\left|S_1(X)\right| \simeq \text{ord}\left(\frac{\lambda}{L}\right) \qquad \text{3.4-63}$$

Thus

$$\delta\phi(X) \simeq \delta\phi_o(X)\exp - \text{ord}\left(\frac{\lambda}{L}\right) \qquad \text{3.4-64}$$

and

$$\delta\phi(X) \simeq \delta\phi_o(X)\left(1 - \text{ord}\,\frac{\lambda}{L}\right) \qquad \text{3.4-65}$$

Thus, for perturbations within the ohmic region, nonlocal contributions to the drain noise current are negligible. The situation when a portion of the FET is within the NDM proceeds in a manner similar to that of equation 3.4-50, except that b(X) is no longer equal to unity, and a(X) will have a form other than that of equation 3.4-47, as may be extracted from Bachtold (1972). Further, $\lambda < 0$ and so a disturbance is enhanced. More generally, from equation 3.4-56 with $\delta\phi_o$ given by equation 3.4-60 and $S_1(X)$ given by equation 3.4-61, we have the first nonlocal quantitative correction to $\delta\phi$.

To calculate the short circuit gate noise it is no longer assumed that $\delta i d = 0$. Instead, it is necessary to solve the equation

$$\lambda\frac{d^2\delta\phi}{dx^2} + \frac{d\delta\phi}{dx} \cdot b(X) + \delta\phi \cdot a(X) = \frac{\delta i d}{\cdot L}\,C(X) \qquad \text{3.4-66}$$

42

where a(X) and b(X) are given by equation 3.4-47, and

$$C(X) = \left(1 - \sqrt{\phi(X) - \phi_g}\right)^{-1} \qquad \text{3.4-67}$$

Equation 3.4-66 is solved in a manner similar to that of equation 3.4-45, except that the presence of the driving term reduces the usefulness of the exponential expansion. Instead, we let

$$\delta\phi = \delta\phi_o(X) + \lambda\delta\phi_1(X) + \lambda^2 \delta\phi_2(X) + \ldots \qquad \text{3.4-68}$$

where

$$\frac{d\delta\phi_o(X)}{dx} + a(X)\, \delta\phi_o(X) = \frac{\delta id}{L}\, C(X) \qquad \text{3.4-69}$$

and

$$\frac{d\delta\phi_1(X)}{dx} + a(X)\, \delta\phi_1(X) = \frac{-d^2\delta\phi_o}{dx^2} \qquad \text{3.4-70}$$

The differential equation 3.4-69 is the same as that of equation 3.4-20. If a disturbance in the form of a noise EMF is generated between X_o and $X_o + \Delta X$, then a solution to equation 3.4-69 in the regions to the left and right of the disturbance, subject to the short circuit conditions

$$\delta\phi(0) = \delta\phi(L) = 0 \qquad \text{3.4-71}$$

yields

$$\frac{\delta i_d X}{L} = \delta\phi_o(X)\, \left(1 - \sqrt{\phi(X) - \phi g}\right) \qquad 0 < X < X_o \qquad \text{3.4-72}$$

$$\frac{\delta i_d (X-L)}{L} = \delta\phi_o(X)\, \left(1 - \sqrt{\phi(X) - \phi g}\right) \qquad X_o + \Delta X < X < L \qquad \text{3.4-73}$$

43

and within each region*

$$\delta\phi_1(X) = {}_{-e} - \int^{X} a(\zeta)d\zeta \int_{o}^{X} d\zeta' e^{\int^{\zeta'} a(\zeta)d\zeta} \frac{d^2\delta\phi_o(\zeta')}{d\zeta'^2}, \quad 0 < X < X_o \qquad 3.4\text{-}74a$$

$$\equiv \frac{Z_I(x)}{L} \, \delta i_d \qquad\qquad 3.4\text{-}74b$$

and

$$\delta\phi_{1+}(X) = {}_{-e} - \int^{X} a(\zeta)d\zeta \int_{x}^{L} d\zeta' e^{\int^{\zeta'} a(\zeta)d\zeta} \frac{d^2\delta\phi_o(\zeta')}{d\zeta'^2}, \quad X_o + \Delta X < X < L \qquad 3.4\text{-}75a$$

$$\equiv \frac{Z_{II}(x)}{L} \, \delta i_d \qquad\qquad 3.4\text{-}75b$$

Across region III the potential is assumed to change by an amount $\Delta\phi\,(X_o)$

Thus

$$\delta\phi(X_o + \Delta X) - \delta\phi(X_o) = \delta\phi_o(X_o + \Delta X) - \delta\phi(X_0) + \lambda\left[\delta\phi_{1+}(X_o + \Delta X) - \right. \qquad 3.4\text{-}76$$
$$\left. \delta\phi_{1-}(X_o)\right] \quad \cdots$$

$$= \frac{-\delta i_d}{1 - \sqrt{\phi(X_o) - \phi g}} + \delta i_d \frac{\lambda}{L} Z_\Delta \qquad 3.4\text{-}77$$

where

$$Z_\Delta = Z_{II} - Z_I \qquad 3.4\text{-}78$$

is independent of current. Thus

$$\delta i_d = \frac{-\Delta\phi(X_o)\left(1 - \sqrt{\phi(X_o) - \phi g}\,\right)}{1 - \frac{\lambda}{L} Z_\Delta\left(1 - \sqrt{\phi(X_o) - \phi g}\,\right)} \qquad 3.4\text{-}79$$

In the $\lambda = 0$ limit, Vander Ziel's (1963) equation (11) is obtained.

*The integration of these equations is direct.

44

The next step in calculating the gate current noise involves computing the fluctuation in gate charge associated with a fluctuation in potential $\Delta\phi$ at X_o. We have seen that such a fluctuation will produce an alteration in the channel potential. If the charge within the depletion layer is changed by an amount

$$\delta Q \doteq eN_o \, W\delta h(X)dx \qquad 3.4\text{-}80$$

Then an equal and opposite amount of charge will be altered on the gate contact. The net charge alteration is

$$\Delta Q = \int_o^L \delta Q \qquad 3.4\text{-}81$$

$$= -eN_o W \int_o^{X_o} \delta h(X)dx - eN_o W \int_{X_o + \Delta X}^L \delta h(X)dx - eN_o W \, \delta h(X)\Delta X \qquad 3.4\text{-}82$$

$$= + \Delta Q_I + \Delta Q_{III} + \Delta Q_\Delta \qquad 3.4\text{-}83$$

Here, in Region I

$$\delta h = \frac{H\delta\phi}{2\sqrt{\phi - \phi g}} \qquad 3.4\text{-}84$$

where, from equations 3.4-72 and 3.4-74

$$\delta\phi = \delta i_d \left\{ \frac{X}{L\,(1 - \sqrt{\phi - \phi g})} + \frac{\lambda}{L} Z_I(X) \right\} \qquad 3.4\text{-}85$$

For comparison, note equation 3.4-65. Thus

$$\Delta Q_I = -\delta i_d \left\{ N_o e \frac{WH}{2L} \int_{X_o}^{X_o} \frac{dx' \, x'}{\sqrt{\phi - \phi_g} \, (1 - \sqrt{\phi - \phi_g})} \right.$$

$$\left. + N_o e \frac{WH\lambda}{2L} \int_o \frac{Z_I(X) \, dx'}{\sqrt{\phi - \phi_g}} \right\} \qquad 3.4\text{-}86$$

Similarly

$$\Delta \phi_{II} = -\delta i_d \left\{ N_o e \frac{WH}{2L} \int_{X_o + \Delta X}^{L} \frac{dx' \, (x' - L)}{\sqrt{\phi - \phi_g} \, (1 - \sqrt{\phi - \phi_g})} \right.$$

$$\left. + N_o e \frac{WH\lambda}{2L} \int_{X_o + \Delta X}^{L} \frac{Z_{II}(X) \, dx'}{\sqrt{\phi - \phi_g}} \right\} \qquad 3.4\text{-}87$$

Thus

$$\Delta Q = -\delta i_d \, \frac{N_o e \, WH}{L} \left\{ \frac{1}{2} \int_o^L \frac{X \, dX}{\theta(X)(1 - \theta(X))} - \frac{1}{2} \int_{x_o + \Delta X}^{L} \frac{L \, dX}{\theta(X)(1 - \theta(X))} \right.$$

$$\left. + \frac{\lambda}{2} \int_o^{X_o} \frac{Z_I(X) \, dX}{\theta(X)} + \frac{\lambda}{2} \int_{X_o + \Delta X}^{L} \frac{Z_{II}(X) \, dX}{\theta(X)} - \frac{1}{2} \int_{X_o}^{X_o + \Delta X} \frac{X \, dX}{\theta(X)(1 - \theta(X))} \right\}$$

$$\frac{-e \, N_o \, WH}{2} \, \frac{\Delta \phi_o}{\theta(X_o)} \quad \Delta X$$

$$3.4\text{-}88$$

46

where $\theta(X_o)$ is given by equation 3.4-62. Integration of the first two terms is direct. Using equation 3.4-19 along with

$$X = -\frac{L}{i_{do}} \left(\phi(X) - \frac{2}{3} \left\{ (\phi(X) - \phi_g)^{3/2} - (-\phi_g)^{3/2} \right) \right) \qquad 3.4\text{-}89$$

we obtain

$$\Delta Q \approx -\delta i_d \, N_o eL \, WH \left\{ \frac{\bar{\theta} - \theta(X_o)}{i_{do}} + \frac{\lambda}{2L} \, \bar{z}_T(X_o) \right\} \qquad 3.4\text{-}90$$

where

$$\bar{z}(X_o) = \frac{1}{L} \left\{ \int_o^{X_o} \frac{z_1(X)dX}{\theta(X)} + \int_{X_o+\Delta}^{L} z_{II} \frac{(X)dX}{\theta(X)} \right\} \qquad 3.4\text{-}91$$

and

$$\bar{\theta} = \frac{1}{L} \int_o^{L} \theta(X)dX \qquad 3.4\text{-}92$$

The first part of equation 3.4-90 we recognize as the same as equation (16) of Van der Ziel (1963).

We are now in a position to compute the mean square noise currents. Recognizing that $\Delta\phi(X_o)$ is caused by thermal noise, its mean squared value is:

$$\overline{\Delta\psi(X_o)}^2 = \frac{4kT \, \Delta f \, \Delta X}{\dfrac{dI_d(X_o)}{d\psi} L} \qquad 3.4\text{-}93$$

or in normalized units, as

$$\overline{\Delta\phi(X_o)}^2 = \frac{4kT\,\Delta f \cdot \Delta X}{G_o\psi_H{}^2 L d_i do/d\phi} \qquad 3.4\text{-}94$$

Hence, for the drain current noise (from equation 3.4-79):

$$\overline{\delta i_d}^2 = \frac{4kT\Delta f \cdot \Delta X}{LG_o\psi_H{}^2 di_{do}(X_o)/d\phi} \cdot \left(\frac{1 - \sqrt{\phi(X_o) - \phi g}}{1 + \frac{\lambda}{L}Z_\Delta(1 - \sqrt{\phi(X_o) - \phi g})}\right)^2 \qquad 3.4\text{-}95$$

and

$$\left\langle \delta i_d^2 \right\rangle = \int_o^L \overline{\delta i_d}^2\, dx \qquad 3.4\text{-}96$$

Noting that

$$\frac{di_d(X_o)}{d\phi} = 1 - \sqrt{\phi(X_o) - \phi_g} \qquad 3.4\text{-}97$$

equation 3.4-95 integrates to

$$\left\langle \delta i_d^2 \right\rangle \cong \frac{4kT\Delta f}{G_o\psi_H{}^2} \left\{ P(\phi_D, \phi_G) - \frac{\lambda}{L}\int_o^L \left(1 - \sqrt{\phi(X_o) - \phi g}\right)^3 Z_\Delta(X)\, dx \right\} \qquad 3.4\text{-}98$$

Or in ordinary units

$$\frac{\left\langle \delta I_d^2 \right\rangle}{\Delta\Omega/2\Pi} = 4kTG_o \left\{ P(\phi_D \phi_G) - \frac{\lambda}{L}\int_o^L \left(1 - \sqrt{\phi(X_o) - \phi g}\right)^3 Z_\Delta(X_o)\, dx \right\} \qquad 3.4\text{-}99$$

where $P(\phi_D, \phi_G)$ is given by equation 3.4-32. We note the similarity of equation 3.4-99 to the more intuitive argument of equation 3.4-41.

For the mean squared fluctuating gate charge

$$\overline{\Delta Q}^2 = (N_o eLWH)^2 \left\{ \frac{\bar\theta - \theta(X_o)}{i_{do}} + \frac{\lambda\overline{Z}(X_o)}{2L} \right\}^2 \overline{\delta i_d}^2 \qquad 3.4\text{-}100$$

48

$$= (N_o eLWH)^2 \left\{ \frac{\bar{\theta} - \theta(X_o)}{i_{do}} + \frac{\lambda \bar{Z}(X_o)}{2L} \right\}^2 \cdot \frac{4kT\Delta f}{LG_o \psi_H^2} \frac{\Delta X}{\frac{di_{do}(X_o)}{d\phi}}$$

$$X \left\{ \frac{1 - \sqrt{\phi(X_o) - \phi g}}{1 + \frac{\lambda Z_\Delta}{L}(1 - \sqrt{\phi(X_o) - \phi g})} \right\}^2$$

The mean squared charge fluctuation along the entire gate is

$$\langle \delta Q \rangle = \int_o^L \overline{\Delta Q}^2 \, dx \qquad 3.4\text{-}102$$

Defining

$$Csg = \frac{N_o eLWH}{\psi_H} \qquad 3.4\text{-}103$$

$$h_1(\phi_d, \phi_g) = \int_o^{\phi_d} \left(1 - \sqrt{\phi(X) - \phi g}\right)^2 d\phi \qquad 3.4\text{-}104$$

$$h_2(\phi_d, \phi_g) = \int_o^{\phi_d} \sqrt{\phi(X) - \phi g} \left(1 - \sqrt{\phi(X) - \phi g}\right)^2 d\phi \qquad 3.4\text{-}105$$

$$h_3(\phi_d, \phi_g) = \int_o^{\phi_d} (\phi(X) - \phi g) \left(1 - \sqrt{\phi(X) - \phi g}\right)^2 d\phi \qquad 3.4\text{-}106$$

[see Vander Ziel (1963)] with (see equation 3.4-32)

$$f_1 = i_{do} \qquad 3.4\text{-}107$$

the uncorrected portion of 3.4-102 integrates to

$$\langle \delta Q \rangle^2 = \frac{4kT\Delta f \cdot C_{sgo}^2}{G_o} \cdot \frac{g_3(\phi_d, \phi_g)}{f_1(\phi_d, \phi_g)^3} \qquad 3.4\text{-}108a$$

where

$$g_3(\phi_d, \phi_g) = \bar{\theta}^2 h_1(\phi_d, \phi_g) - 2\bar{\theta} h_2(\phi_d, \phi_g) + h_3(\phi_d, \phi_g) \qquad 3.4\text{-}108b$$

49

The total, including corrected contributions, is

$$\frac{\left\langle \delta Q^2 \right\rangle}{\Delta\Omega/2\pi} = \frac{4kT}{G_o} \; C_{sg}^2 \cdot \left\{ \frac{g_3(\phi_d,\phi_g)}{f_1(\phi_d,\phi_g)} + \frac{\lambda}{L}\left[\int_o^L d\phi \frac{(1-\theta)^2(\bar{\theta}-\theta)Z(\bar{X}_o)}{i_{do}^2} \right.\right.$$

$$\left.\left. - \; 2Z_\Delta \frac{(1-\theta)^3 \, (\bar{\theta}-\theta)^2}{i_{do}^3} \right]\right\} \qquad 3.4\text{-}109$$

The mean square gate current is

$$\left\langle \delta I_g \right\rangle^2 = \Omega^2 \left\langle \delta Q \right\rangle^2 \qquad 3.4\text{-}110$$

For the correlation coefficient

$$\Delta Q \delta i_d = N_o eLWH \left\{ \frac{\bar{\theta}-\theta(X_o)}{i_{do}} + \frac{\lambda}{2L} \; Z(\bar{X}_o) \right\} \; \delta i_d^2 \qquad 3.4\text{-}111$$

or

$$\Delta Q \delta I_d = \Delta Q \delta i_d \; G_o \psi_H \qquad 3.4\text{-}112$$

and

$$\Delta Q \delta I_d = \frac{N_o eLWHG_o \psi_H \cdot 4KT\Delta f}{G_o \psi_H^2 L} \; \frac{\Delta X}{i_{do}/d\phi} \qquad 3.4\text{-}113$$

$$\times \; \left\{ \frac{\bar{\theta}-\theta(X_o)}{i_{do}} + \frac{\lambda \bar{Z}(X_o)}{2L} \right\} \left\{ \frac{1 - \sqrt{\phi(X_o) - \phi_g}}{1 + \frac{\lambda Z_\Delta}{L}(1 - \sqrt{\phi(X_o) - \phi g})} \right\}^2$$

Thus,

$$\frac{\left\langle \Delta Q \delta I_d \right\rangle}{\Delta\Omega/2\Pi} = \int_o^L \Delta Q \delta I_d \; dx \qquad 3.4\text{-}114$$

50

$$= -4kTCg s_o \left[\begin{array}{c} g_2(\phi_d, \phi_g) \\ L \end{array} \right.$$

3.4-115

$$\frac{-\lambda}{L} \left\{ \frac{1}{2} \int_o^L Z(X_o)\, (1 - \sqrt{\phi(X_o) - \phi g})^2\, d\phi \right.$$

$$\left. \frac{-1}{i_{do}} \int_0^L Z_\Delta\, \left(1 - \sqrt{\phi(X_o) - \phi g}\right)^3\, (\bar{\theta} - \theta(X))d\phi \right\}$$

where

$$g_2(\phi_d, \phi_g) = \bar{\theta} h_1\,(\phi_d, \phi_g) - h_2\,(\phi_d, \phi_g)$$

3.4-116

Note the first part of equation 3.4-115 is found in Vander Ziel (1969). If

$$\delta I_g = -j\Omega\, \Delta Q$$

3.4-117

$$\langle \delta I_g\, \delta I_d \rangle = -j\Omega\, \langle \Delta Q \delta I_d \rangle$$

3.4.5 Conclusions

Equations 3.4-99, 3.4-109 and 3.4-115 represent the first significant analytical generalization of FET noise theory to account for nonlocal effects of space charge within the conduction channel of the FET. The application was only to ohmic conduction, but an apparent generalization to transport within the NDM region is clear. The importance of this calculation lies in the fact that the current sources depend significantly on the space charge distribution within the FET, and that disturbances within the NDM regime will be amplified.

The effect of coupling this to the external circuit is unclear. Consider for example equation 3.4-44 which represents the effect of drain circuit and noise source on the noise figure of the FET. At low values of drain bias, figure 3-9 indicates that at all but dc conditions, the imaginary part of Y_{21} is the dominant contribution. Similarly, for the imaginary part of Y_{11}. But, in this case there is no enhanced

noise due to gain from within the NDM region. Nevertheless, under dc conditions, the situation appears as

$$\left\langle \delta I_d^2 \right\rangle \frac{1}{g_m^2} \qquad\qquad 3.4\text{-}118$$

Equation 3.4-118 prevails at high bias levels when domains are present and introduces two competing contributions. On the one hand, increased noise is expected from $<\delta I_d^2>$, but this is partially compensated by an increase in the transconductance. Thus, the net effect may be an apparent decrease in noise due to the drain current contribution.

The frequency dependence at bias levels sufficiently high to generate domain is more direct. Here, Y_{11} is dominated by capacitive contributions while Y_{21} is still primarily real. Thus, the drain component of noise is approximately

$$\left\langle \delta I_d^2 \right\rangle \frac{1 + \omega^2 \, Y_s^2 \, C_{11}^2}{g_m^2} \qquad\qquad 3.4\text{-}119$$

and shows an increase with increasing frequency, as discussed experimentally [Liechti (1976)]. As far as the frequency dependence of the gate noise current, there is no contribution from the circuit as long as Ys is real. All frequency dependence is contained in $< \delta I_g^2 >$. With regard to the correlation coefficient, its frequency dependence is on the square root of the drain component.
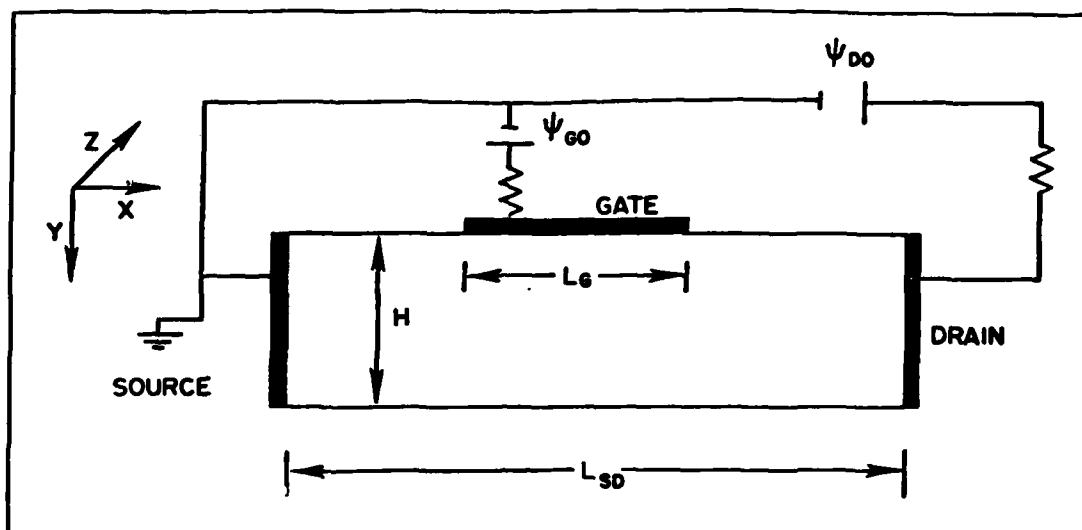
Figure 3-1. Two dimensional device circuit configuration for the small signal calculations. The semi-conductor studied was gallium arsenide with a nominal doping $N_0 = 10^{15}/CM^3$. The low doping was chosen to reduce computational time. Relevant dimensions are $L_G = 1.2\mu m$, $L_{SD} = 10\mu m$ and $H = 1.95\mu m$.
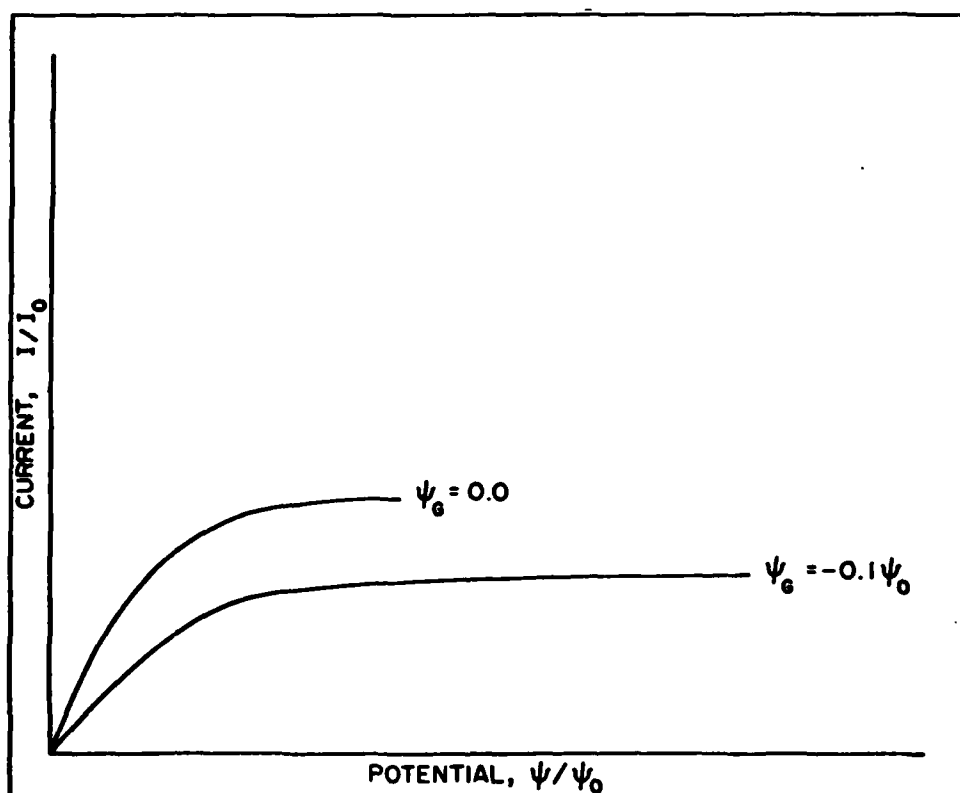
Figure 3-2. Steady state drain current versus drain potential for two values of gate bias. Here $I_0 = N_0 e V_p A$ and $\psi_0 = F_p L$, where V_p is the peak gallium arsenide carrier velocity, and F_p is the threshold field for negative differential mobility.
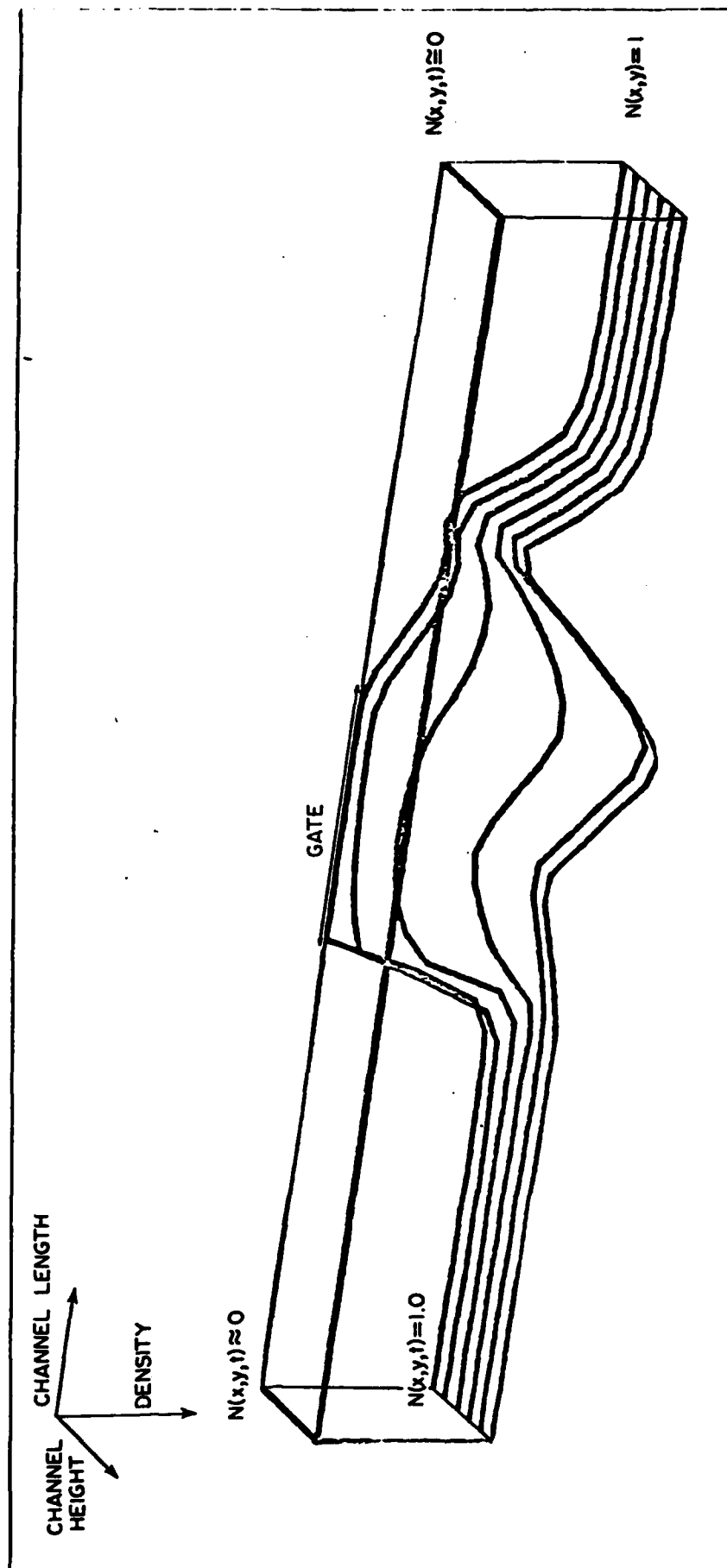
Figure 3-3. Projection of electron density within the FET. Channel height increases toward the bottom of the channel. Channel length is along a direction of increasing x. Density, which is in normalized units, increases in the downward direction. Thus at the gate the electron density is approximately equal to zero. Near the source and drain regions the electron density is approximately equal to unity. Under the gate there is an accumulation of carriers. A dipole layer has formed. For this calculation $\psi_G = 0.0$, and $\psi_D = 1.0\psi_0$.
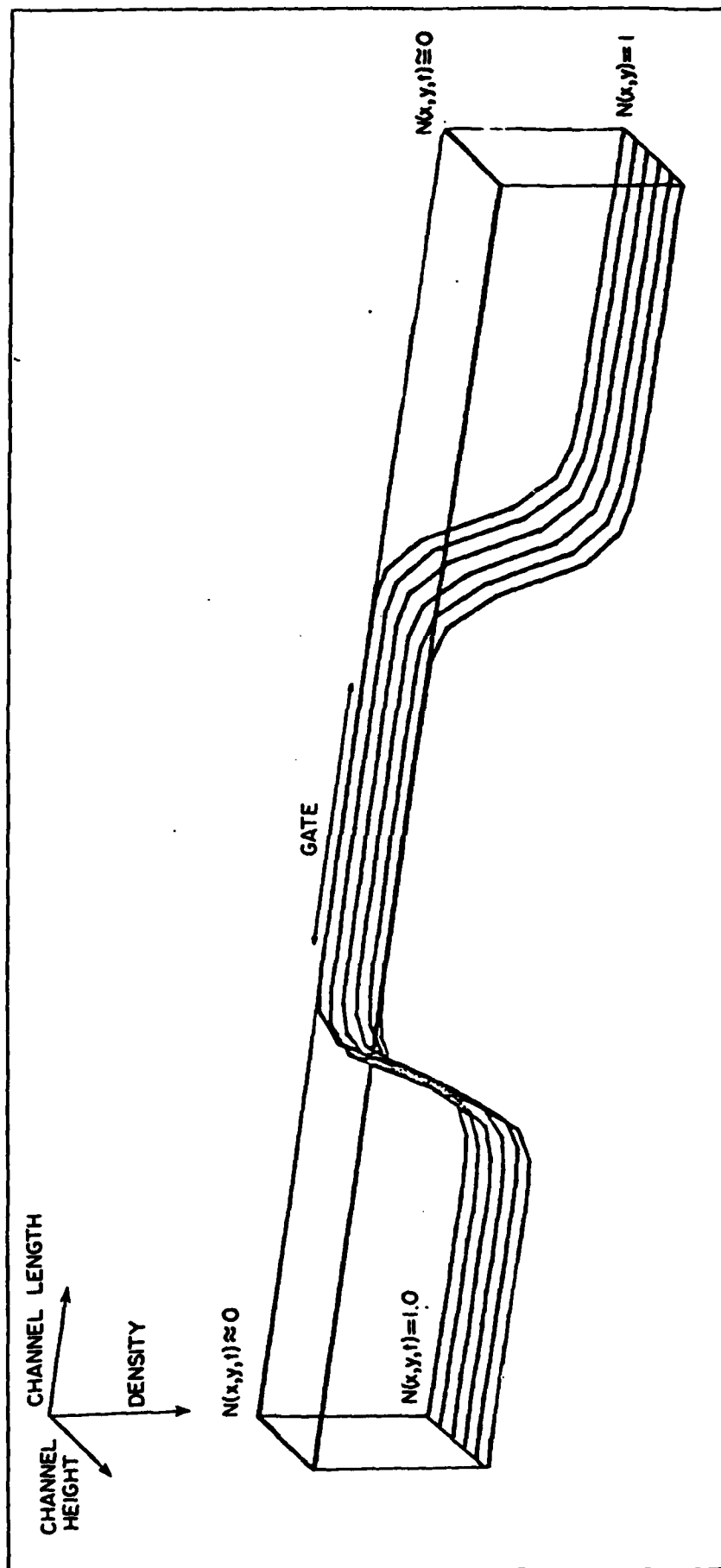
Figure 3-4. Carrier density showing a broad, almost symmetric, carrier density. For this calculation $\psi_G = -0.6\psi_0$, and $\psi_D = 0.4\psi_0$. The current density for this case is $I_D \approx 0.0$.
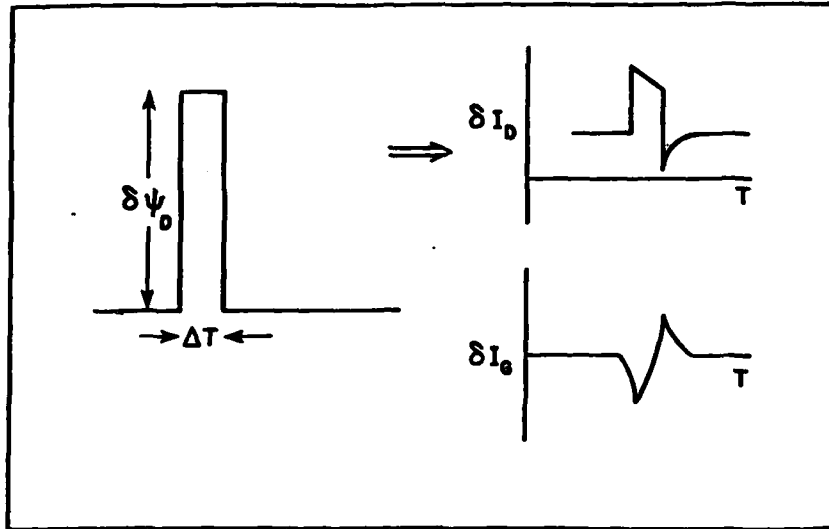
Figure 3-5. Representation of the small signal distrubance. A square wave pulse is applied to the drain contact, altering the drain contact boundary condition: $\psi_D \rightarrow \psi_D + \delta\psi_D$. There is a subsequent change in the drain and gate currents, δI_D and δI_G.
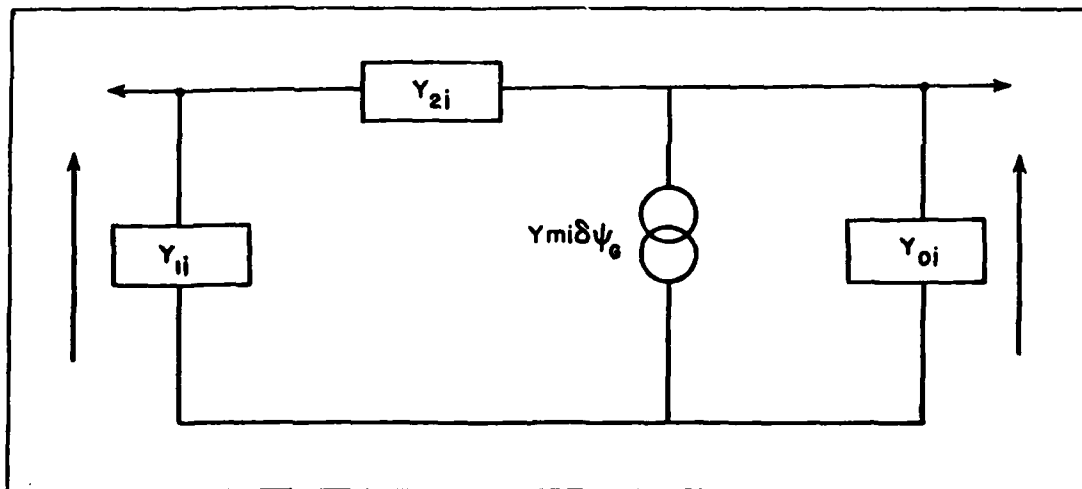
Figure 3-6 – General form of the FET intrinsic circuit model with reference to equations 3.2-11 and 3.2-12: $Y_{oi} = Y_{22} + Y_{12}$, $Y_{1i} = Y_{11} + Y_{12}$, $Y_{2i} = -Y_{12}$ and $Y_{mi} = Y_{21} - Y_{12}$. See also Cobbold (1970), figure 5.3.
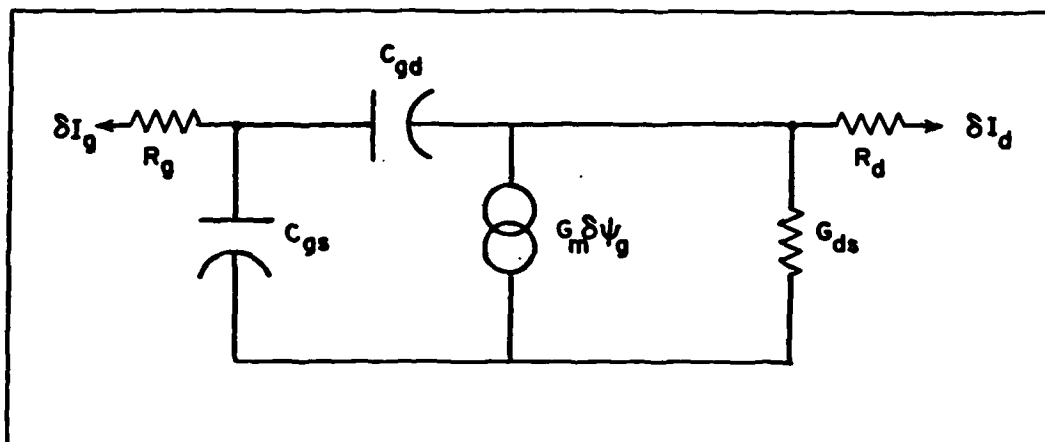
Figure 3-7 - First order equivalent circuit for the small
signal FET calculations.
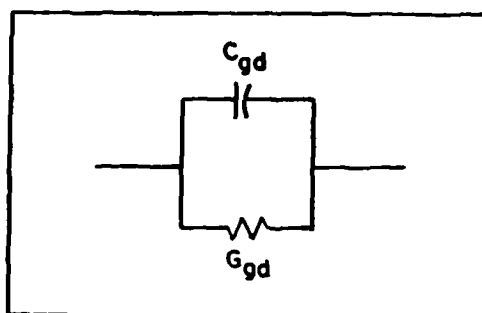
Figure 3-8 - Schematic representation of the gate-drain admittance in the presence
of a high field domain. G_{gd} represents a small signal conductance
which exhibits a frequency dependent region of negative differential
conductivity when a high field domain is present.
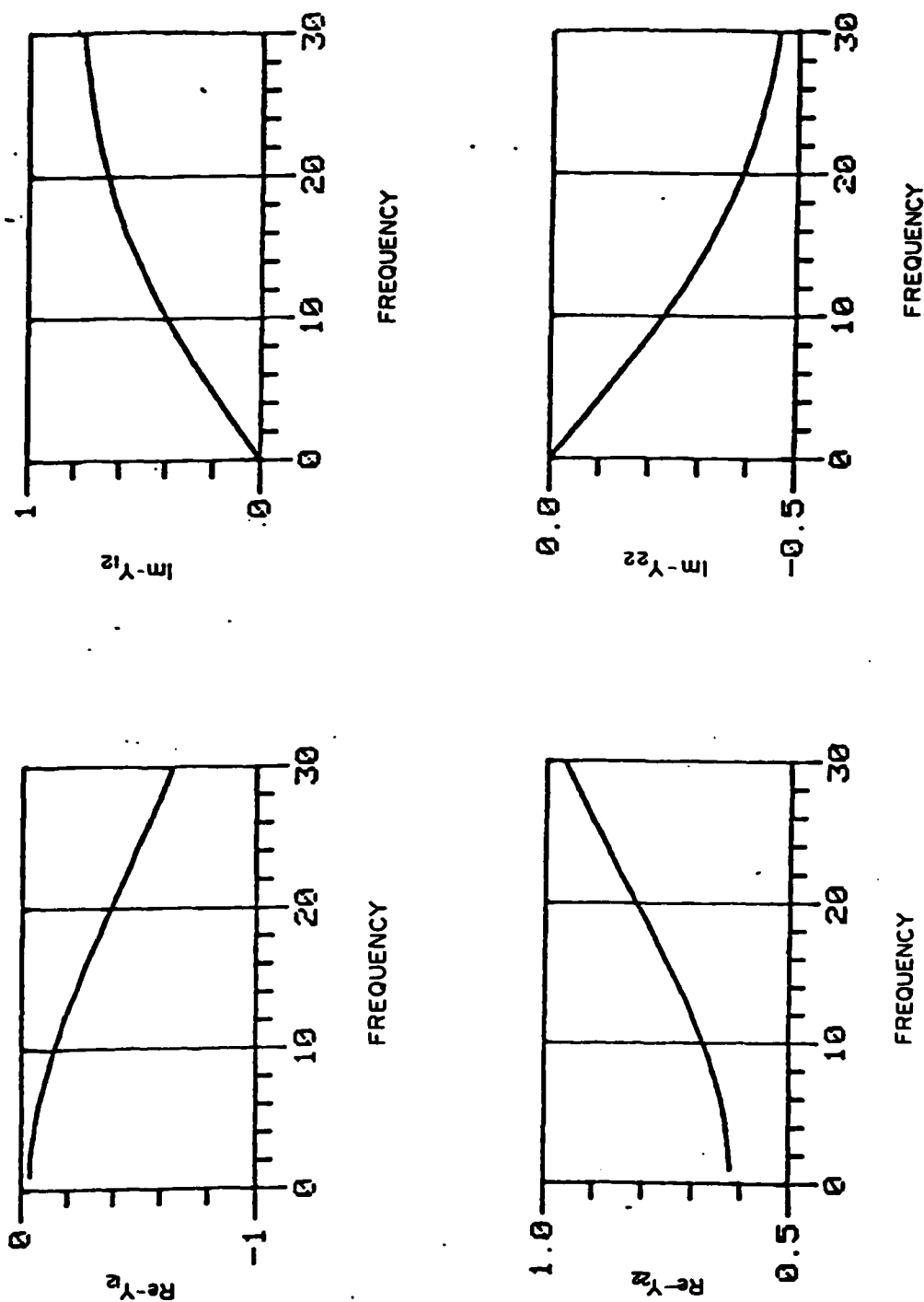
Figure 3-9a - Frequency dependent admittance parameters Y_{12} and Y_{22}, obtained by Fourier analysis of the gate and drain currents when the drain is subjected to a square wave voltage pulse. Admittance parameters are in multiples of G_o (see equation 3.2-38) and the frequency is in multiples of $f_o = 0.542$ GHz. The dc bias levels for this calculation are $V_{DO} = 0.1V_o$ and $V_{GO} = -0.1V_o$. V_o is defined in figure 3.2.

58
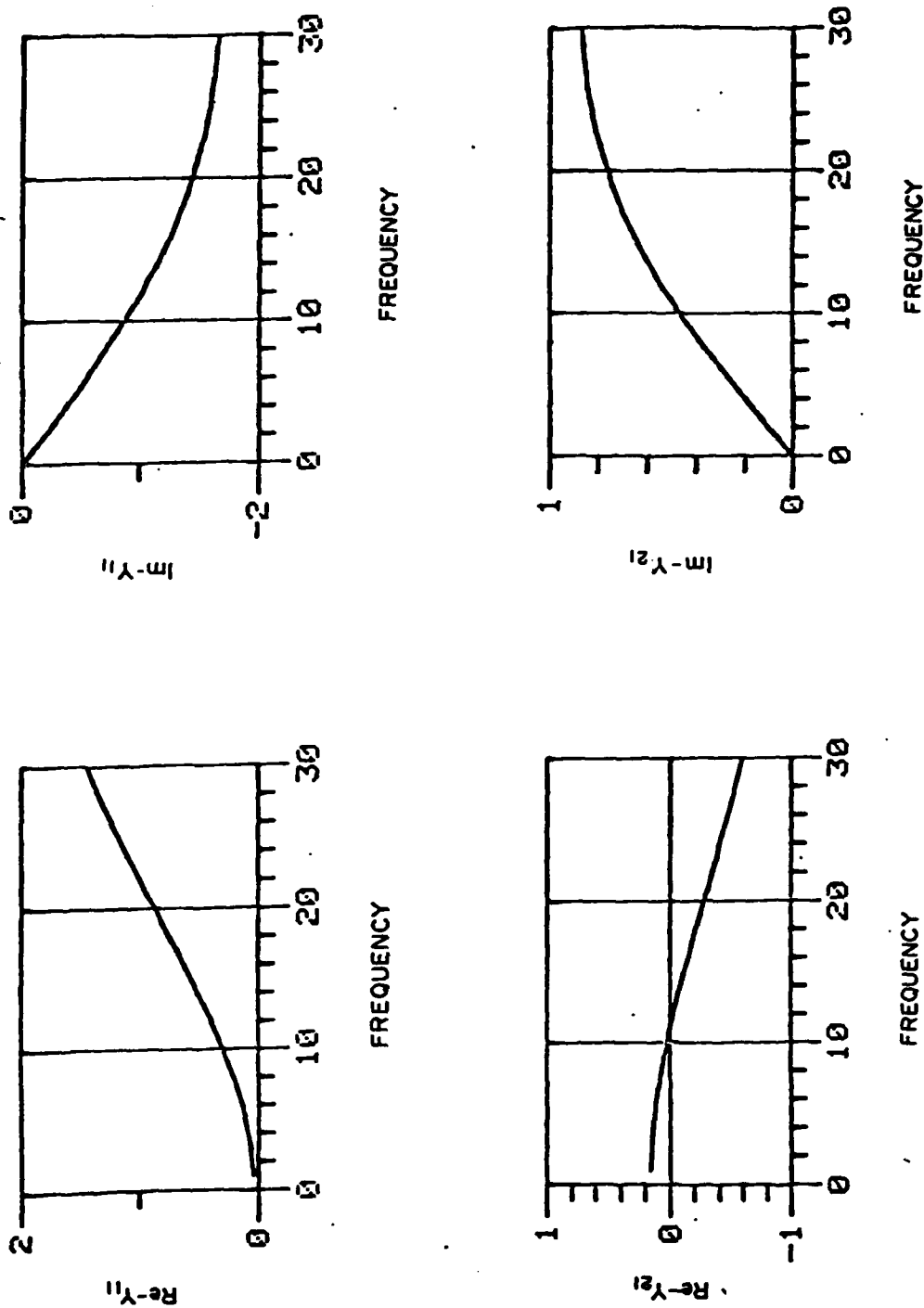
Figure 3.9b – Frequency dependent admittance Y_{11} and Y_{21} obtained by Fourier analysis of gate and drain currents, when the gate is subjected to a square wave pulse.
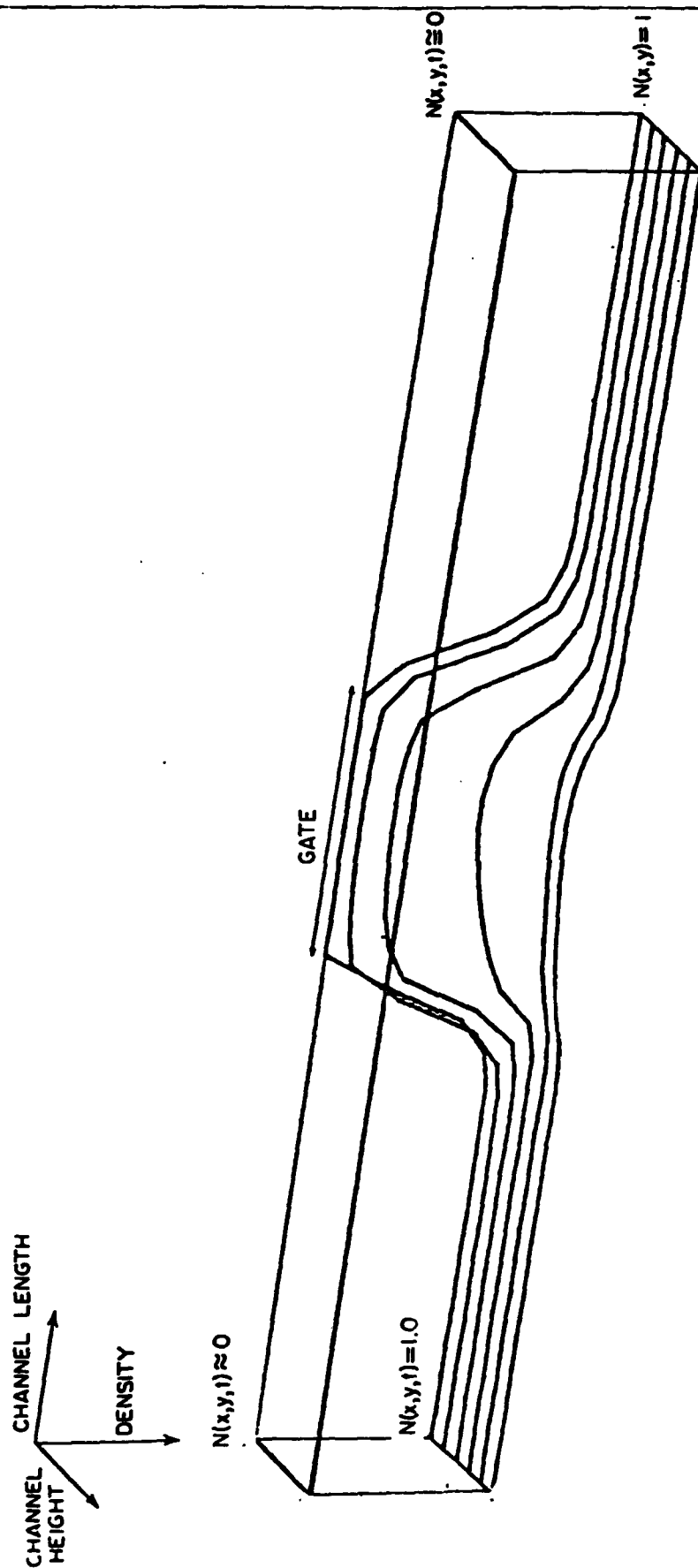
Figure 3.9c - Projection of steady state electron density for this bias level.
See figure 3.3 for a discussion of projection characteristics.
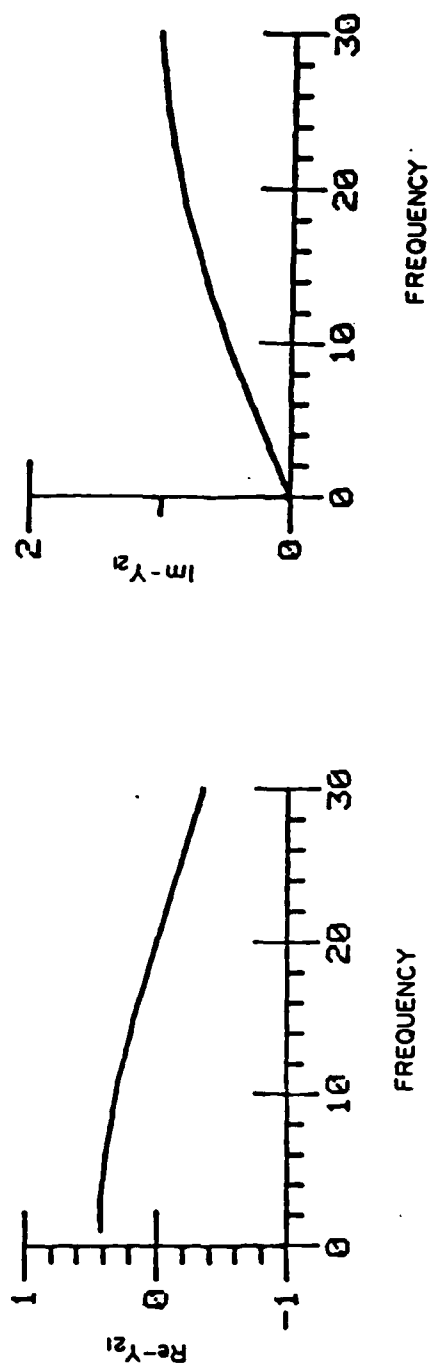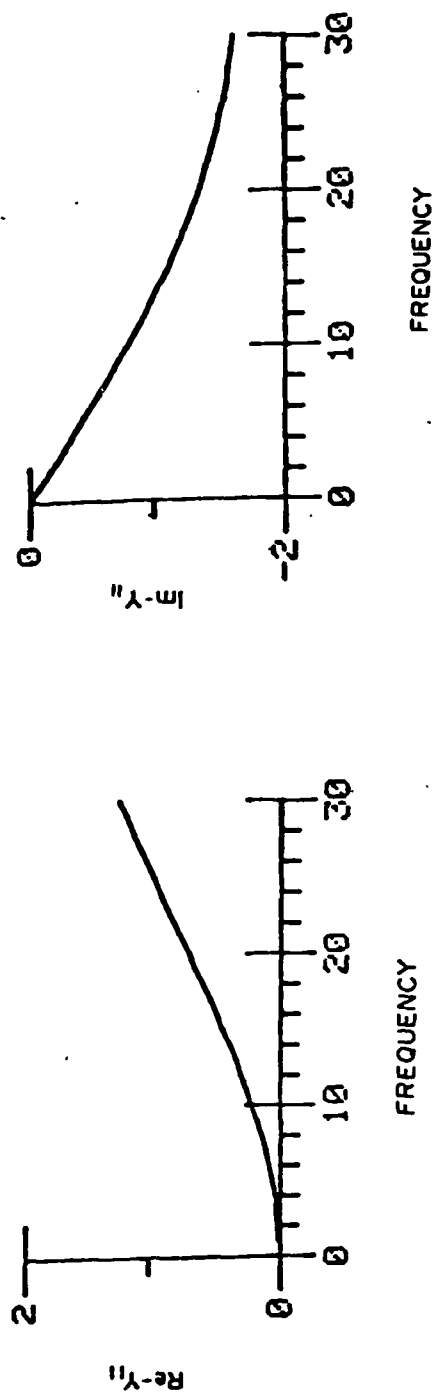
Figure 3-10a, b and c - As in figure 3-9, but for $\Psi_{DO} = 0.25\Psi_0$ and $\Psi_{GO} = 0.1\Psi_{GO}$.

Fig. 3-10 b.

Y - PARAMETERS

ELECTRON DENSITY

Fig. 3-10c:

$N(x,y,1) \cong 0$

$N(x,y) = 1$

GATE

CHANNEL LENGTH

DENSITY

CHANNEL HEIGHT

$N(x,y,1) \approx 0$

$N(x,y,1) = 1.0$
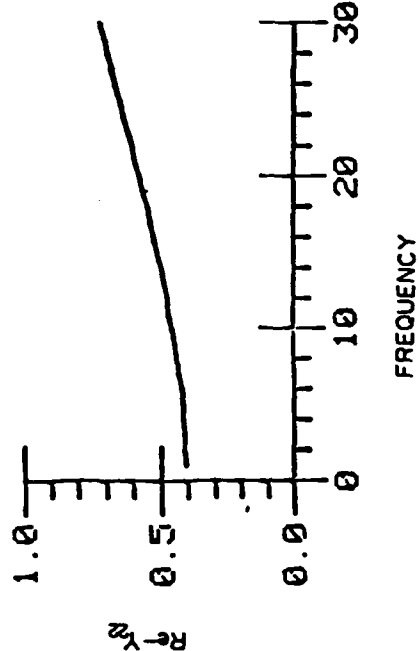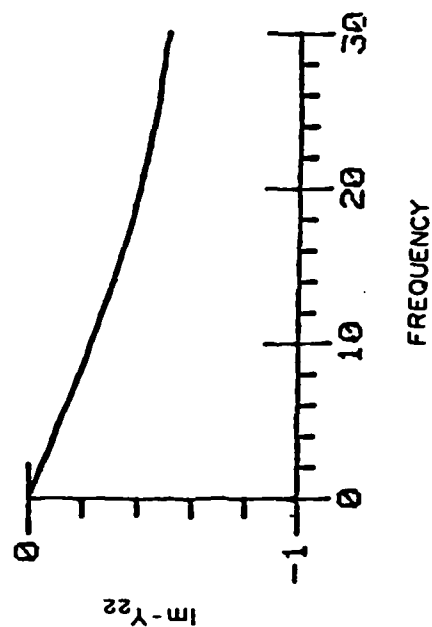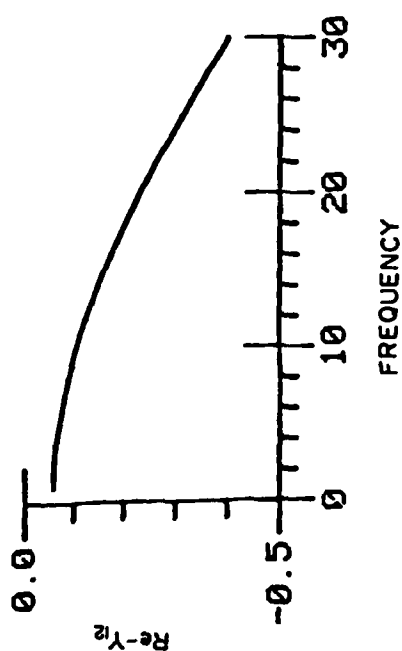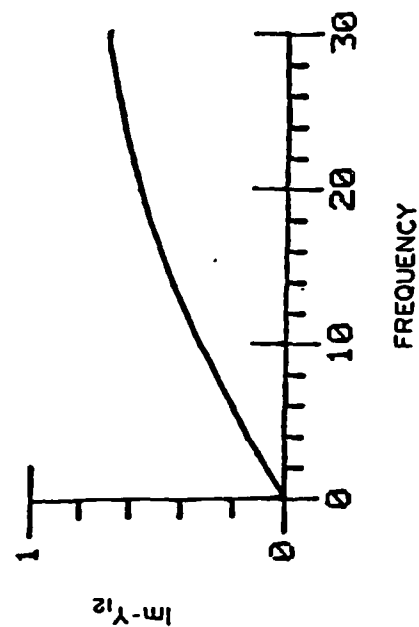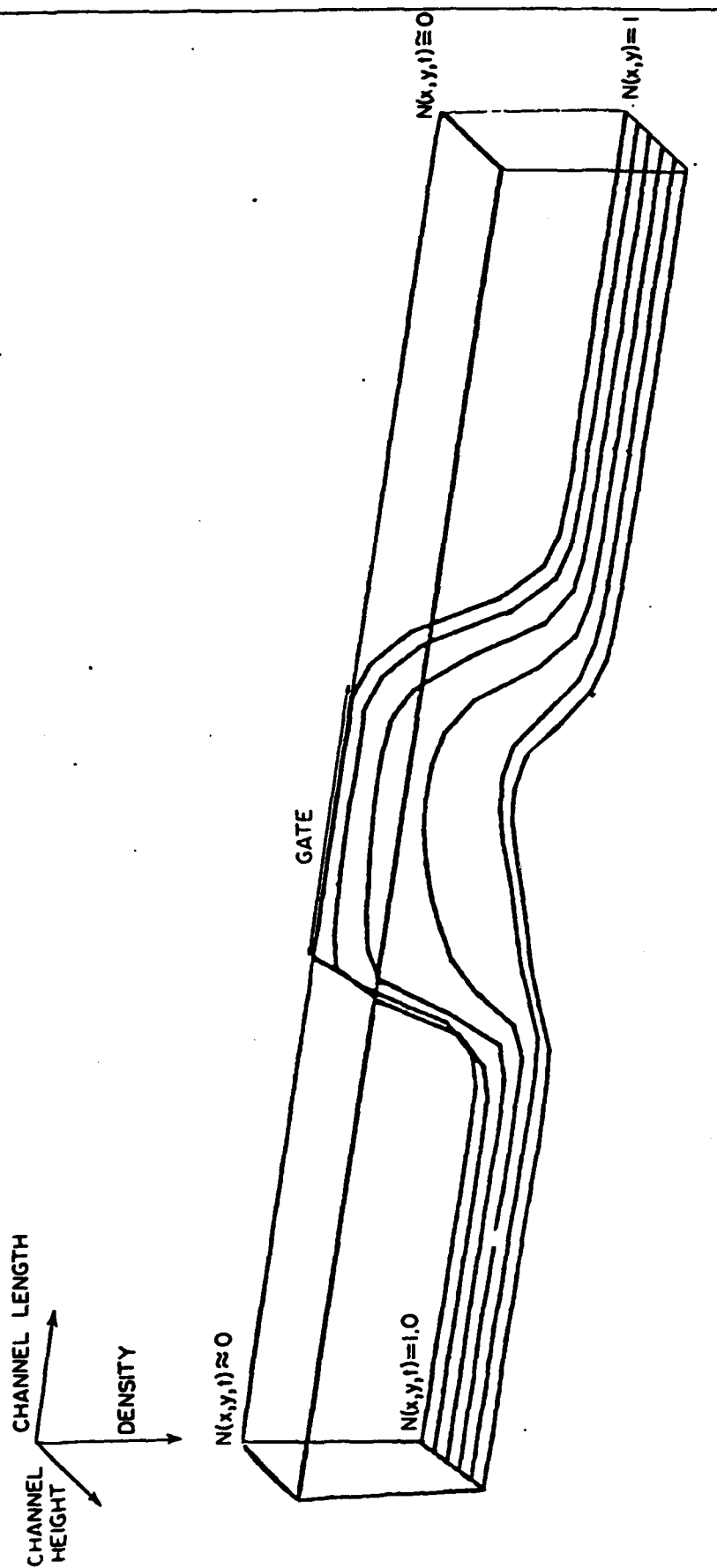
Fig. 3-11a.

Y - PARAMETERS
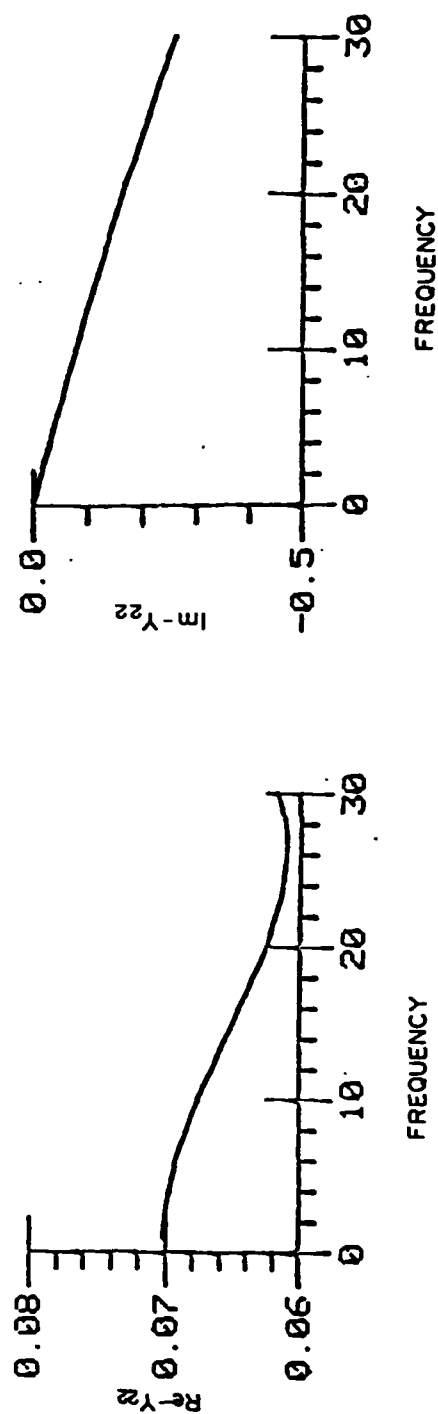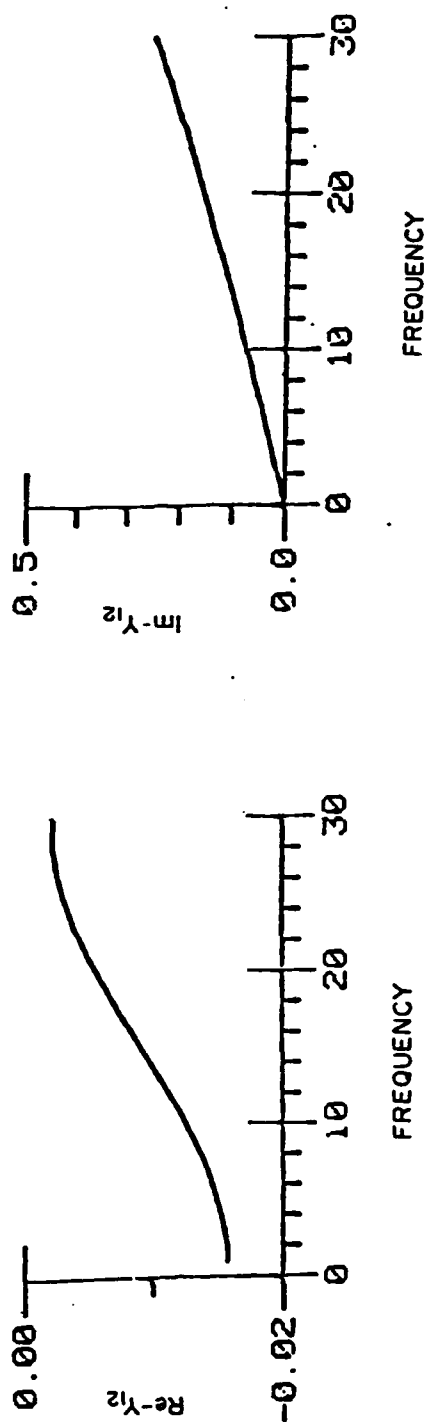
Figure 3-11a, b and c - As in figure 3-9, but for $\Psi_{DO} = 0.5\Psi_O$ and $\Psi_{GO} = 0.1\Psi_O$.

64

Fig. 3-11b.

Y - PARAMETERS

Fig. 3-11c.

ELECTRON DENSITY

CHANNEL LENGTH

CHANNEL HEIGHT

DENSITY

$N(x,y,1) \approx 0$

$N(x,y,1) = 1.0$

GATE

$N(x,y,1) \cong 0$

$N(x,y) = 1$

Fig. 3-12a.

Y – PARAMETERS

FREQUENCY

FREQUENCY

FREQUENCY

FREQUENCY

Im-Y_{12}

Im-Y_{22}

Re-Y_{12}

Re-Y_{22}
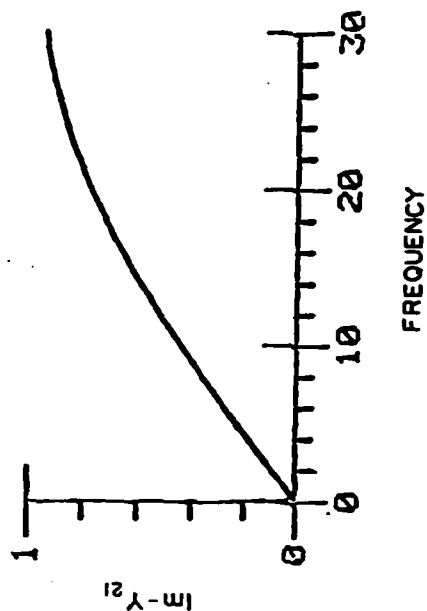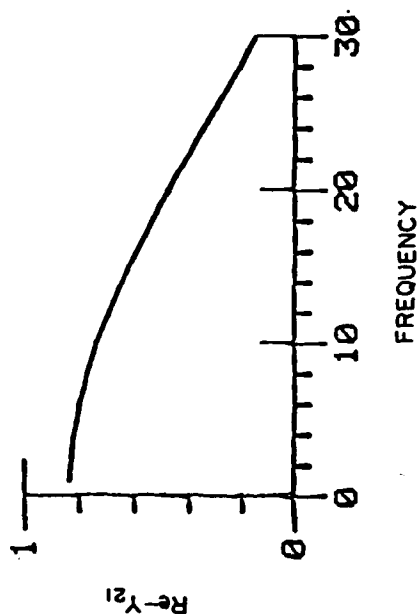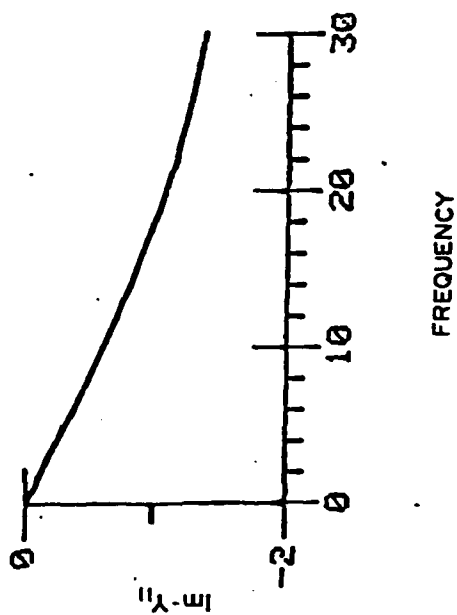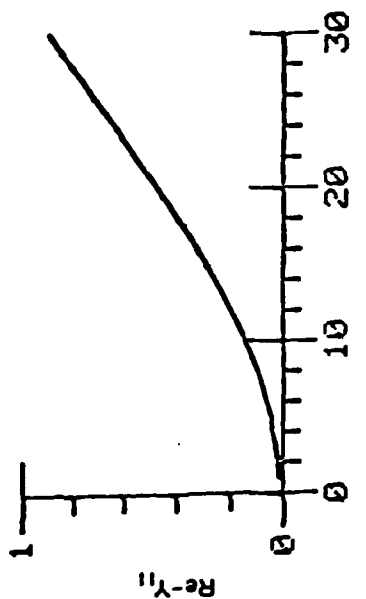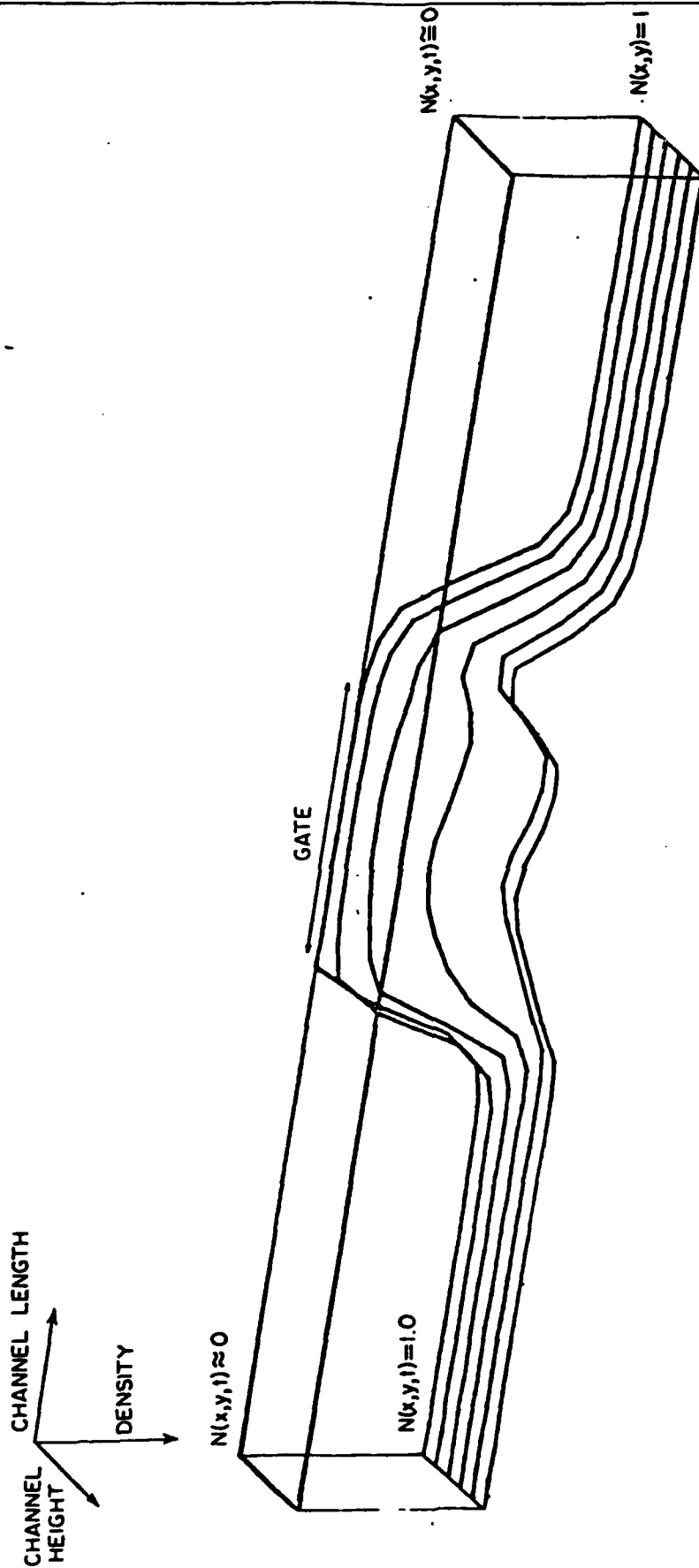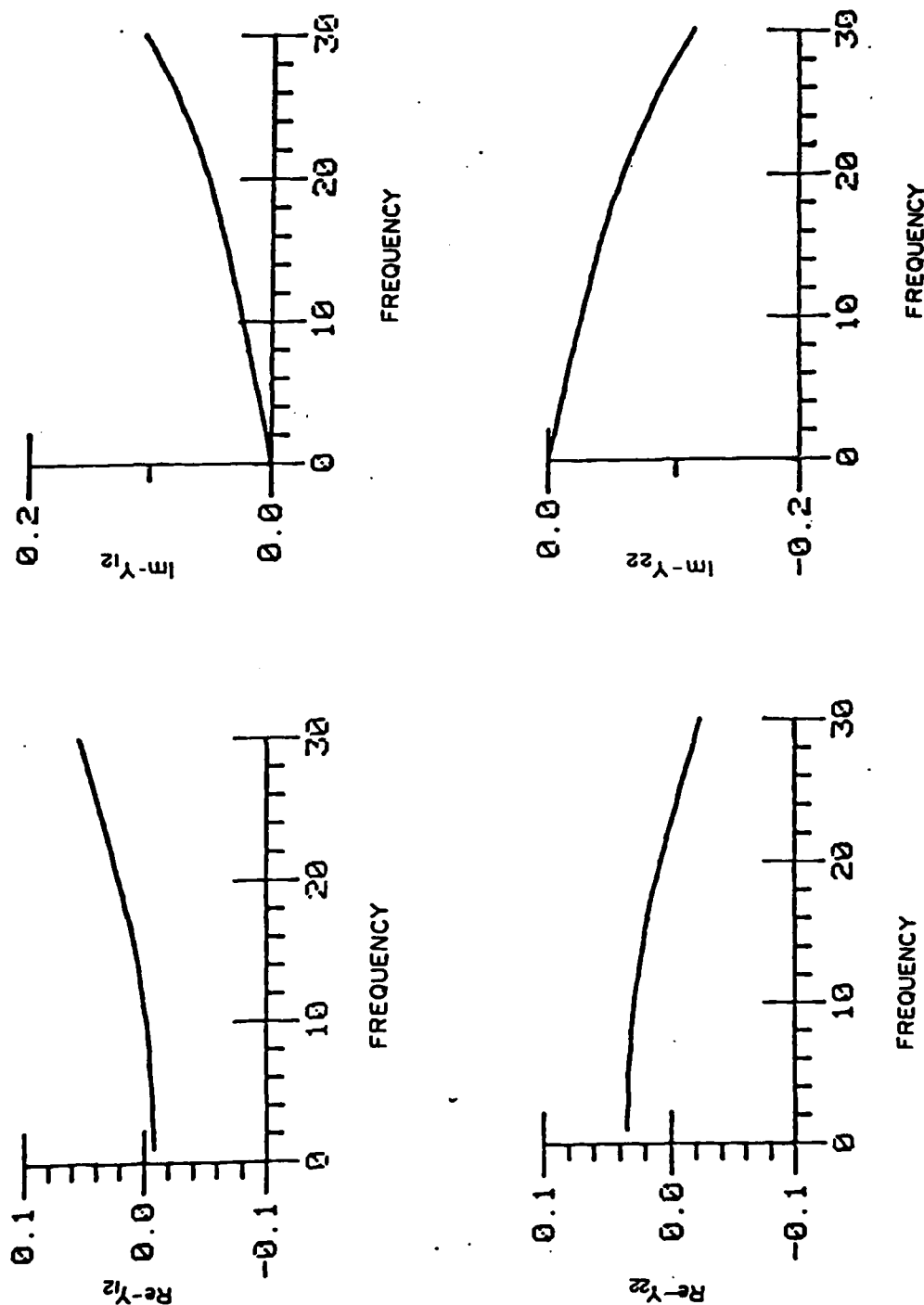
Figure 3-12a, b and c – As in figure 3-9, but for Y_{DO} = 1.0Y_{o} and Y_{GO} = -0.1Y_{o}.

67

Fig. 3-12b.

Y – PARAMETERS
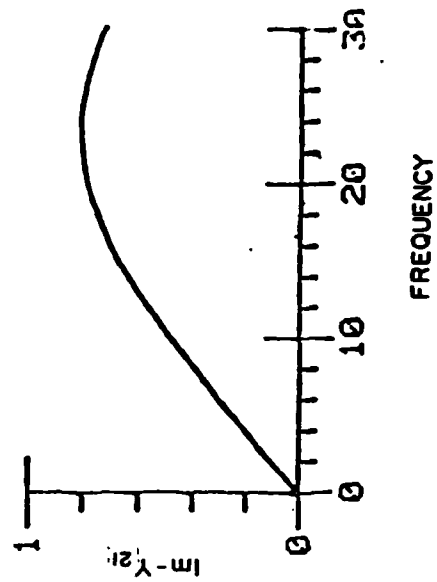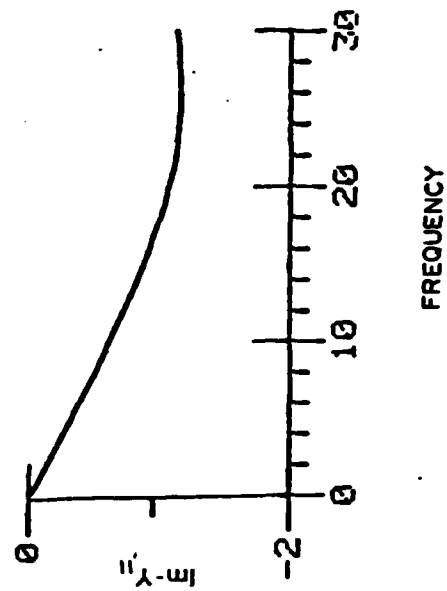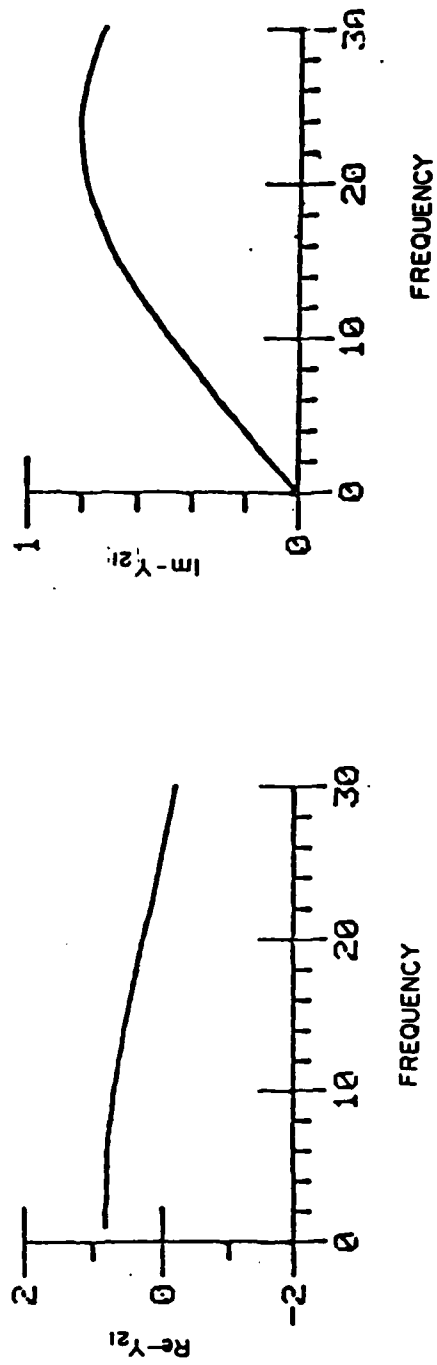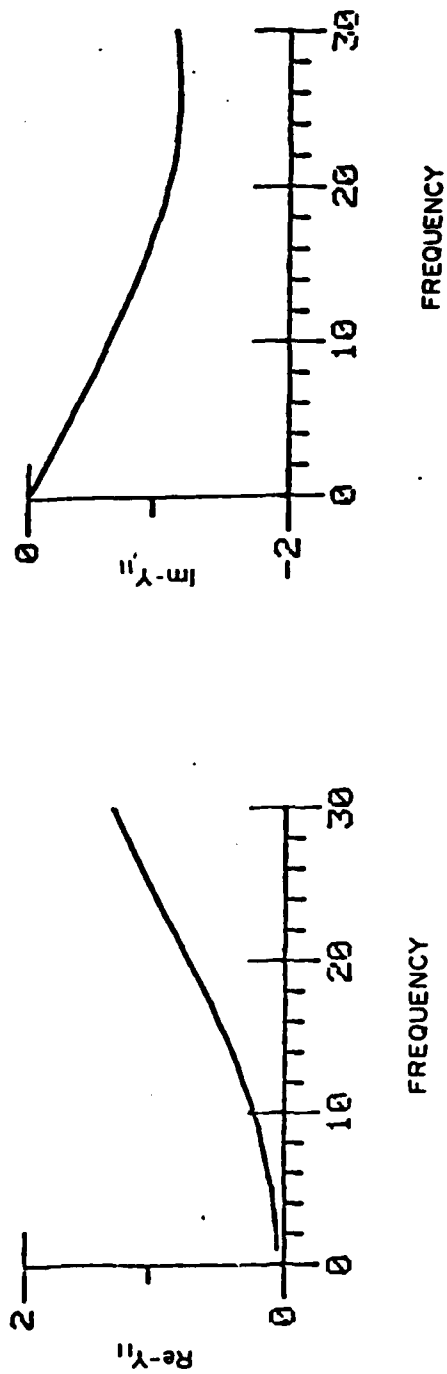
Fig. 3-12c.

ELECTRON DENSITY

GATE

CHANNEL LENGTH

DENSITY

CHANNEL HEIGHT

$N(x,y,1) \cong 0$

$N(x,y,1) = 1$

$N(x,y,1) \approx 0$

$N(x,y,1) = 1.0$

69
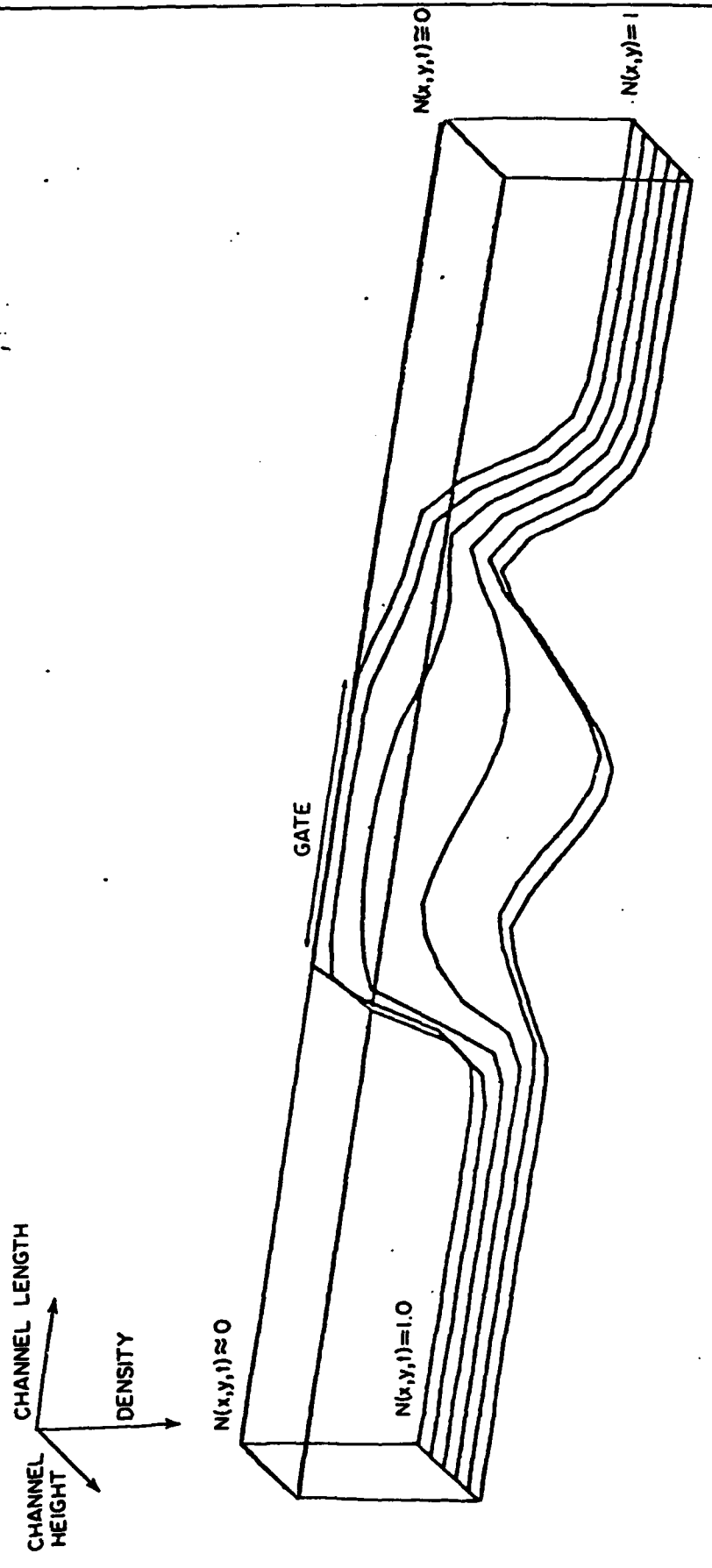
Fig. 3-13a.
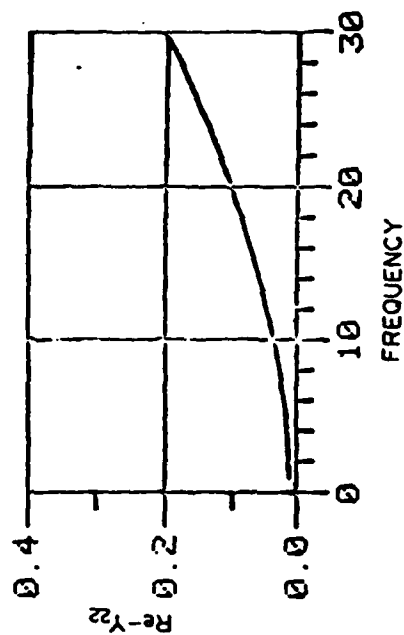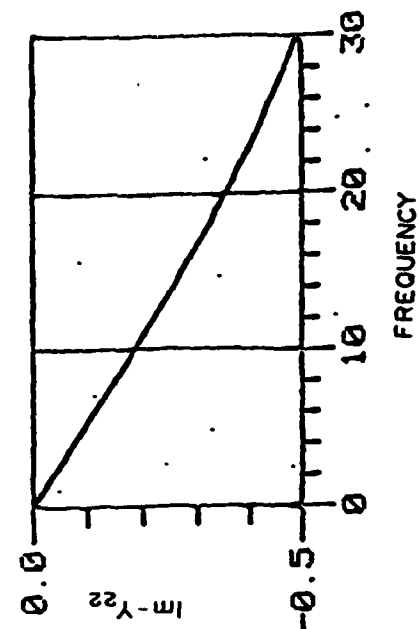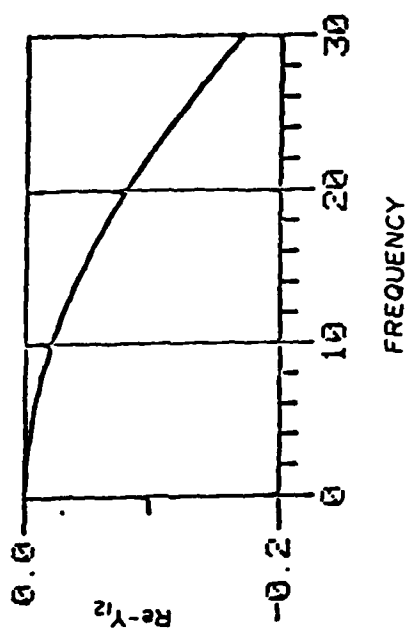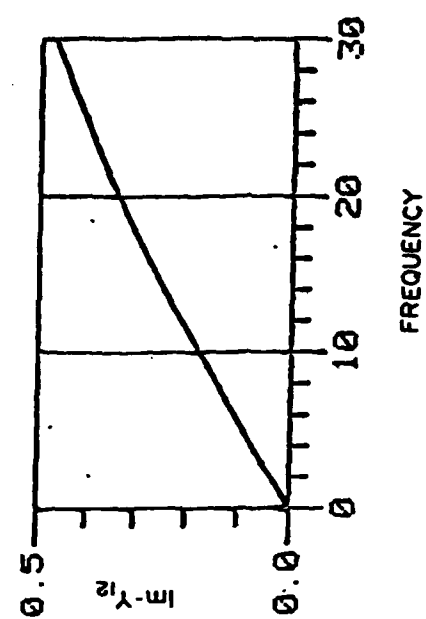
Y - PARAMETERS

Figure 3-13a, b and c - As in figure 3-9, but with $Y_{DO} = 0.1Y_o$ and $Y_{GO} = -0.4Y_o$.

Fig. 3-13b.

Y - PARAMETERS

71

ELECTRON DENSITY

Fig. 3-13 c.

72

Figure 3-14a, b and c - As in figure 3-9, but for $V_{DO} = 0.1V_o$.

73
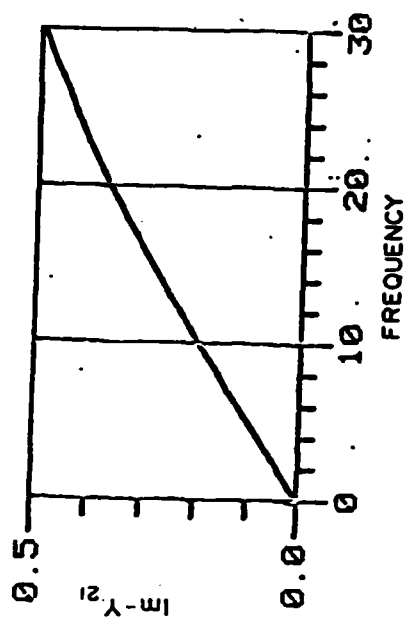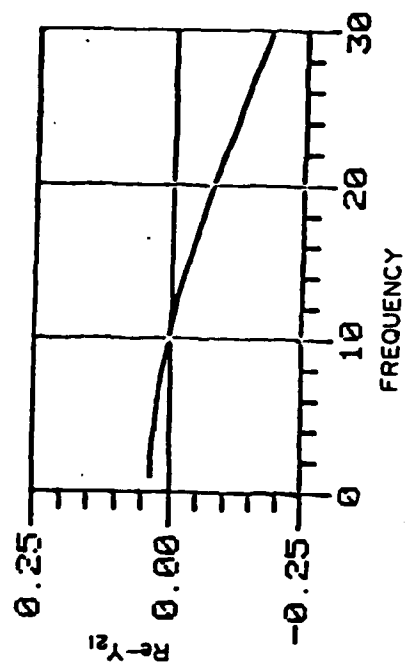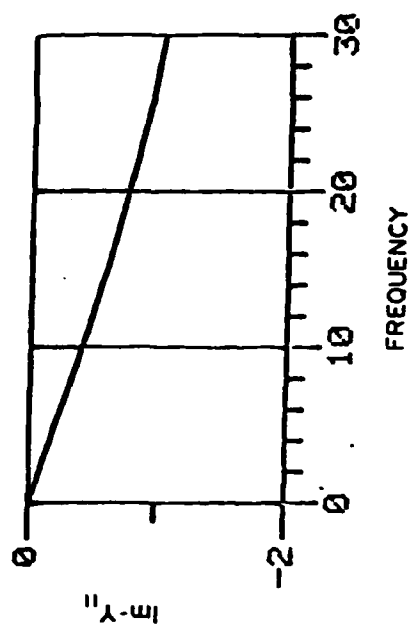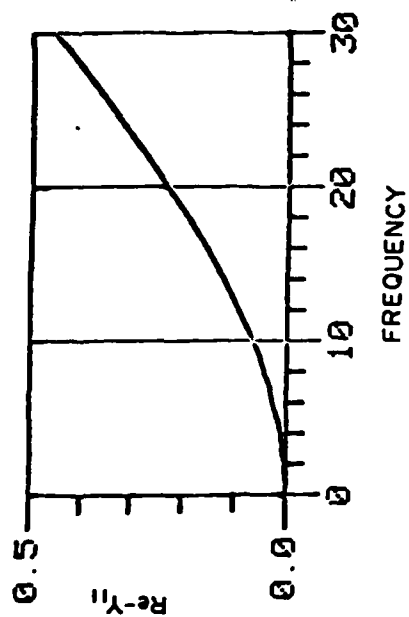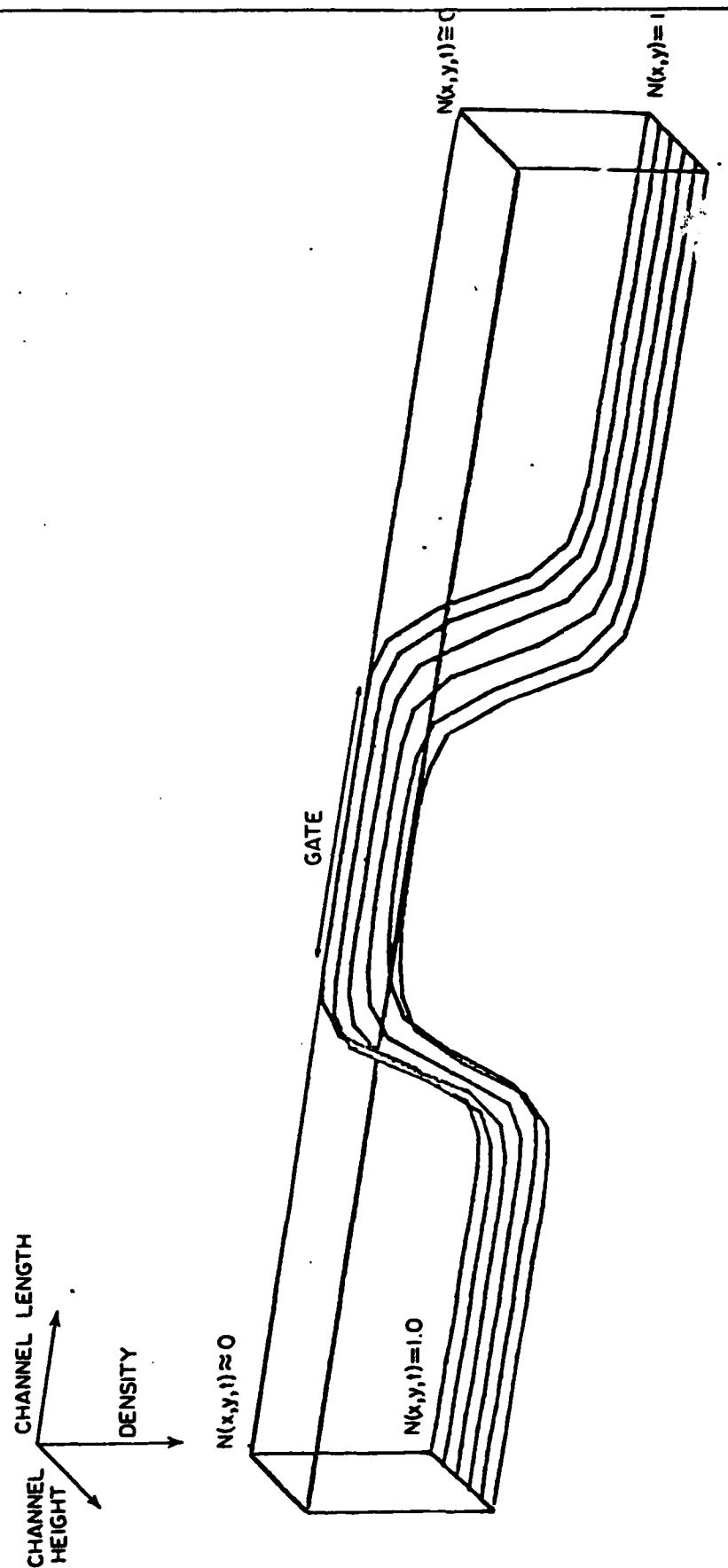
Fig. 3-14b.

Y - PARAMETERS
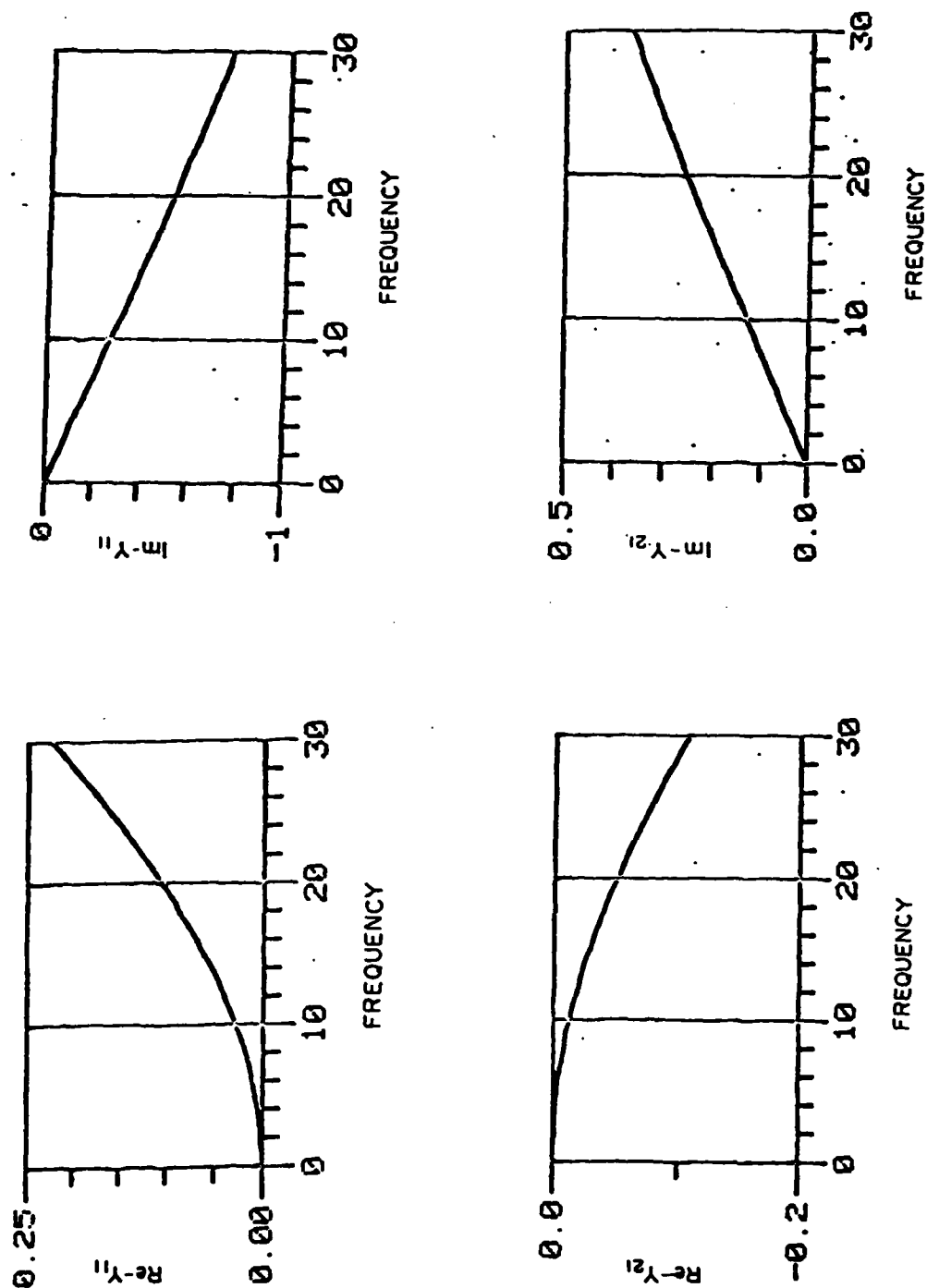
Fig. 3-14c.

ELECTRON DENSITY

CHANNEL LENGTH

CHANNEL HEIGHT

DENSITY

$N(x,y,1) \approx 0$

$N(x,y,1) = 1.0$

GATE

$N(x,y,1) \cong 0$

$N(x,y)=1$

75
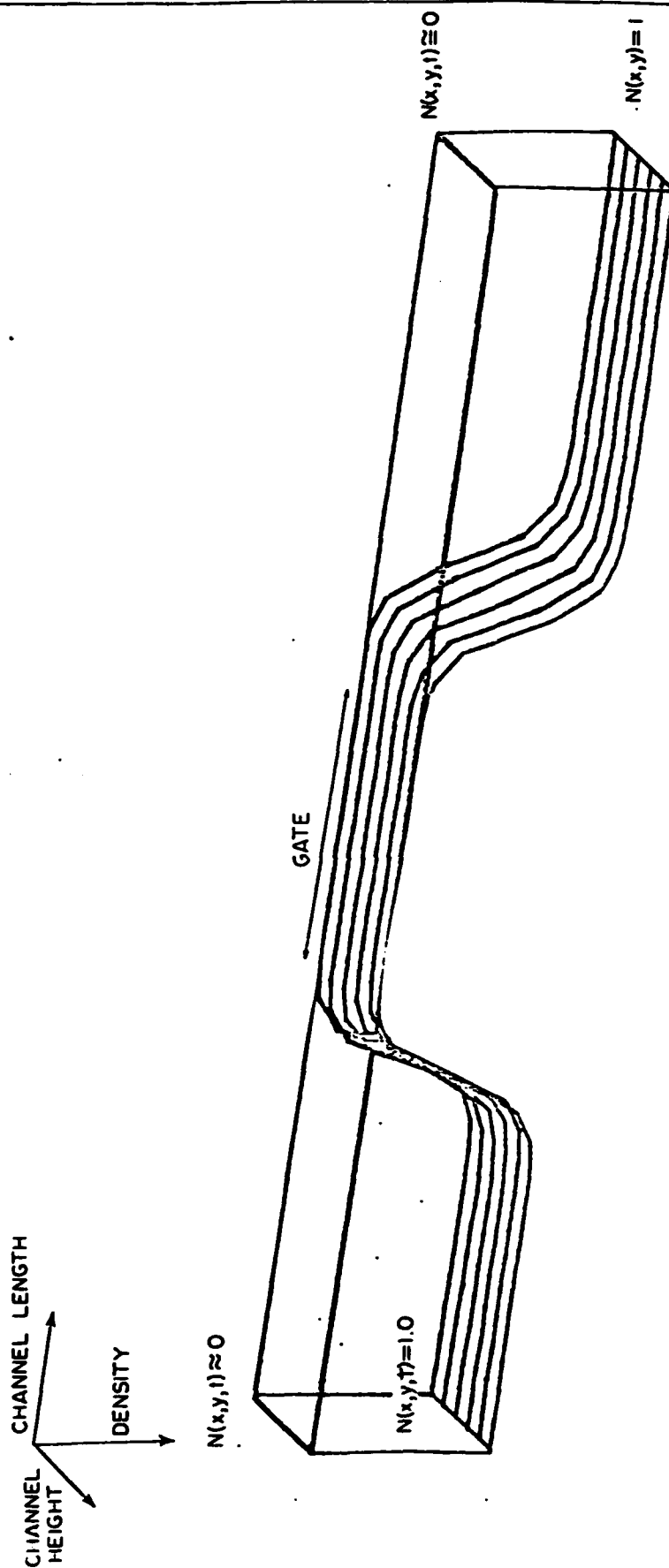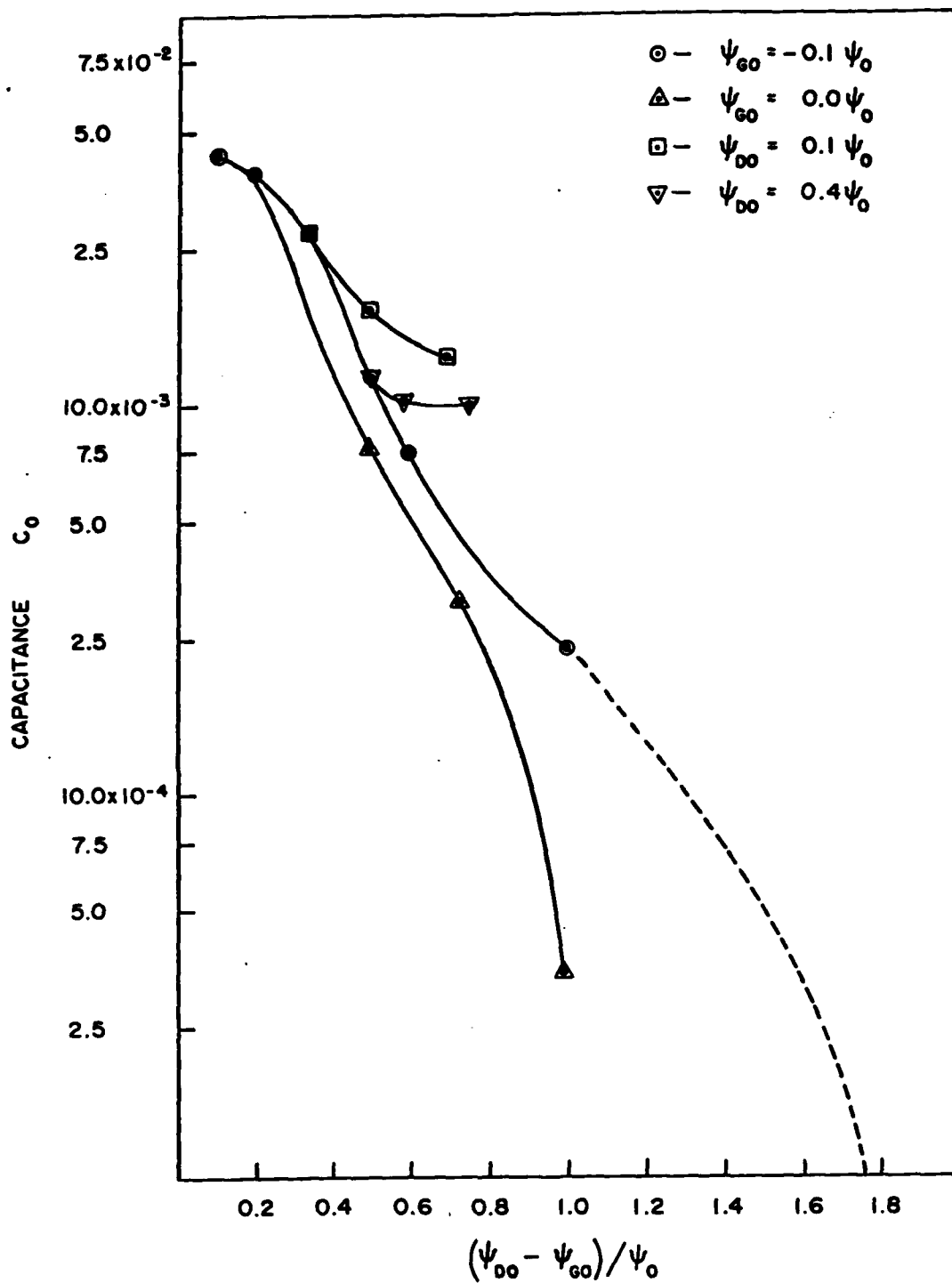
Figure 3-15 – Gate to drain capacitance versus $(\Psi_{DO} - \Psi_{GO})/\Psi_o$. Circular and triangular results are for a fixed gate bias. Square and inverted triangular data are for a fixed drain bias. For this calculation $C_o = 3.25 \times 10^2 \, \varepsilon HW/L$.
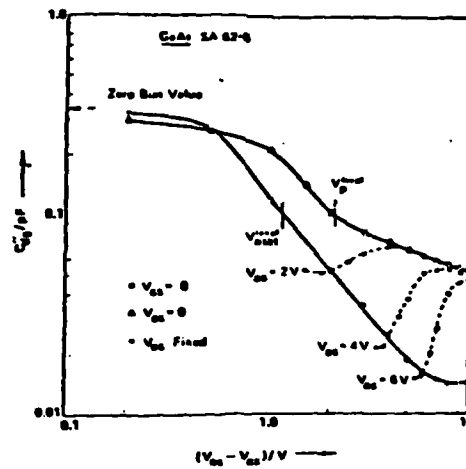
Figure 3-16 - Experimental measurement of C_{gd} versus bias. From Englemann, et al (1977).
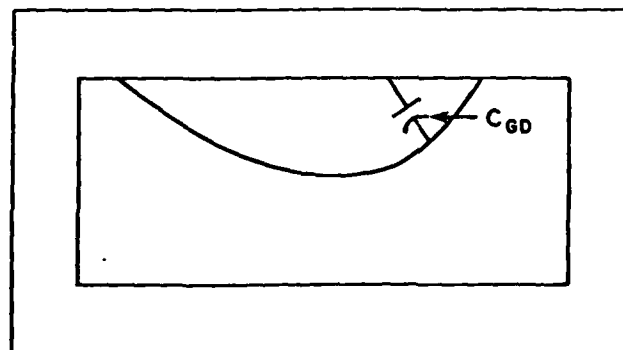
Figure 3-17 - Schematic of the gate-to-drain capacitance as a measure of the change in channel depletion charge resulting from changes in drain bias.
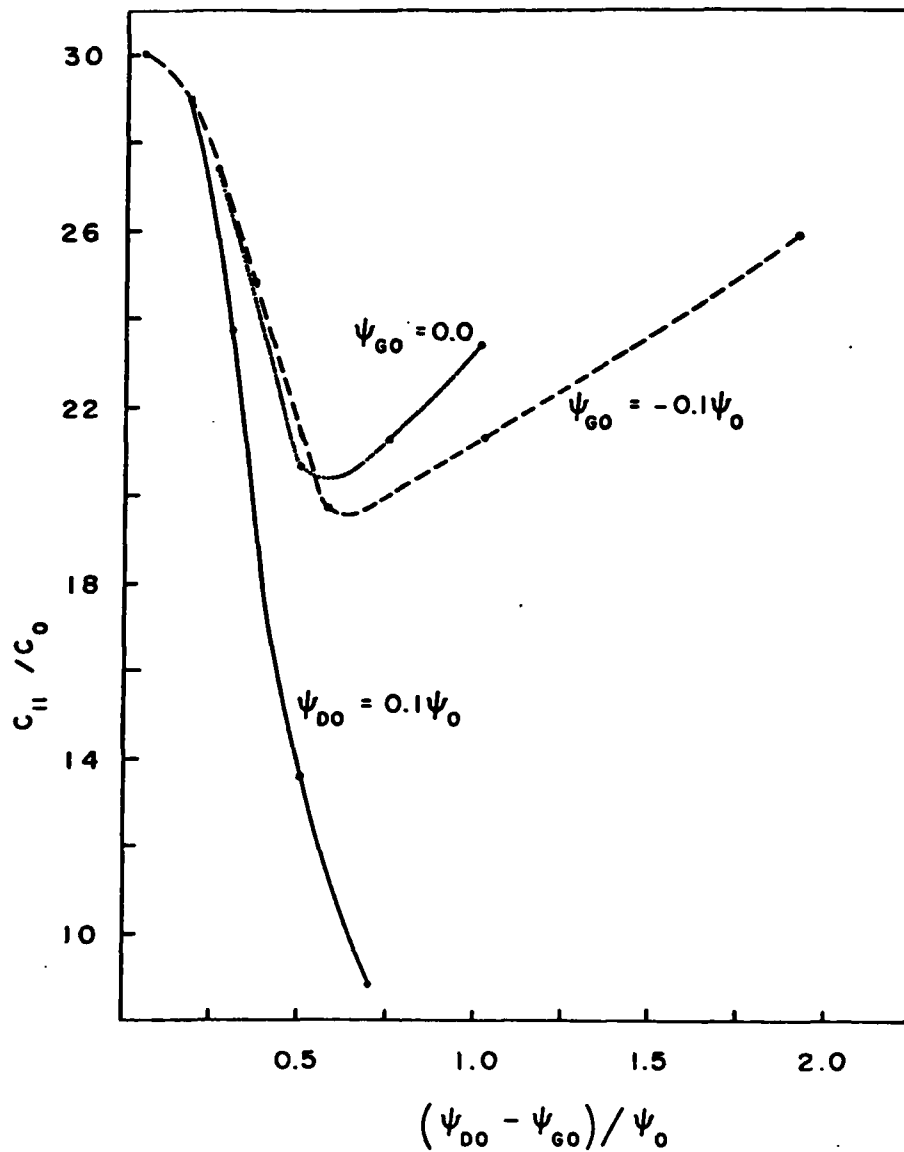
Figure 3-18 - Capacitance C_{11} (see equation 3.2-41) versus $(\Psi_{DO} - \Psi_{GO})/\Psi_o$. For this calculation $C_o = \epsilon HW/L$. Note $C_{11} \doteq C_{gs} + C_{gd}$.
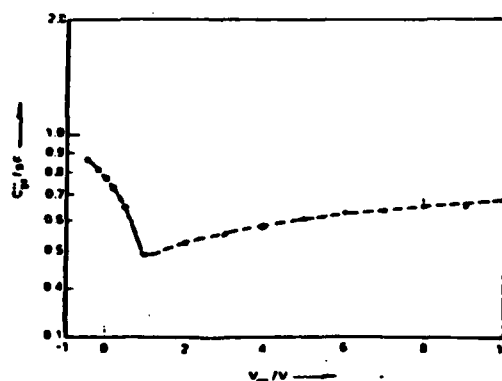
Figure 3-19 - Experimental measurements of the gate-drain capacitance. From Englemann, et al (1977).
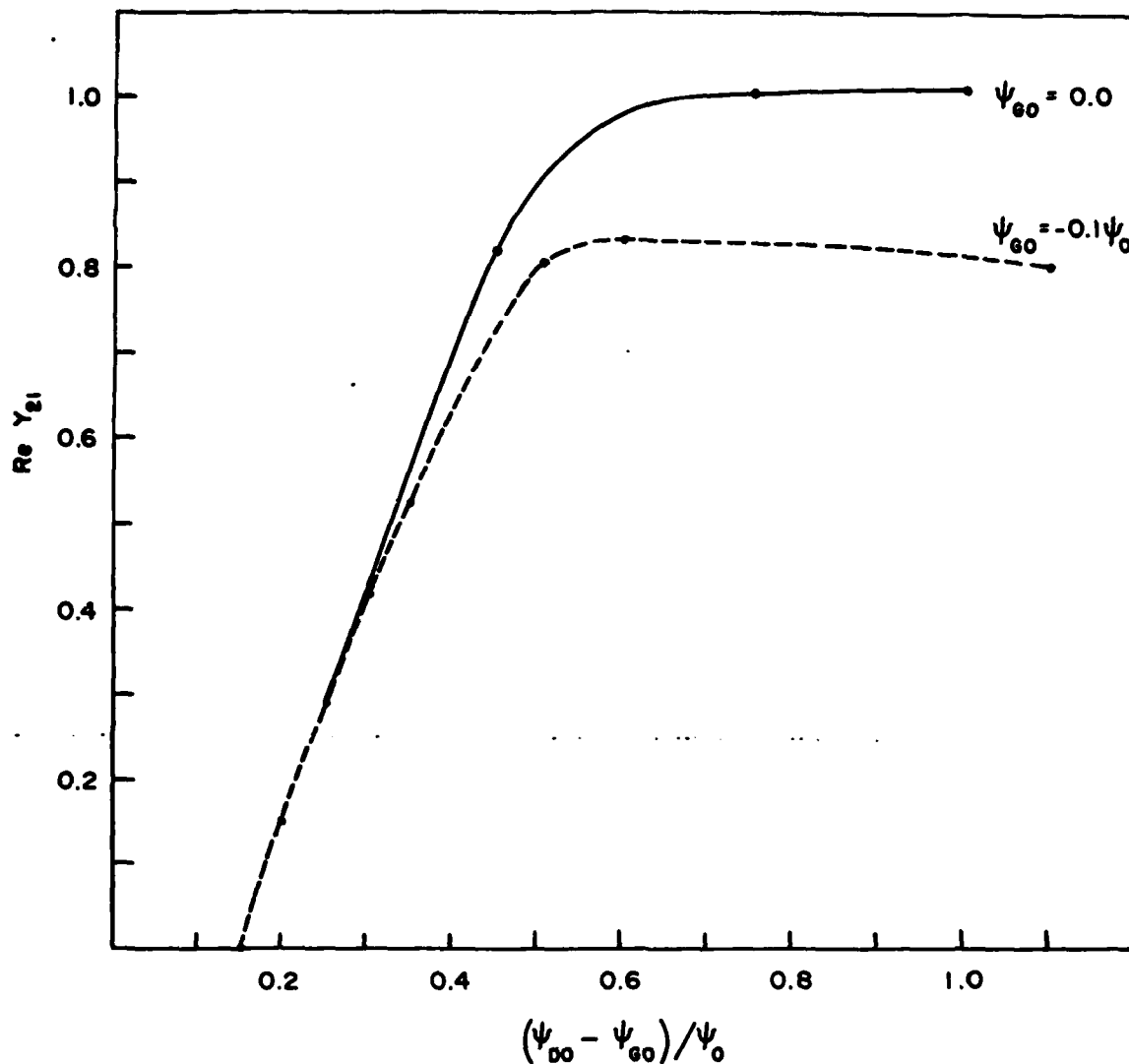
Figure 3-20 - Re Y_{21} (in multiples of G_o) versus $(\Psi_{DO} - \Psi_{GO})/\Psi_o$. There is saturation at high bias levels. The slight decrease in transconductance at high bias levels for $\Psi_{GO} = -0.1\Psi_o$ may be a numerical artifact. It is being studied.
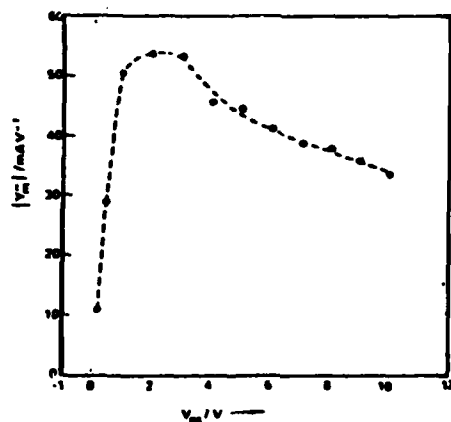
Figure 3-21 - Experimental measurement of transconductance versus drain bias. From Englemann, et al (1977).
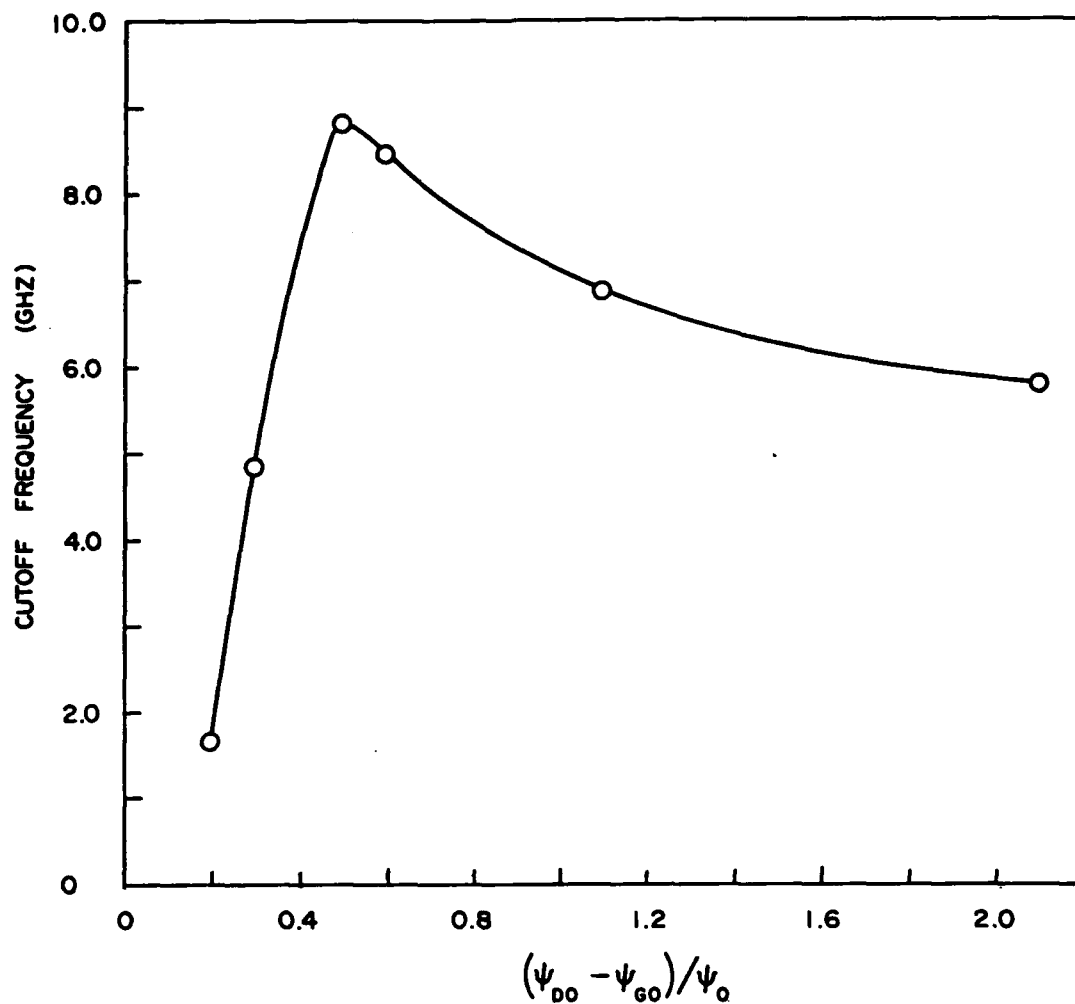
Figure 3-22 - Cutoff frequency versus $(\Psi_{DO} - \Psi_{GO})/\Psi_o$ for $\Psi_{GO} = -0.1\Psi_o$.
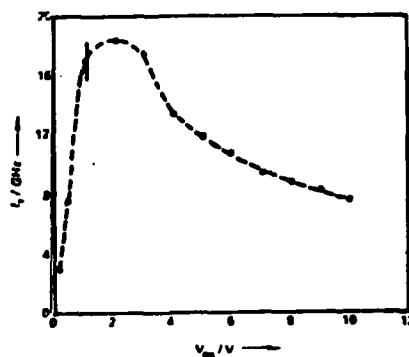
Figure 3-23 - Experimental measurements of the cutoff frequency versus $(\Psi_{DO} - \Psi_{GO})/\Psi_o$. From Englemann, et al (1977).
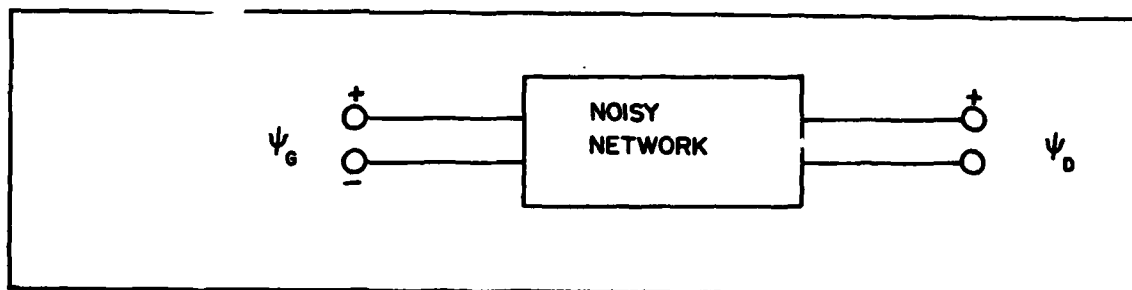
Figure 3-24 - Circuit representation of an FET with noise.
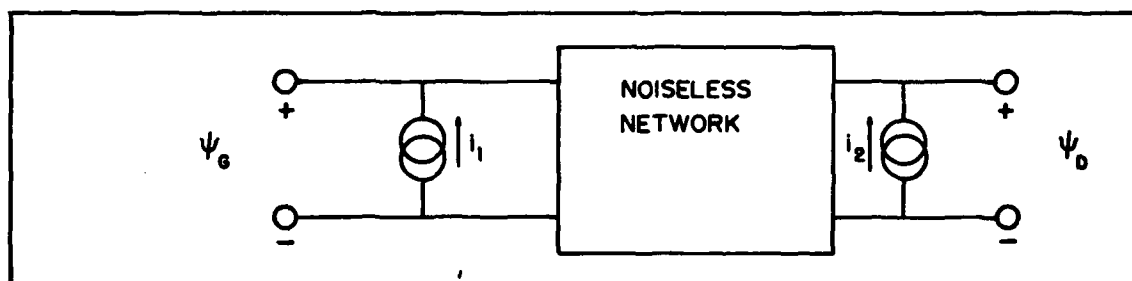
Figure 3-25 - Circuit representation of a noisy FET as a noiseless network with two noise sources. [See, e.g., Talpey (1959)].

81
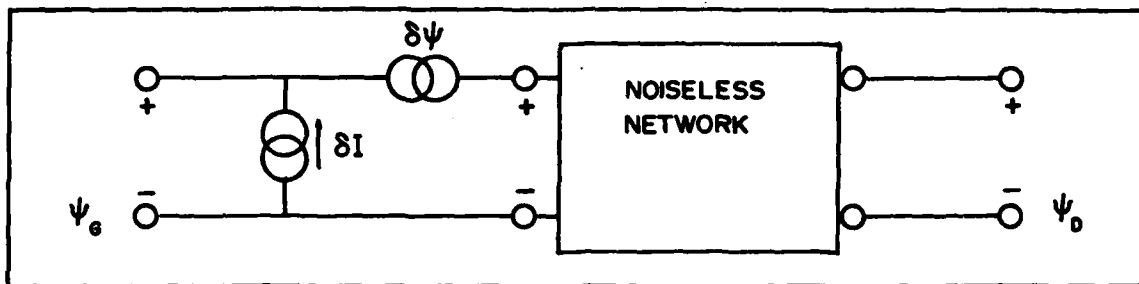
Figure 3-26 - Circuit representation of a noisy FET as a noiseless network with a voltage and current source. [See Talpey (1959)].
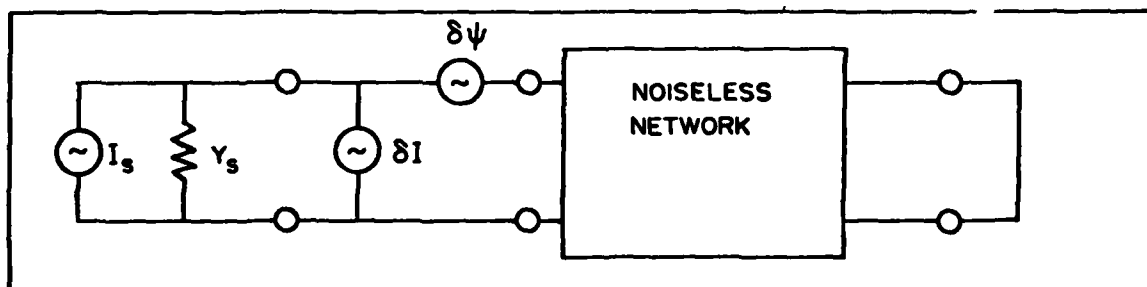
Figure 3-27 - As in figure 3-26, but with signal noise source. [From Talpey (1959)].
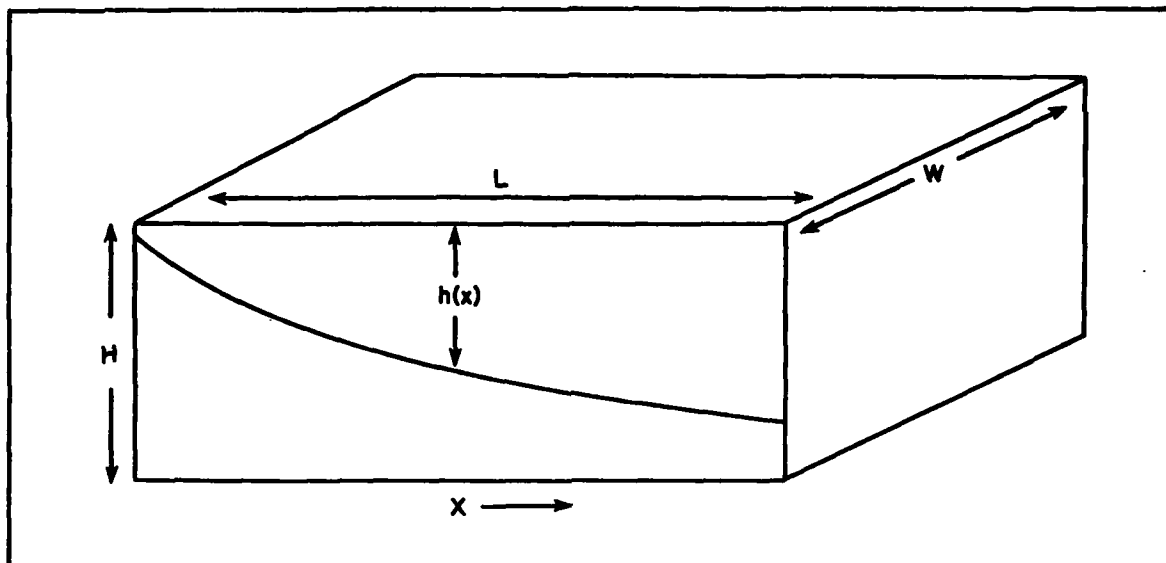
Figure 3-28 – Structure of FET and definitions of variables used in gradual
channel approximation steady.

4. Thermal Variations in Semiconductor Devices

4.1 Introduction

When a material such as gallium arsenide or indium phosphide is operating
as a Gunn diode, where the operation is dependent upon transit of a high
field domain, the resulting frequency is dependent in a significant way on the
saturated drift velocity of the semiconductor. The saturated drift velocity of
the carriers is significantly dependent upon the high field electron-phonon
scattering rates and in a marginal way upon scattering by ionized impurities.
At high fields the saturated drift velocity decreases with increasing temperature,
as seen in figure 4-1. In addition to changes in the high field temperature,
dependent properties of the velocity-field curve there is also a decrease in the
low field mobility with increasing temperature. Thus, it may be expected that
increases in the operating temperature will degrade device performance.

If we move away from the Gunn device and toward a compound semiconductor
IMPATT it becomes necessary to include hole as well as electron transport.
Furthermore, temperature variations in a direction normal to the principle
direction of current flow are known to cause measurable changes in the
performance of IMPATTS [Haitz (1968)]. Thus, two-dimensional simulations are
necessary. The two-dimensional nature of the problem becomes even more
dramatic when it is realized that gallium arsenide FETs and three-terminal
transferred electron logic devices are extremely sensitive to temperature varia-
tions [Grubin, et al (1980, 1982)]. Under the present ARO contract, two-dimensional
transient variations for both hole and electron transport were formulated. However,
numerical calculations we performed for only one space dimension, and it is
within this context that our results are presented.

The temperature dependent results discussed below must be regarded as
initial effects on this problem. Additional calculations are still necessary
before preparation for publication.

4.2 Formulation and Analytical Results

Thermal effects are examined by generalizing equation 2.23 to include
temperature effects:

$$J(T) = NeV(E, \mathcal{T}) - e \left[D(E, \mathcal{T}) \frac{\partial N(X,T)}{\partial X} + D(E, \mathcal{T})N(X,T) \frac{\partial \mathcal{T}}{\partial X} \right] + \epsilon \frac{\partial E}{\partial T} \qquad 4.2\text{-}1$$

The third term on the right side of Eq. 4.2-1 represents temperature gradient contributions to the current density. It is included for formal reasons only, and by analogy to the situation in which classical statistics apply and the scattering parameter is independent of position. Its contribution will, however, be ignored. The quantities considered below are the field-dependent velocity and diffusion coefficients which now include a temperature dependence. The temperature dependence of the velocity-electric field curve has been calculated by Ruch, et al (1970) and shown to be in good agreement with the experimental measurements of Ruch, et al (1968). A fit to the velocity-field curve of Ruch, et al (1970) was given by Freeman, et al (1972)

$$V(E, \mathcal{T}) = \frac{2.25 \times 10^9 E}{\mathcal{T}} \left\{ \left[1 + \frac{0.265(E/E_o)^3}{(1 - 5.3 \times 10^{-4} \mathcal{T})} \right] \bigg/ \left[1 + \left(\frac{E}{E_o} \right)^4 \right] \right\} \qquad 4.2\text{-}2$$

and is said to be valid for any temperature between 300 and 600°K. The fit for 300 and 500°K is shown in Fig. 4-1. In Eq. 4.2-2, E_o is 4 k V/cm, yielding a threshold electric field of approximately 3.5 k V/cm. Freeman, et al (1972) also argued that the temperature dependence of the diffusion curve between 300 and 600°K could be represented by multiplying the room temperature values by the factor 300°K/$\mathcal{T}$. Analytical representations of the velocity field curve, as given by equation 4.2-2 are the type used in the simulation.

To simulate the temperature dependence of the device, equation 4.2-1 was solved simultaneously with the equation for heat conduction

$$C\rho \frac{\partial \mathcal{T}}{\partial T} = \frac{\partial}{\partial X} \left(\kappa(\mathcal{T}) \frac{\partial \mathcal{T}}{\partial X} \right) + J(T)E(X,T), \qquad 4.2\text{-}3$$

where ρ is the mass density of the material and C its specific heat [see Carslaw and Jaeger (1959)]. In studying this problem, two time constants emerge. The thermal time constant [see e.g., Shaw, et al [1979] equation 7-30)

$$\tau_{th} = 4C\rho \ell_n^2/\pi^2 \kappa \approx (1.5 \times \ell_n^2/cm^2)s, \qquad 4.2\text{-}4$$

and a characteristic electric time constant. For $\ell_n \approx 10\mu m$ $\tau_{th} = 1.6 \times 10^{-6}$ sec. In the one-dimensional gallium arsenide calculations, the doping profile were chosen to yield a localized high field domain which was potentially capable of sustaining a time-dependent oscillation. At sufficiently high bias an oscillation did result. The time constant; associated with this oscillation were of the

85

order of ℓ_n/V, and for the device studied $\ell_n = 5\mu m$ leading to

$$\tau_{el} \doteq \ell_n/V \approx 5 \times 10^{-11} \text{ sec} \approx 3 \times 10^{-5} \tau_{th} \qquad 4.2-5$$

The results are expected to lead to a slow increase in temperature from the source to the drain. However, in view of the disparate values of the thermal and electrical time constants, we chose not to resolve the long thermal time to equilibrium. Instead, we concentrated on the steady state time-independent solutions. Before discussing these solutions, it is useful to make reference to an earlier analytical calculation, first discussed by Knight (1967) and summarized by Shaw, et al (1979).

We consider the device structure shown in figure 4-2 and seek time-independent solutions to equation 4.2-3 for the situation when the quantity of heat generated at the n^+n interface and within the n^{++} region is negligible, are [Shaw, et al (1979)]

$$\mathcal{T}(X) = \mathcal{T}_{n/n^{++}} \exp\left\{\frac{JE}{300}(\ell_n^2 - X^2)\right\}, \quad 0 < X < \ell_n, \qquad 4.2-5$$

where $\mathcal{T}_{n/n^{++}}$ is the temperature at the n/n^{++} interface and ℓ_n is the thickness of the n region.

$$\mathcal{T}(X) = \mathcal{T}_{ms} \exp\left[(JE\ell_n/120)(\ell_n + \ell_{n^{++}} - X)\right],$$

$$\ell_n < X < \ell_{n^{++}} + \ell_n \qquad 4.2-6$$

where $\ell_{n^{++}}$ is the thickness of the n^{++} layer and $\mathcal{T}_{ms}$ is the temperature at the metal/semiconductor interface. From equation 4.2-5 and 4.2-6

$$\mathcal{T}_{n/n^{++}} = \mathcal{T}_{ms} \exp(JE\ell_n\ell_n^{++}/120), \qquad 4.2-7$$

and the temperature distribution within the n layer is

$$\mathcal{T}(X) = \mathcal{T}_{ms} \left[\exp JE\ell_n \left(\frac{\ell_n^{++}}{120} + \frac{\ell_n}{300}\right)\right] \left[\exp\left(-\frac{JEX^2}{300}\right)\right],$$

$$0 < X < \ell_n \qquad 4.2-8$$

We are interested in the temperature difference $\mathcal{T}(0) - \mathcal{T}(\ell) = \Delta\mathcal{T}$

Thus

$$\Delta \tau = \tau_{ms} \left[\exp JE\ell_n \left(\frac{\ell_n^{++}}{120} + \frac{\ell_n}{300} \right) \right] \left\{ 1 - \exp \left(-\frac{JE\ell_n^2}{300} \right) \right\} \qquad 4.2\text{-}9$$

If $\ell_n^{++} << \ell_n$

$$\Delta \tau \approx \tau_{ms} \left[\exp \left(\frac{JE\ell_n^2}{300} \right) - 1 \right] \qquad 4.2\text{-}10$$

For the parameters of Table 2, and a power density associated with the maximum field and current prior to an instability, $JE\ell_n = 5.75 \times 10^3$ W/cm^2, and

$$\Delta \tau \equiv \tau_{ms} [01] \qquad 4.2\text{-}11$$

For $\tau_{ms} = 300°$, $\Delta \tau = 3°$K for a field of 90KV/cm

$$\Delta \tau \equiv \tau_m [0.11] \qquad 4.2\text{-}12$$

and again for $\tau_{ms} = 300°$, $\Delta \tau \equiv 34°$K

Thus, for very short devices large temperature gradients are not expected until high fields are reached. These same general conclusions emerge from the numerical calculation. The results, including the doping profile are shown in figures 4-3 through 4-6. With the exception of one calculation, all were performed for a thermal conductivity of $X = 0.5$ W/cm$°$K. The temperature dependent boundary conditions were: @ $X = 0$, $\tau = 300°$K, @ $X = L$, $\partial \tau / \partial X = 0$.

4.3 Numerical Calculations and Conclusions

Figure 4-3 shows the carrier density, electric field profile, and temperature variation for a 5μm long gallium arsenide element with a centrally placed notch of magnitude $\Delta n = .6N_o$. The potential drop across this element is 1 volt. Note the other negligible temperature variation across the device. The current level for these calculations yielded an average velocity $<v> = J/N_o e = 1.46 \times 10^7$ cm/sec. Further increases in voltage generated transit time oscillations.

Figure 4-4 displays a similar calculation. This time, however, with a doping notch of $\Delta n = 0.1N_o$. For this case, the field variation is more

87

extreme than in figure 4-3, but the current level is below that of the former; a result consistent with the cathode boundary field model [See, e.g., Shaw, et al (1979)]. Note that for both figure 4-3 and 4-4 the temperature variation is negligible, as expected from equation 4.2-11. With regard to figure 4-4, we point out that the structure in N(X), downstream from the notch is a consequence of the region of negative differential mobility.

Large temperature variations, for a sample of fixed length, are a consequence of either a low thermal conductivity and/or high fields. We illustrate both cases. To illustrate the low thermal conductivity case, we use gallium arsenide parameters with a thermal conductivity equal to 0.05 W/cm °K. The result is shown in figure 4-5. While the current density is virtually unchanged, the temperature variation has increased by an order of magnitude.

The situation in which an average field is increased to 90 kv/cm, and the thermal conductivity taken as 0.5 W/cm °K, is displayed in figure 4-6. While structure in carrier density and field is seen everywhere throughout the device, the field profile is relatively uniform. For this calculation, the origin of all field nonuniformities is the notch, and we see that the temperature difference between cathode and anode is approximately 30°K. This was predicted analytically in equation 4.2-12.

While additional calculations are necessary, particularly with regard to ellucidating the role of field nonuniformities on the temperature profile, the results of both the analytical and numerical study indicate that for short micron scale devices large thermal gradients are not likely to be prominent until high fields are present across the device structure.

TABLE 2

GaAs Parameters

$V_p = 2.25 \times 10^7$ cm/sec

$E_p = 3.2$ kV/cm

$\ell = 5 \times 10^{-4}$ cm

$N_o = 10^{15}/cm^3$

area $= 1.5 \times 10^{-4}$ cm^2

$R_o = 3.03\Omega$

$C_o = 2.94 \times 10^{-13} f$

$J_p = N_o e V_p$

$\quad = 3.6 \times 10^3$ A/cm^2

$E_p \ell = 1.6$ volts
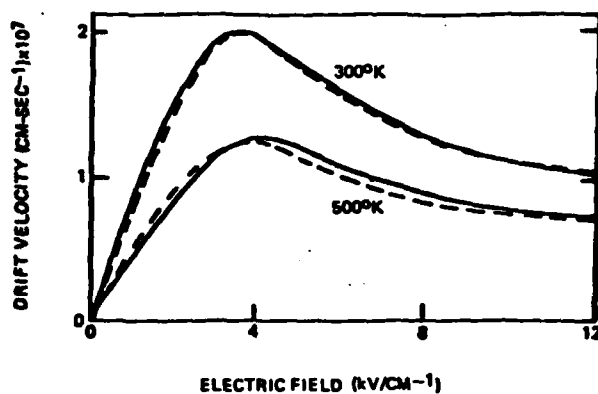
Figure 4-1 – Analytical fit (---) of the drift velocity electric field
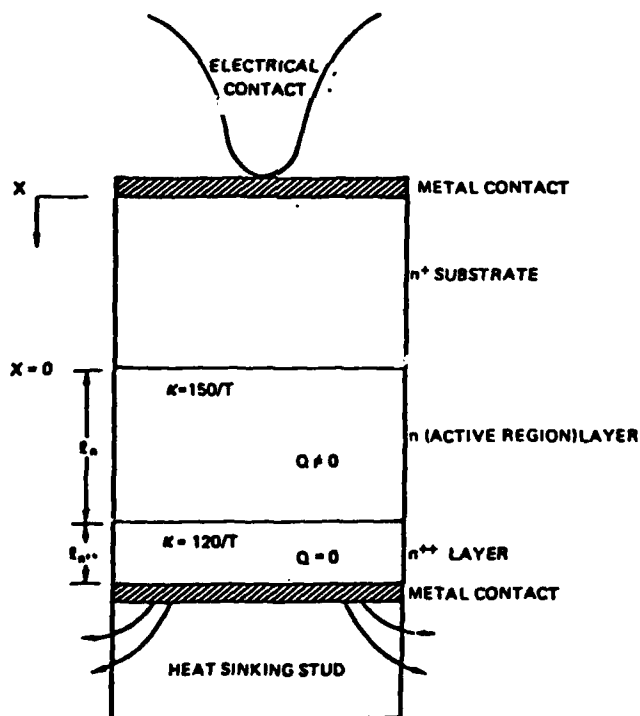relation for electrons in GaAs. (From Freeman et al (1972).
For the data (—), see Ruch et al 1968.

Figure 4-2 – Device structure for doing temperature-dependent calculations.
(From Knight (1967).
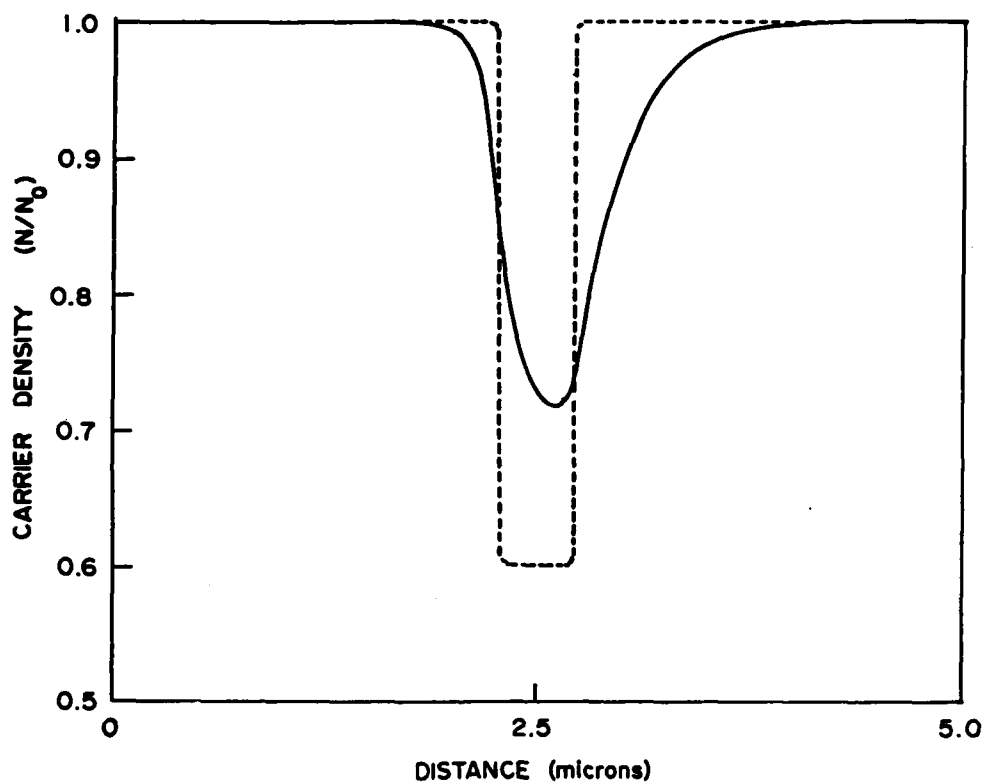
Figure 4-3(a) — Normalized carrier density, $N'/10^{15}/an^3$ and
normalized background doping $N_o(x)/10^{15}/cm^3$
for a five micron long gallium arsenide element
subjected to an average field of 2kv/cm. The
thermal conductivity is $\kappa = 0.5W/cm°K$.
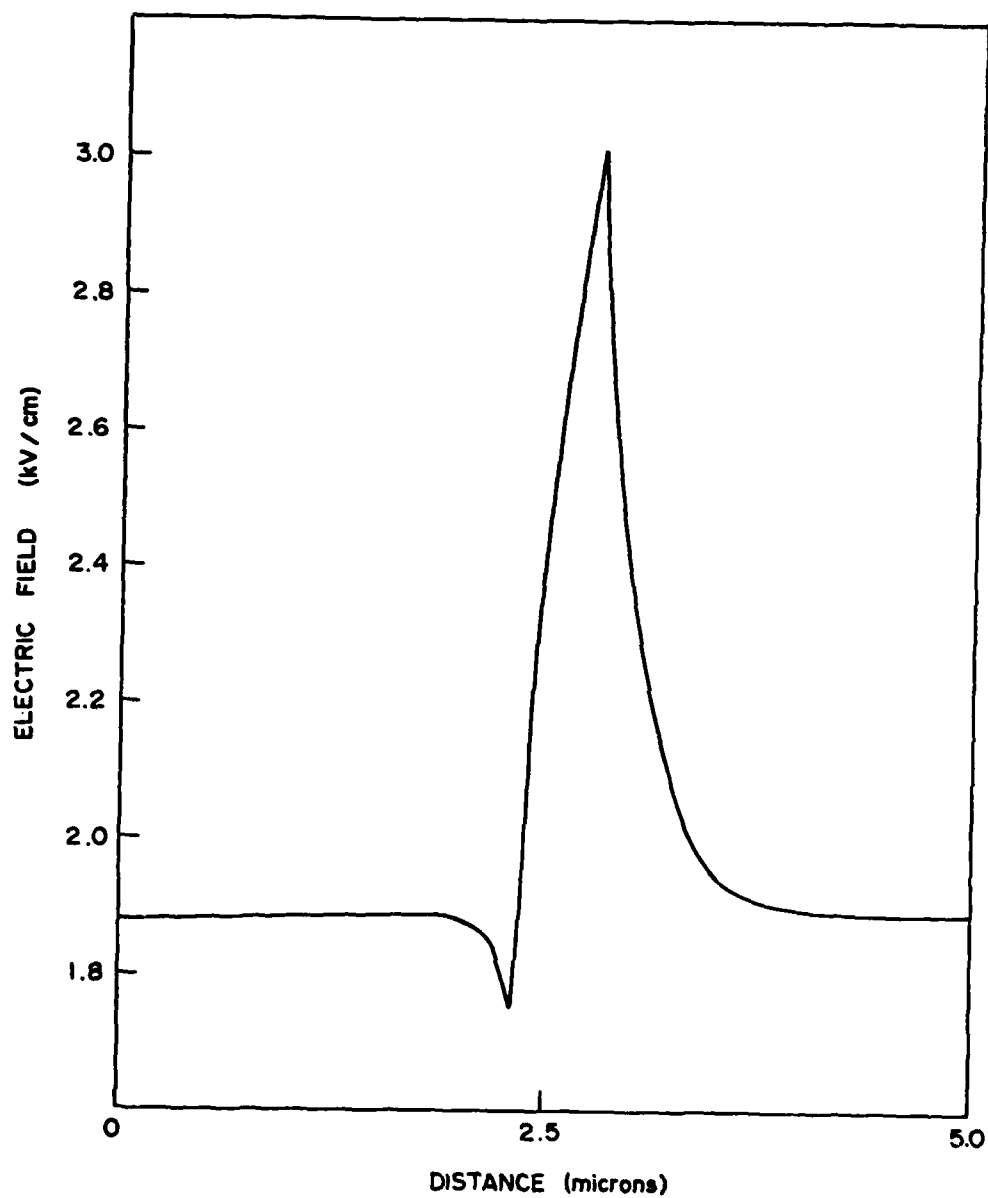
Figure 4-3(b) - Electric field versus distance.

END

DATE
FILMED

83

DTIC
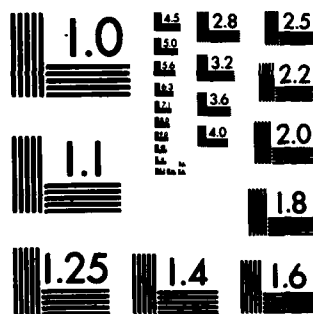
MICROCOPY RESOLUTION TEST CHART

NATIONAL BUREAU OF STANDARDS-1963-A
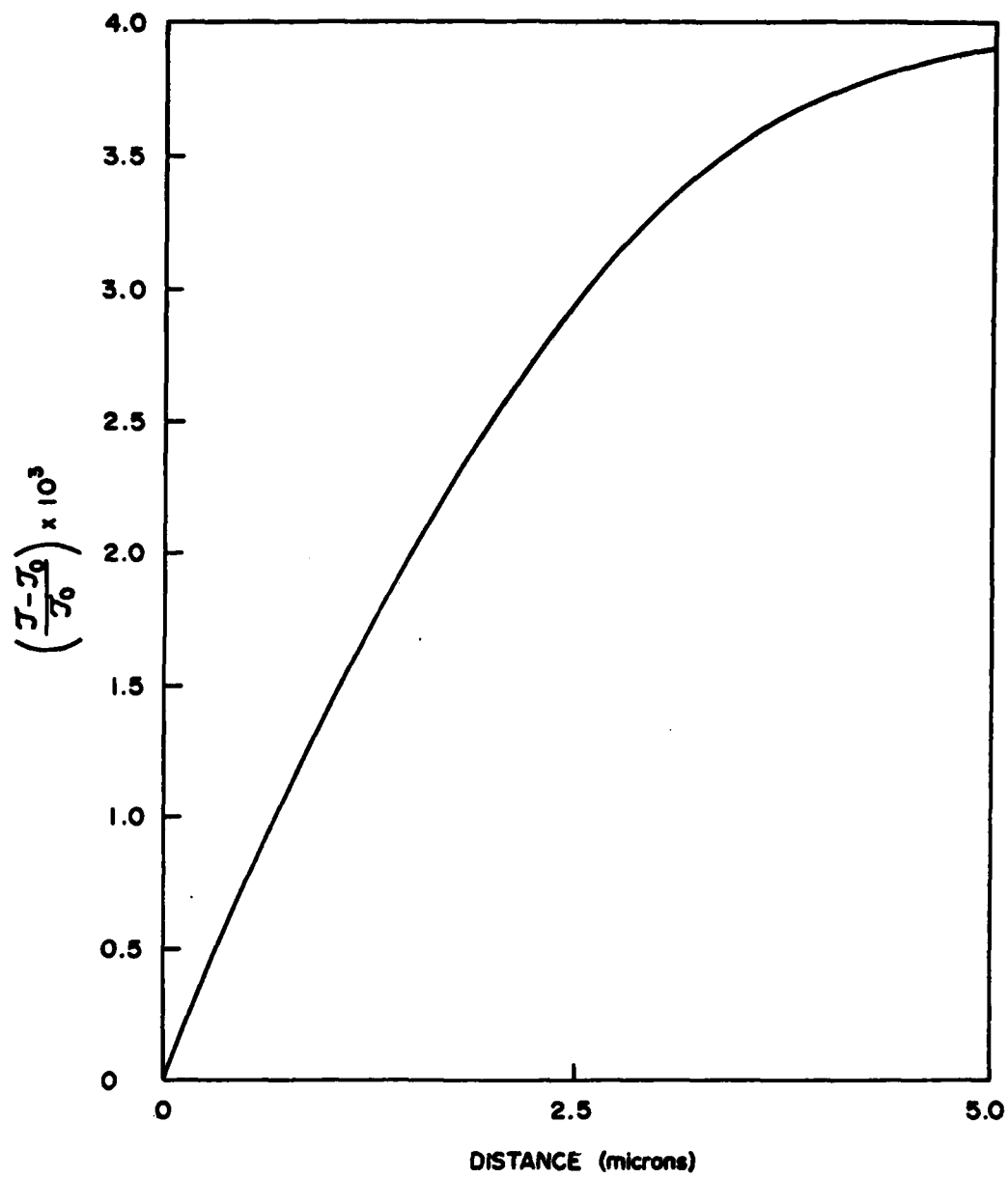
Figure 4-3(c) — Fractional temperature variation across device.
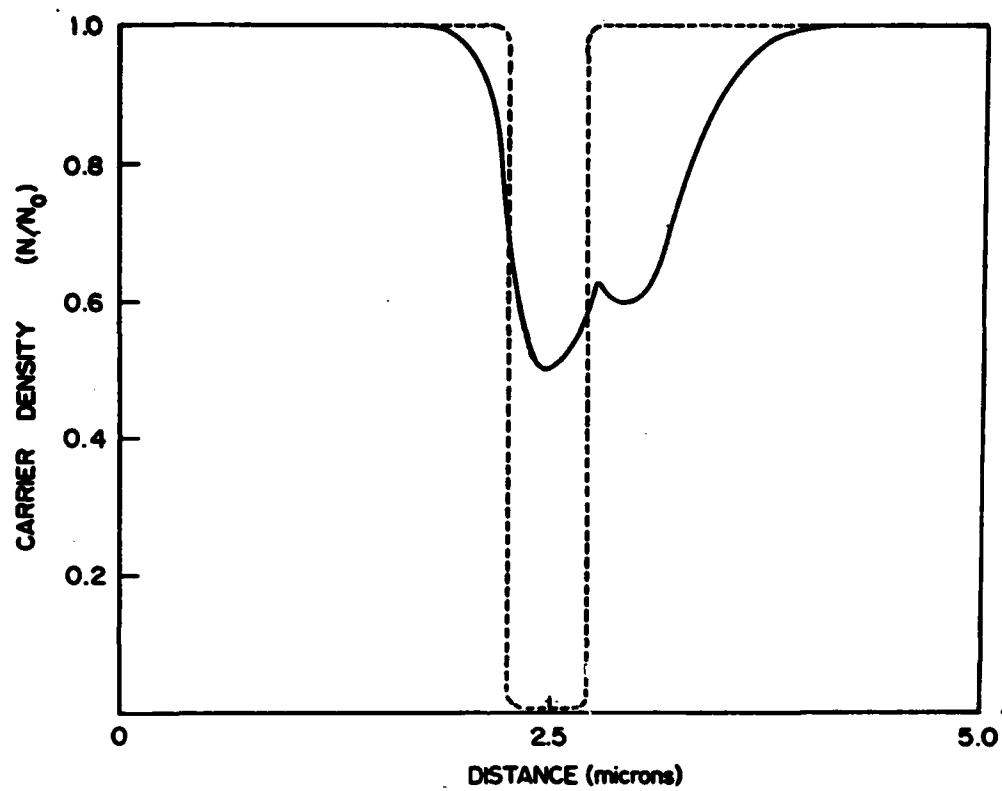
Figure 4-4 a,b and c — As in Figure 4-3, but for a different notch depth.

94
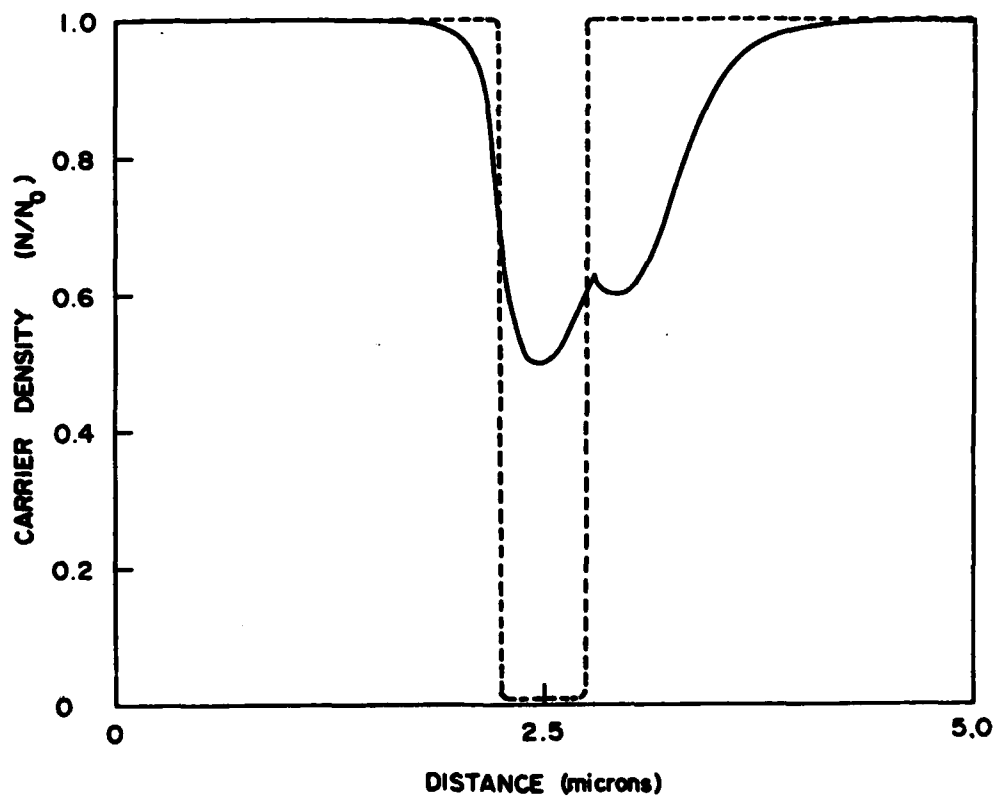
Figure 4-4(b)

95

Figure 4-4(c)

96
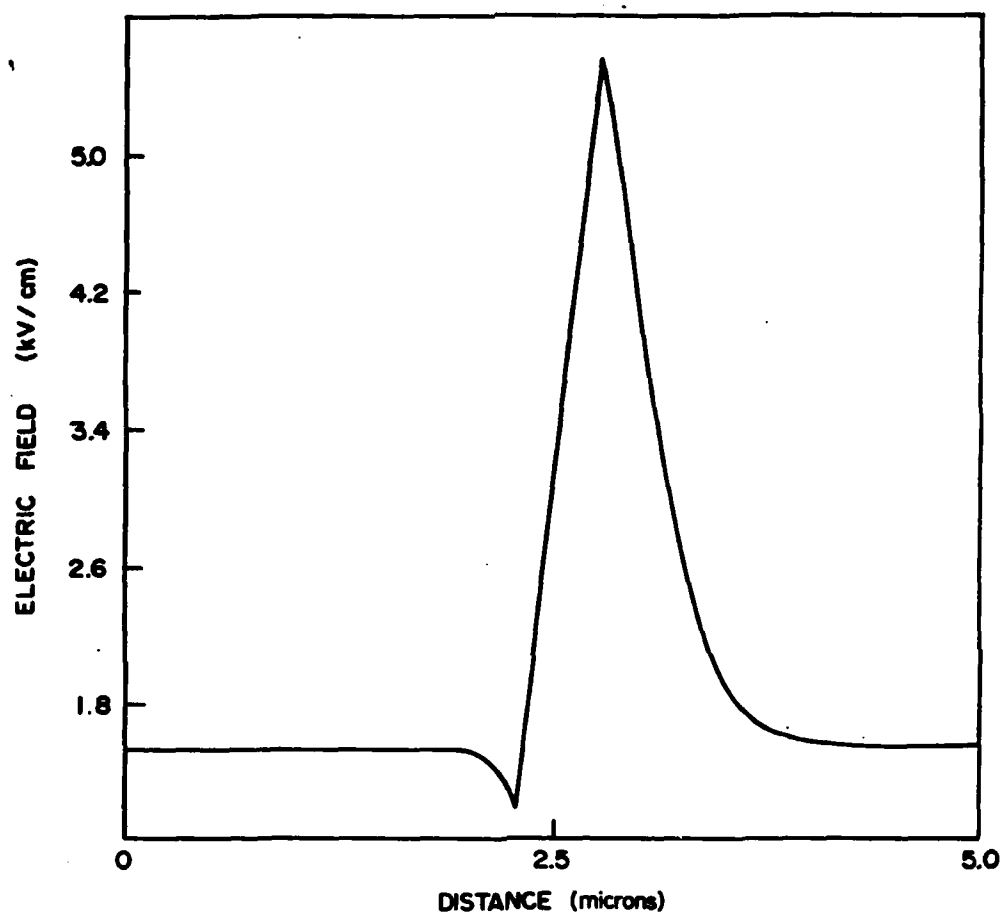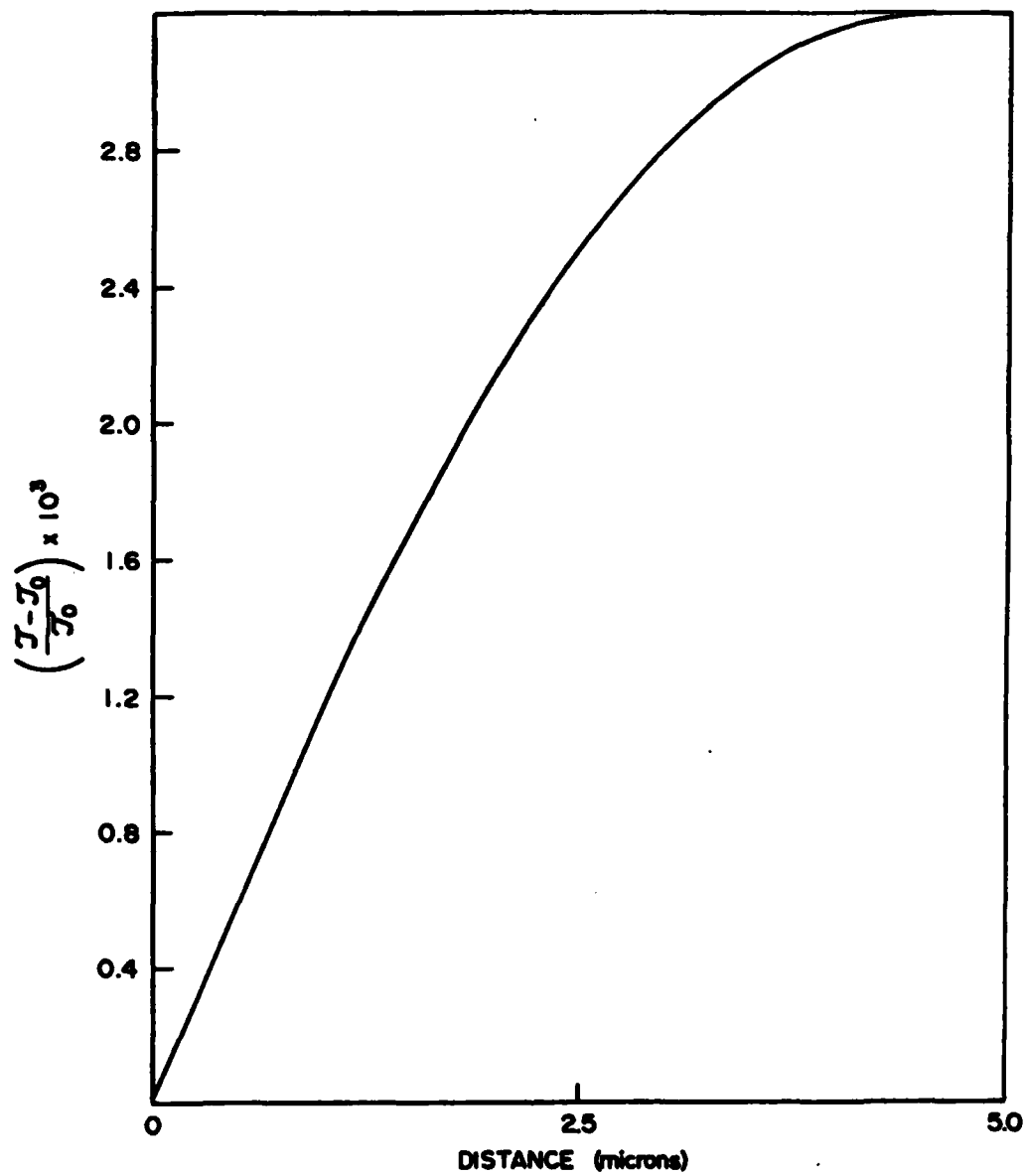
Figure 4-5 a,b and c - As in Figure 4-4, but for a reduced
thermal conductivity, $\kappa = 0.05W/cm°K$.

Figure 4-5(b)
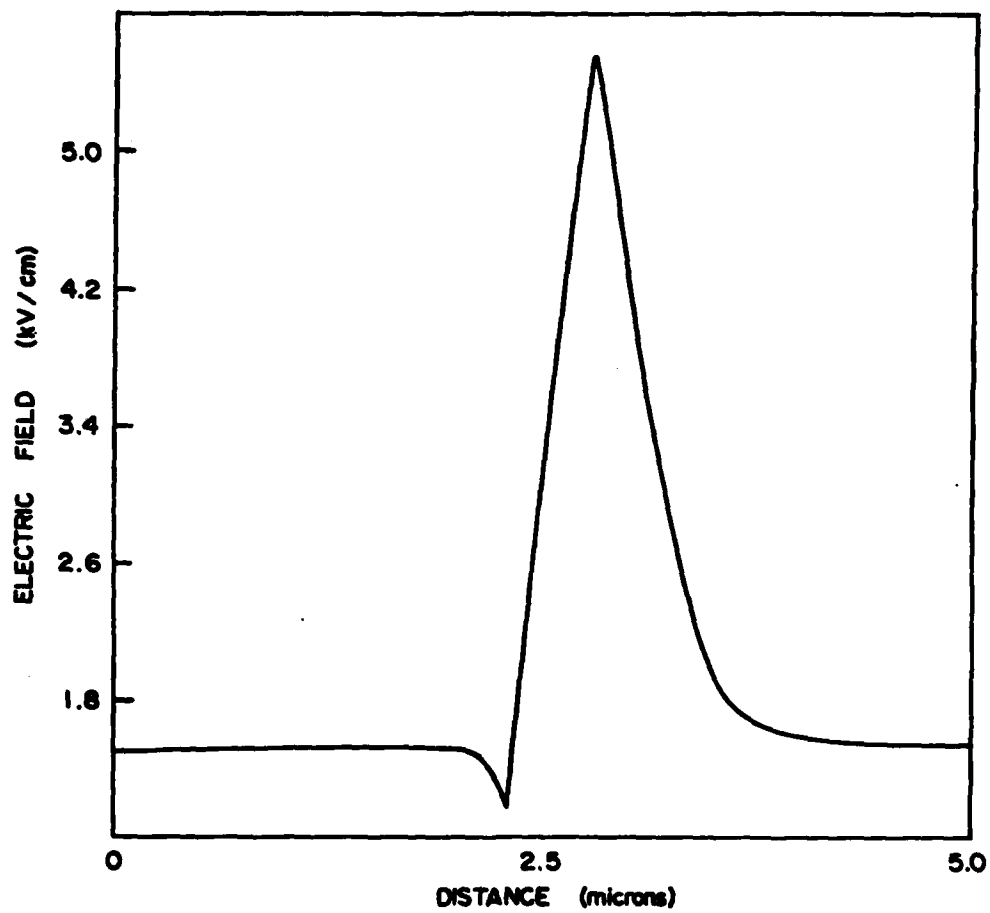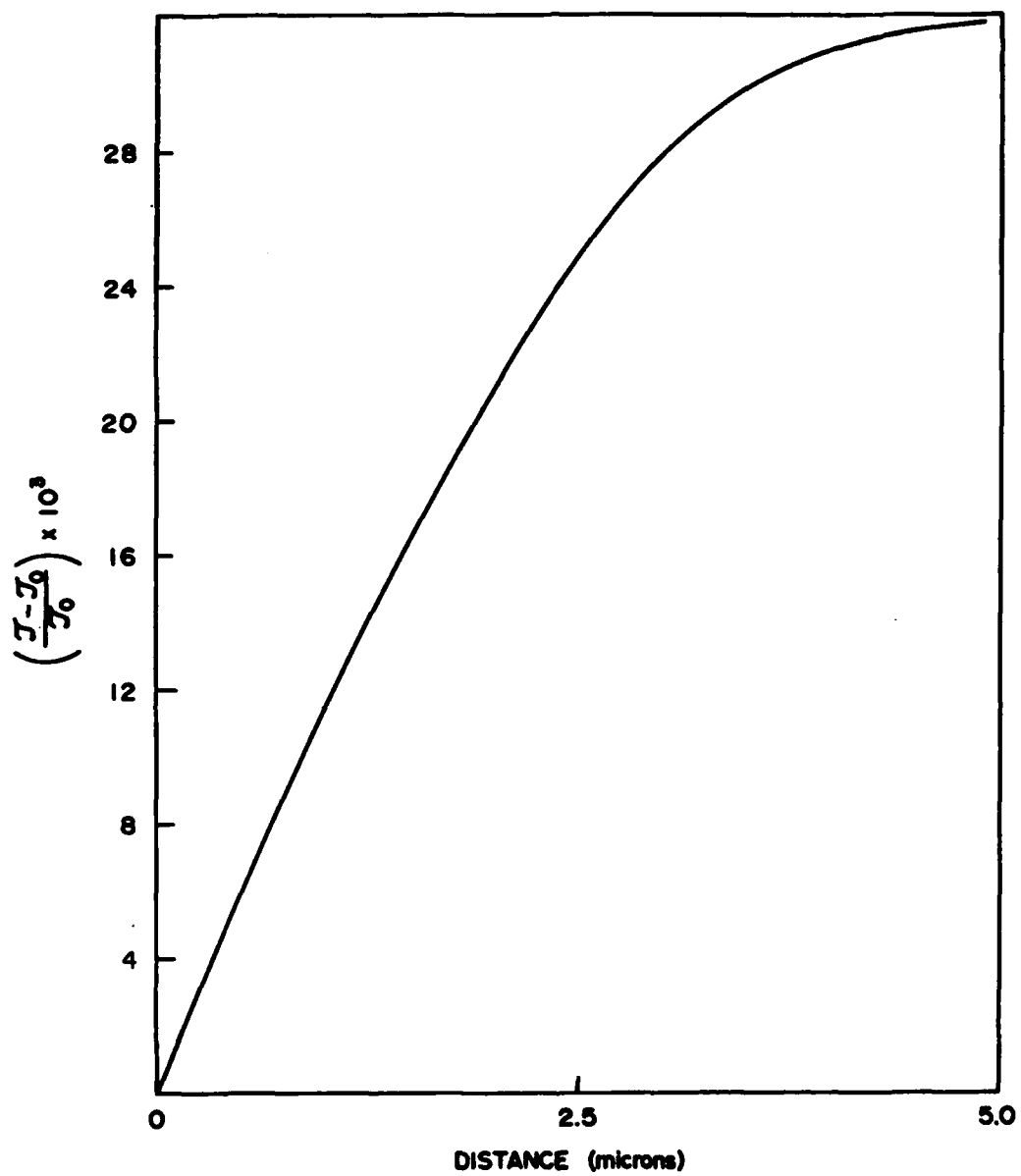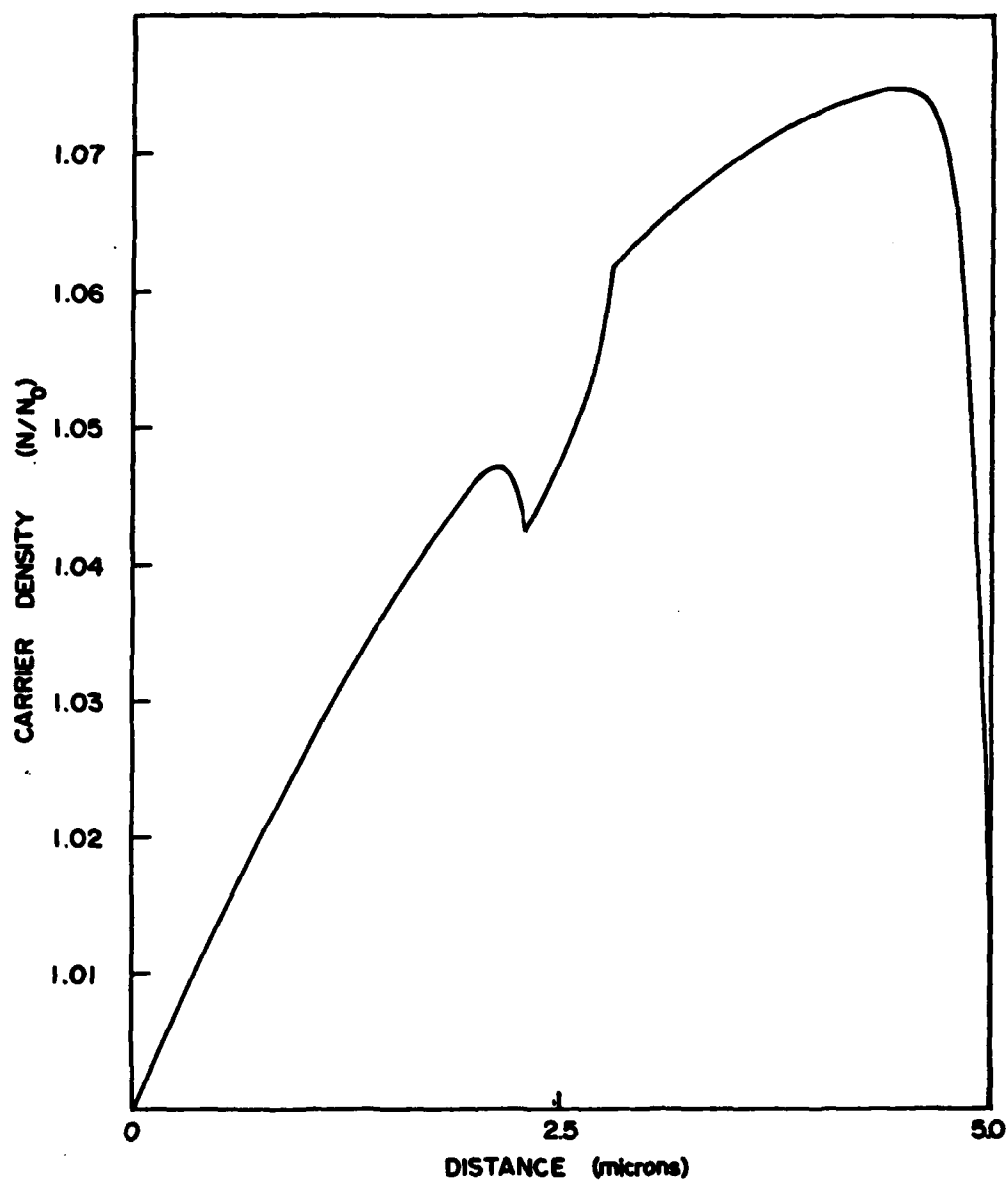
Figure 4-5(c)

99

Figure 4-6 a,b and c — As in Figure 4-4, but for an average
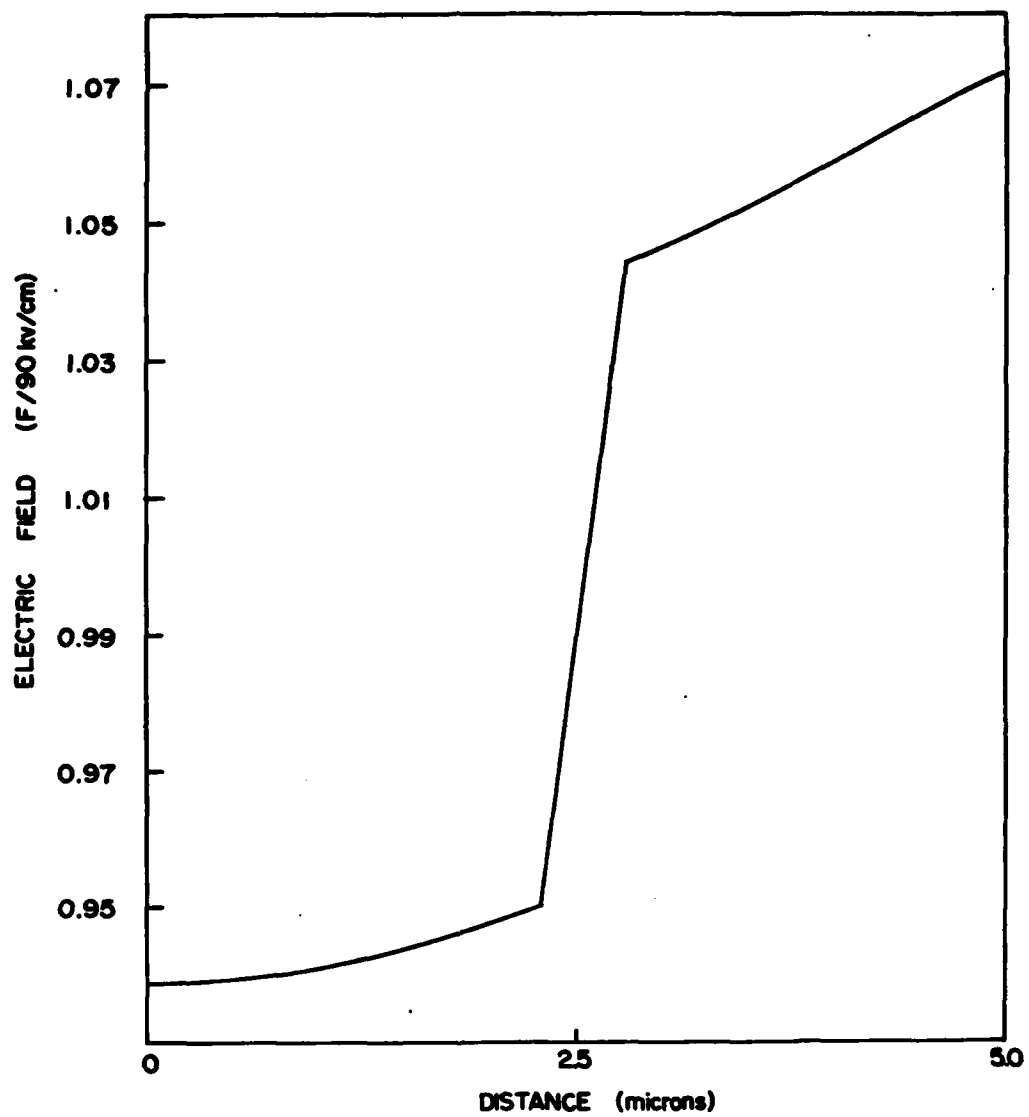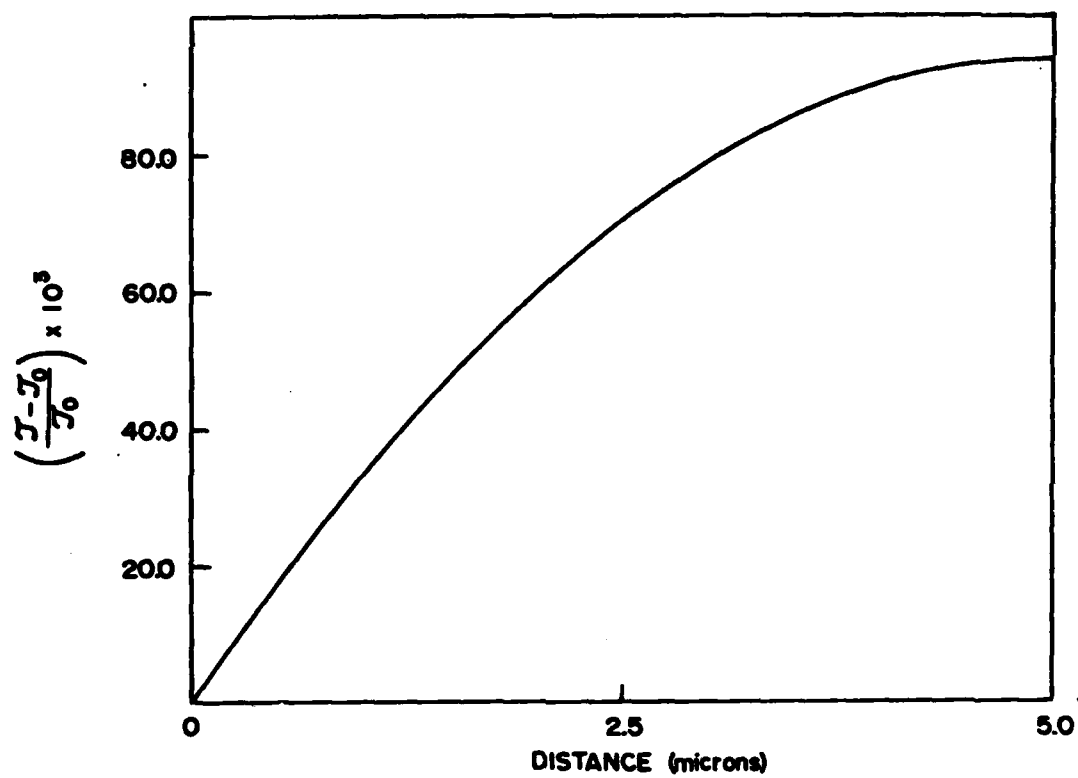field of 90kv/cm.

100

Figure 4-6(b)

101

Figure 4-6(c)

102

5. Drift and Diffusion Description of Injection Field Effect Transistors

5.1 Introduction

A recent study by Fauquemberque, et al (1983) on a submicron gate injection-type field effect transistor suggests some rather interesting electrical characteristics. In particular, for a gate length of 0.15µm, a gain-bandwidth product of 400 GHZ was predicted. The predicted behavior of the device was based on a Monte Carlo solution, and short channel velocity overshoot effects were included. The immediate question is: To what extent are submicron dimensions important for this pehnomena. A study to answer this question was recently initiated. The initial study was for a micron scale device.

The calculations were performed for a device whose basic structure is shown in figure 3-1. However, the semiconductor material used for this calculation was InP with a nominal doping level of $10^{16}/cm^3$, H = 0.64 micron and L = 3.0 microns.

5.2 Numerical Results

Two types of calculations were performed. In one calculation N_o was uniform and at sufficiently high bias the device sustained current oscillations in the form of propagating high field domains. In the second calculation, the background was reduced to $10^{14}/cm^3$ over a distance of 1.5µm. No instabilities were observed in the latter case and, of course, the current levels were significantly reduced. The space charge distribution for the uniformly doped material was qualitatively similar to that obtained for the gallium arsenide structure discussed in section 3. The distribution for the injection FET is qualitatively different, and is displayed in figure 5-1, where we see strong injection.

The first collection of calculations for the injection FET provide a series of current voltage characteristics, two branches of which are shown in figure 5-2. The initial results find a dramatic improvement in the trans-conductance for the injection FET. For example; For the uniformly doped FET and a drain potential of approximately 0.5 volts the transconductance near V_G = -0.1 was

5.2-1

$$gm \approx .5\ G_o$$

where

$$Go = \frac{N_o e \mu H W}{L}$$
5.2-2

For the injection FET G_o is reduced by almost two orders of magnitude:

$$Goinj \approx G_o/50$$
5.2-3

while the transconductance is reduced by significantly less

$$g_m \approx 0.14 \ G_o$$
5.2-4

The results of these studies are currently being evaluated, but several points are noted:

For a routinely configured FET, the change in drain current due to changes in gate bias is largely a consequence of a modulation in the cross-sectional area of the conducting channel. When domains form as discussed in section 3, modulation is accompanied by space charge injection into the depletion region. For the injection FET the space charge density at moderate value of gate bias levels exceeds the background. Modulation is then accompanied by both a variation in channel height as well as an alternation in the net mobile carrier density. The behavior of the injection FET appears operationally different from the classical FET, and its device potential should be explored.
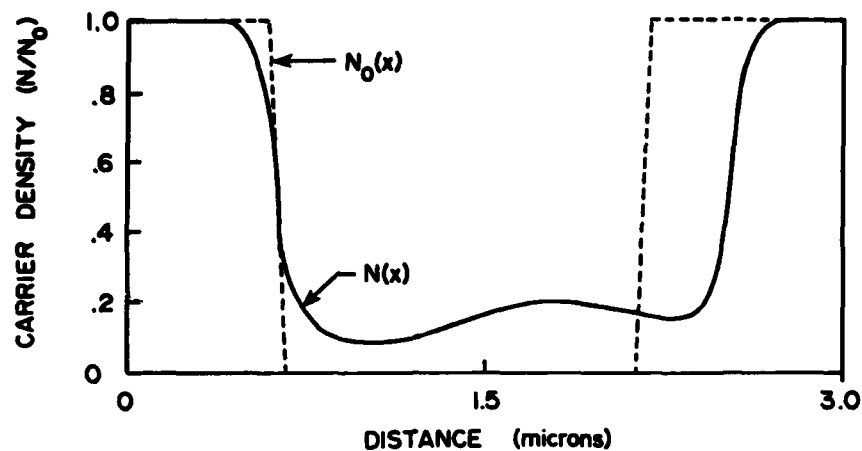
Figure 5.1a - Spatial distribution of carrier density N(X) at the **bottom of the channel** of the injection FET. Also shown is the background density $N_o(X)$ for the device.
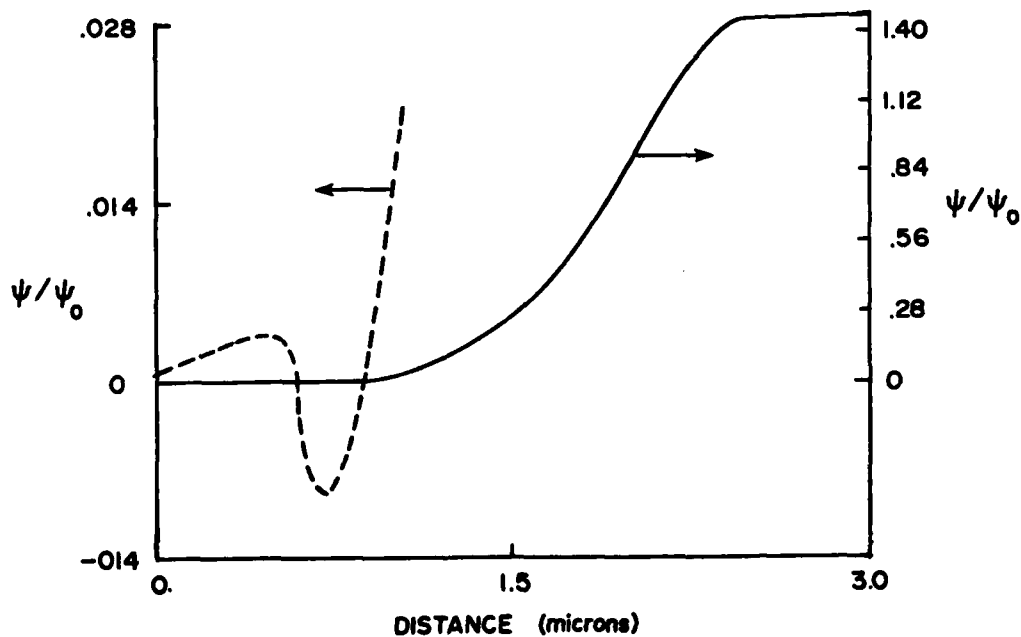

Figure 5.1b - Potential distribution along the bottom of the channel. Most of the potential drop is across the injection region, as shown by the solid line whose axis is toward the right hand side of the figure. There is structure in the potential near the source. This is shown by the dashed curve. For this calculation Y_o = 3 volts.
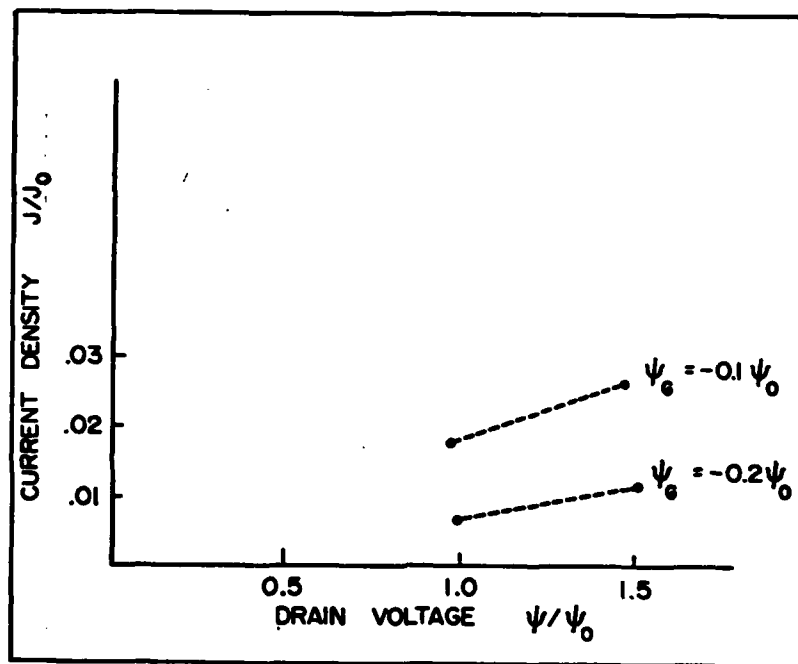
Figure 5.2 – Drain current versus drain voltage for an InP injection FET. Here $J_o = N_o e V_p A$ and $\Psi_o = 3$ volts.

REFERENCES

Baechtold, W. (1974), IEEE Trans. Electron Devices, ED-19, 674 (1972).

Carslaw, H.S. and J.C. Jaeger (1959) Conduction of Heat in Solids 2nd ed. Oxford Univ. Press, London and N.Y. (1959).

Cobbold, R.S.C., (1970) Theory and Applications of Field Effect Transistors, Wiley-Interscience, New York (1970).

Englemann, R.W.H. and C. Liechti (1977) IEEE Trans. Electron Devices, ED-24, 1977).

Fauquemberque R., M. Pernisek, and E. Constant, (1983) Proc. of 1982 Workshop on the Physics of Submicron Structures Plenum Press to be published (1983)

Freeman, K.R. and G.S. Hobson (1972), IEEE Trans. Electron Devices ED-19, 62 (1972).

Grubin, H.L. and R. Kaul (1975), IEEE Trans. Electron Devices, ED-22, 240, 1975.

Grubin, H.L., D.K. Ferry and K.R. Gleason (1980) Solid State Electronics 23, 158 (1980).

Grubin, H.L., W. Anderson, and A. Christoo (1982) 1982 WOCSEMMAD February, Scottsdale, Arizona.

Gunn, J.B. (1964), IBM J. Res. Develop. 8, 141 (1964).

Haitz, R. (1968), IEEE Trans. Electron Devices ED-15, 350, 1968.

Knight, S. (1967) Proc. IEEE 55, 112 (1967).

Liechti, C. (1976) IEEE Trans. Microwave Theory and Tech. MTT-24, 279 (1976).

Pucel, R.A., H.A. Haus and H. Statz (1975) in Advances in Electronics and Electron Physics, Academic Press, N.Y. (1975).

Richer, I., (1975) Solid State Electronics 8, 381 (1965).

Ruch, J.G. and G.S. Kino (1968) Phys. Rev. 174, 921 (1968).

Ruch, J.G. and W. Fawcett (1970) J. Appl. Phys. 41, 3843 (1970).

Shaw, M.P., H.L. Grubin and P.R. Solomon (1979), The Gunn-Hilsum Effect, Academic Press, New York (1979).

Shockley, W., J.A. Copeland and R.P. James (1966), Quantum Theory of Atoms, Molecules and the Solid State (P.O. Lowdin, ed.), pp. 537-563, Academic Press, New York (1966).

Sitch, J.E. and P.N. Robson (1976), IEEE Trans. Electron Devices, ED-23, 1086 (1976).

Talpey, T.E. (1959) in Noise in Electron Devices, MIT and John Wiley and Sons, N.Y., (1959).

Thim, H.W. (1971), Electronics Letts. 7, 106 (1971).

Thornber, K.K., (1973), Solid State Electronics 17, 95 (1973).

Van der Ziel (1962), Proc. IEEE, 50, 1808 (1962).

Van der Ziel, A. (1963), IEEE Trans. Electron Devices (ED-10, 461 (1963).

Van der Ziel, A. and Ero (1964) IEEE Trans. Electron Devices ED-11, 128 (1964).

PARTICIPATING PERSONNEL

H. L. Grubin   Vice-President, Solid State Device Research

J. P. Kreskovsky   Senior Research Scientist

LIST OF PUBLICATIONS

1. Grubin, H.L. and Ferry, D.K.: Conceptual Problems in Modeling Submicron Device Physics. J. Vac. Sci. Tech. 19, 540 (1981).

2. Ferry, D.K. and Grubin, H.L.: The Role of Transport in Very Small Devices for VLSI. Microelectronics J. 12 (2), 5 (1981).

3. Iafrate, G.J., Grubin, H.L., and Ferry, D.K.: Utilization of Quantum Distribution Functions for Ultra-Submicron Device Transport. Journal de Physique, Colloque C7, Supplement au n°10, Tome 42, Octobre 1981, page C7-307.

4. Iafrate, F.J., Grubin, H.L., and Ferry, D.K.: The Wigner Distribution Function. Physics Letters, Vol. 87A, No. 4, January 4, 1982.

5. Ferry, D.K., Grodin, R.O., and R.K. Reich: Considerations on the Finite, Very-Small Semiconductor Device and Superlattice Arrays. Presented at Workshop on Physics of Submicron Structures, June 28-30, 1982.

6. Grubin, H.L. and Kreskovsky, J.P.: Physics and Modeling Considerations for VLSI Devices. Presented at Workshop on Physics of Submicron Structures, June 28-30, 1982.

7. Grubin, H.L., Ferry, D.K., Iafrate, G.J., and Barker, J.R.: The Numerical Physics of Micron-Length and Submicron-Length Semiconductor Devices. VLSI Electronics: Microstructure Science, Vol. 3.

8. Grubin, H.L.: The Role of Boundaries on High Speed Semiconductor Devices. Presented at Second Annual Symposium on Interfaces. (Trieste, Italy 1982) To appear in Surface Science.